

## Supporting Information

### Bio-Based Vinylogous Urethane Vitrimers from Waste-Wood Lignosulfonate and Enzymatic Lignin: Explorations in Stress Relaxation Behavior and Mechanical Strength

Florian C. Klein, Nils Sobania, and Volker Abetz\*

Table S1: Summary of the masses of the educts, the grinding, and the heat compression conditions of the lignin vitrimer samples.

Sample <sup>a)</sup>	Acetoacetylated Lignin Species Mass	APPD Mass	Priamine™ 1073 Mass	Grinding Condition Frequency Duration	Heat compression Temperature Duration Pressure
VU-(ALs-Pri) <sub>0.4</sub>	ALs 1.333 g	-	1.588 g	Cryogenic 20 Hz 60 s	160 °C 30 min 1.9 MPa
VU-(ALs-Pri) <sub>0.5</sub>	ALs 1.467 g	-	1.482 g	Cryogenic 20 Hz 60 s	150 °C 30 min 1.9 MPa
VU-(ALs-Pri) <sub>0.6</sub>	ALs 1.586 g	-	1.361 g	Cryogenic 20 Hz 60 s	150 °C 30 min 1.9 MPa
VU-(ALs/APPD <sub>5</sub> -Pri) <sub>0.6</sub>	ALs 1.549 g	0.153 g	1.327 g	Ambient 20 Hz 60 s	180 °C 30 min 1.9 MPa
VU-(ALs/APPD <sub>10</sub> -Pri) <sub>0.6</sub>	ALs 1.388 g	0.304 g	1.319 g	Cryogenic 20 Hz 60 s	180 °C 30 min 1.9 MPa
VU-(ALs/APPD <sub>15</sub> -Pri) <sub>0.6</sub>	ALs 1.223 g	0.459 g	1.321 g	Cryogenic 20 Hz 60 s	180 °C 30 min 1.9 MPa
VU-(ALnC-Pri) <sub>0.7</sub>	ALnC 1.505 g	-	1.494 g	Ambient 30 Hz 60 s	180 °C 30 min 2.5 MPa
VU-(ALnC-Pri) <sub>0.8</sub>	ALnC 1.608 g	-	1.408 g	Ambient 30 Hz 60 s	180 °C 30 min 2.5 MPa
VU-(ALnC-Pri) <sub>0.9</sub>	ALnC 1.699 g	-	1.309 g	Ambient 30 Hz 60 s	180 °C 30 min 2.5 MPa
VU-(ALnP-Pri) <sub>0.7</sub>	ALnP 1.665 g	-	1.331 g	Ambient 30 Hz 60 s	180 °C 30 min 2.5 MPa
VU-(ALnP-Pri) <sub>0.8</sub>	ALnP 1.764 g	-	1.231 g	Ambient 30 Hz 60 s	180 °C 30 min 2.5 MPa
VU-(ALnP-Pri) <sub>0.9</sub>	ALnP 1.848 g	-	1.150 g	Ambient 30 Hz 60 s	180 °C 30 min 2.5 MPa

a) The lignin vitrimers were abbreviated following this nomenclature: First, the vinylogous urethane chemistry is introduced (VU), then, the lignin source (ALs/ALnC/ALnP) and the Priamine™ 1073 (Pri) are abbreviated, and the *R*-value (acetoacetate/amine ratio) is displayed in the index.



Figure S1: A heat compression mold with a diameter of 5 cm was used for the reprocessing of the vitrimers.

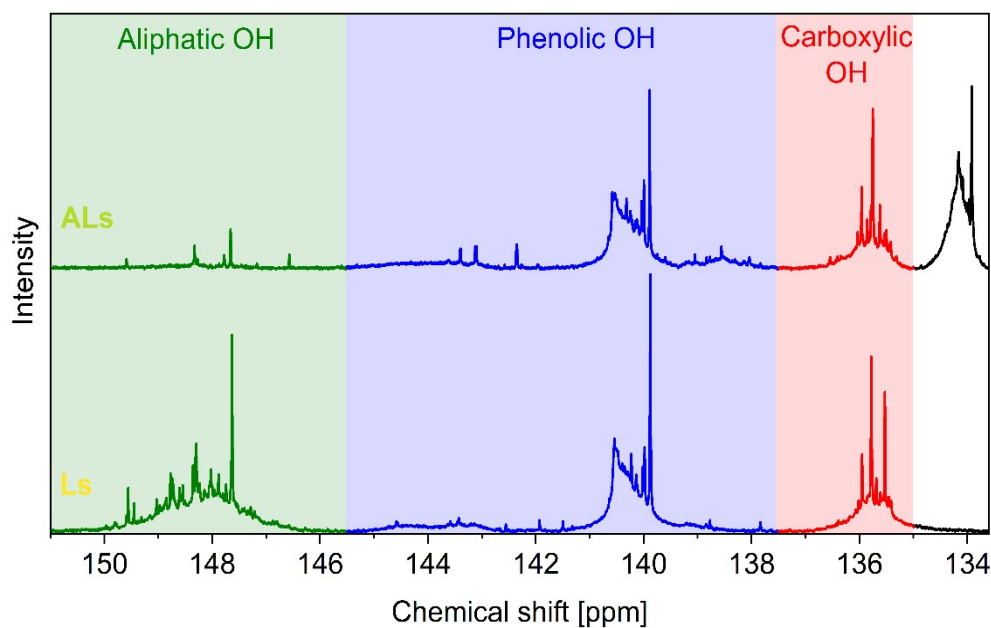


Figure S2:  $^{31}\text{P}$  NMR spectra of lignosulfonate (bottom) and acetoacetylated lignosulfonate (top). The regions corresponding to aliphatic (green), phenolic (blue), and carboxylic (red) hydroxy groups are indicated. Notably, the intensity of the aliphatic hydroxy groups is decreased in the corresponding acetoacetylated species. A broad range of signals around 134 ppm appears as a result of the enolization of the acetoacetate moieties.  $^{31}\text{P}$  NMR (243 MHz,  $\text{DMF-}d_7/\text{DMF}/\text{pyridine}$ , 298 K). Preparations and measurements were carried out according to the procedure outlined in the experimental section, using DMF as the solvent.

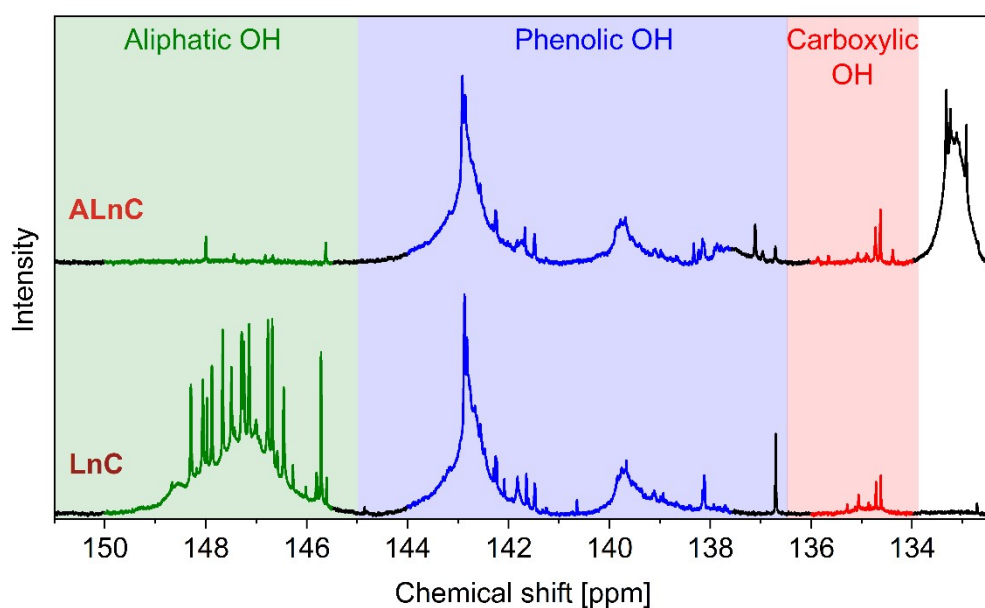


Figure S3:  $^{31}\text{P}$  NMR spectra of Lignova™ Crude (bottom) and acetoacetylated Lignova™ Crude (top). The regions corresponding to aliphatic (green), phenolic (blue), and carboxylic (red) hydroxy groups are indicated. Notably, the intensity of the aliphatic hydroxy groups is decreased in the corresponding acetoacetylated species. A broad range of signals around 133 ppm is observed as a result of the enolization of the acetoacetate moieties.  $^{31}\text{P}$  NMR (243 MHz,  $\text{CDCl}_3/\text{pyridine}$ , 298 K). Preparations and measurements were conducted following the procedure outlined in the experimental section, using  $\text{CDCl}_3$  as the solvent.

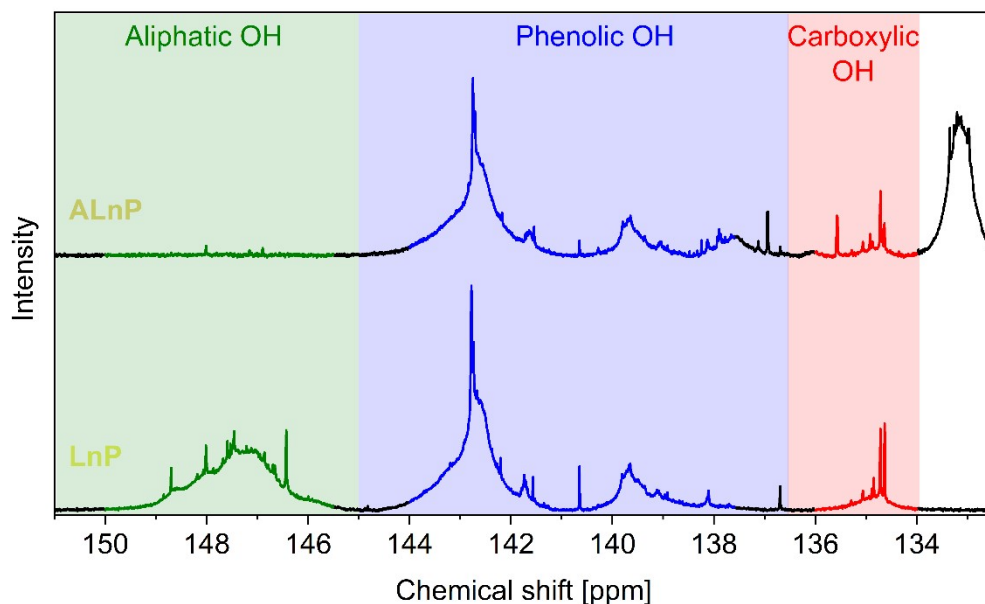


Figure S4:  $^{31}\text{P}$  NMR spectra of Lignova™ Pure (bottom) and acetoacetylated Lignova™ Pure (top). The regions corresponding to aliphatic (green), phenolic (blue), and carboxylic (red) hydroxy groups are indicated. Notably, the intensity of the aliphatic hydroxy groups is decreased in the corresponding acetoacetylated species. A broad array of signals around 133 ppm appears as a result of the enolization of the acetoacetate moieties.  $^{31}\text{P}$  NMR (243 MHz,  $\text{CDCl}_3/\text{pyridine}$ , 298 K). Preparation and measurements were conducted in accordance with the procedure described in the experimental section, using  $\text{CDCl}_3$  as the solvent.

#### Equation S1

$$\text{OH group moieties [mmol/g]} = \frac{n_{\text{OH}}}{m_{\text{Lignin}}} = \frac{I_{\text{OH}}}{I_{\text{NHND}}} \cdot \frac{n_{\text{NHND,NMR}}}{m_{\text{Lignin,NMR}}}$$

$n_{\text{OH}}$	: Amount of hydroxy groups [mmol]
$m_{\text{Lignin}}$	: Mass of lignin [g]
$I_{\text{OH}}$	: Integral of spectral region of OH moieties [-]
$I_{\text{NHND}}$	: Integral of NHND region [-]
$n_{\text{NHND,NMR}}$	: Amount of NHND in the NMR sample [mmol]
$m_{\text{Lignin,NMR}}$	: Mass of lignin in the NMR sample [g]

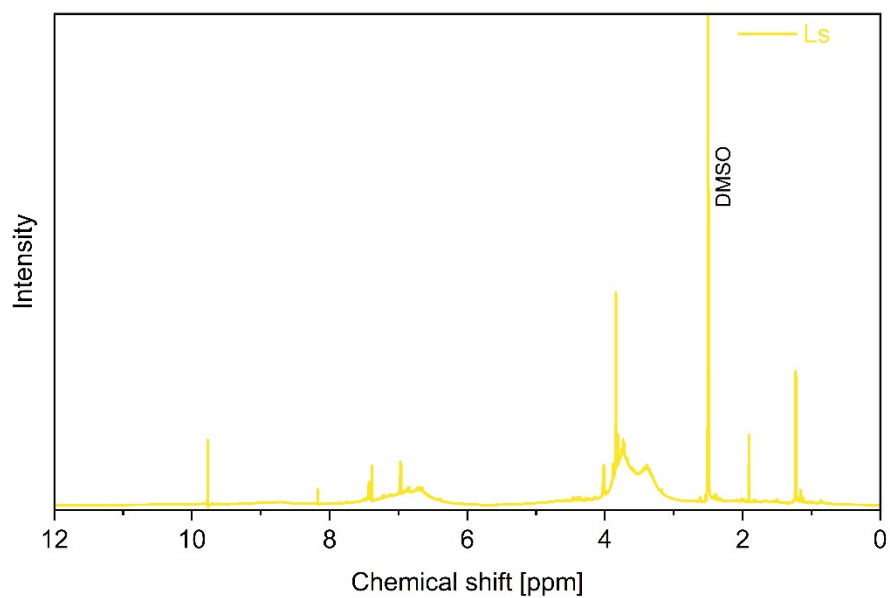


Figure S5: The  $^1\text{H}$  NMR spectrum of lignosulfonate displays the characteristic signals and intensities associated with the lignin backbone.  $^1\text{H}$  NMR (400 MHz,  $\text{DMSO-}d_6$ , 298 K)

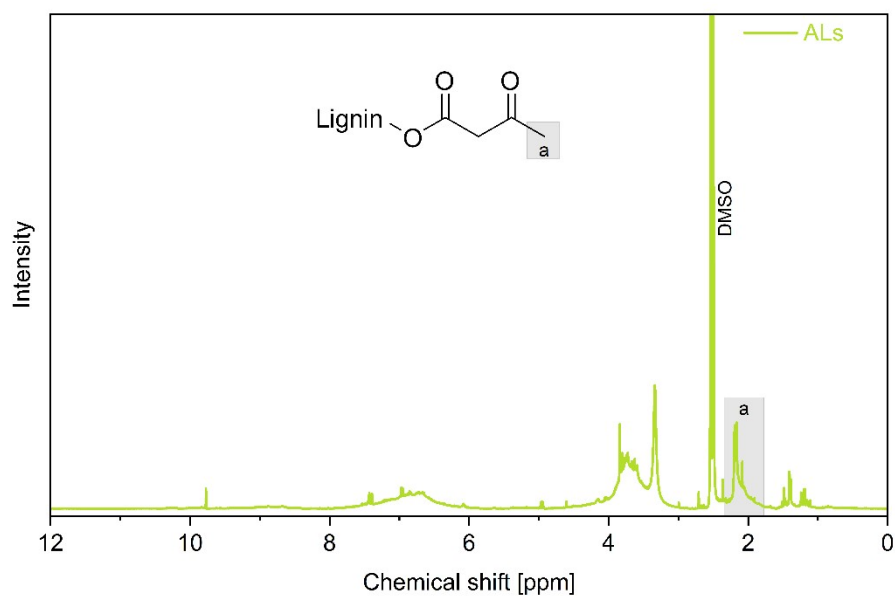


Figure S6: The  $^1\text{H}$  NMR spectrum of acetoacetylated lignosulfonate shows the methyl group of the acetoacetate moieties, along with the characteristic signals and intensities of the lignin backbone. The signal corresponding to the methyl group of the acetoacetate moieties is indicated in gray.  $^1\text{H}$  NMR (600 MHz,  $\text{DMSO-}d_6$ , 298 K)

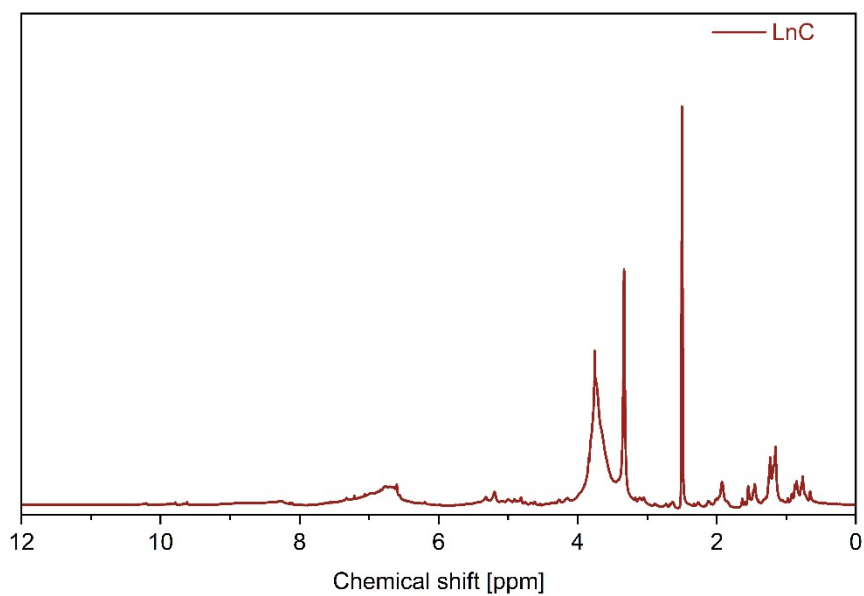


Figure S7: The  $^1\text{H}$  NMR spectrum of LignoCrude displays the characteristic signals and intensities associated with the lignin backbone.  $^1\text{H}$  NMR (400 MHz,  $\text{DMSO-}d_6$ , 298 K).

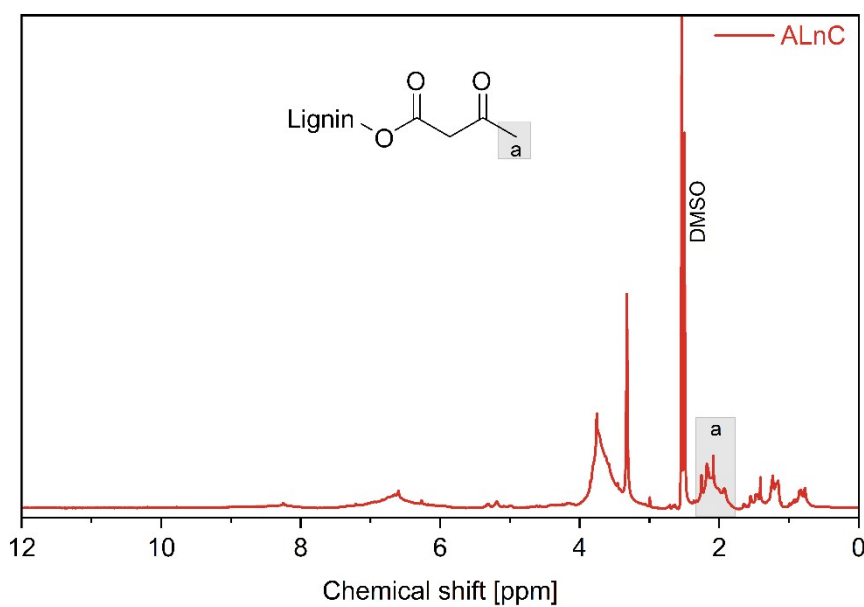


Figure S8: The  $^1\text{H}$  NMR spectrum of acetoacetylated LignoCrude shows the characteristic signals and intensities of the lignin backbone. The signal corresponding to the methyl group of the acetoacetate moieties is indicated in grey.  $^1\text{H}$  NMR (400 MHz,  $\text{DMSO-}d_6$ , 298 K).

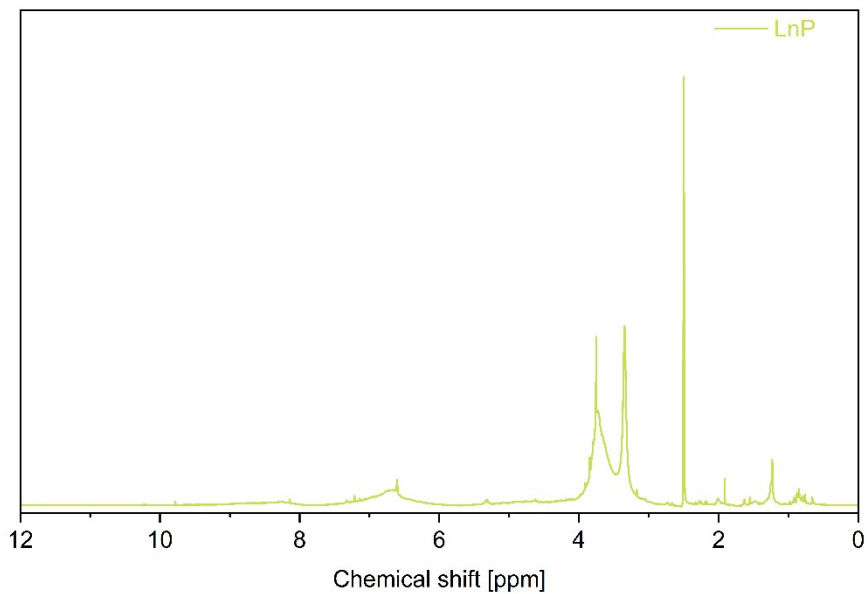


Figure S9:  $^1\text{H}$  NMR spectrum of Lignova™ Crude displays the characteristic signals and intensities associated with the lignin backbone.  $^1\text{H}$  NMR (400 MHz,  $\text{DMSO-}d_6$ , 298 K).

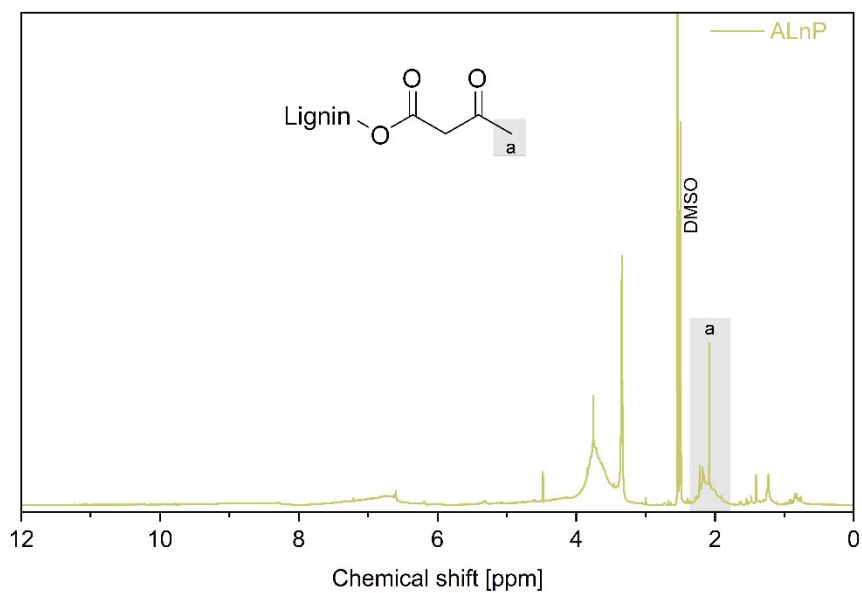


Figure S10:  $^1\text{H}$  NMR spectrum of acetoacetylated Lignova™ Pure displays the characteristic signals and intensities associated with the lignin backbone. The signal corresponding to the methyl group of the acetoacetate moieties is indicated in grey.  $^1\text{H}$  NMR (400 MHz,  $\text{DMSO-}d_6$ , 298 K).

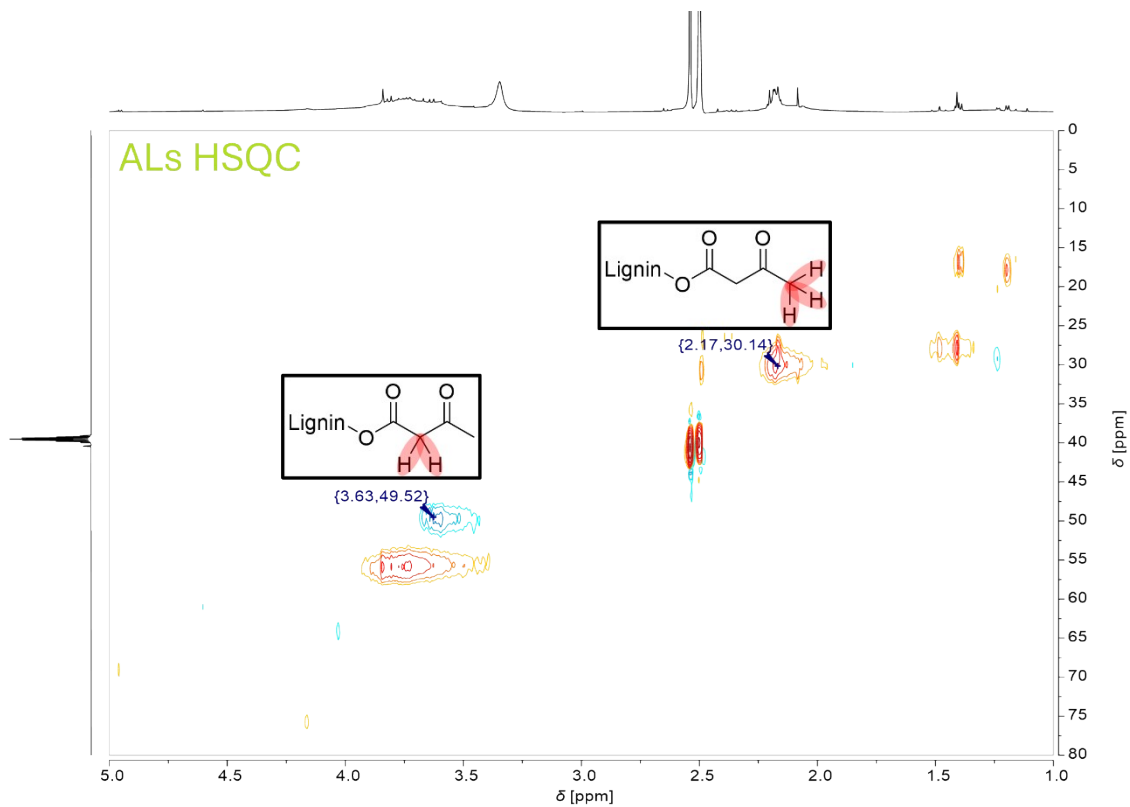


Figure S11: HSQC spectrum of ALs. The  $^1J$  couplings of the terminal methyl group and the  $^1J$  of the methylene group of the acetoacetate functionalities are presented. Measured with an AVIII600 600 MHz spectrometer in  $\text{DMSO-}d_6$ .

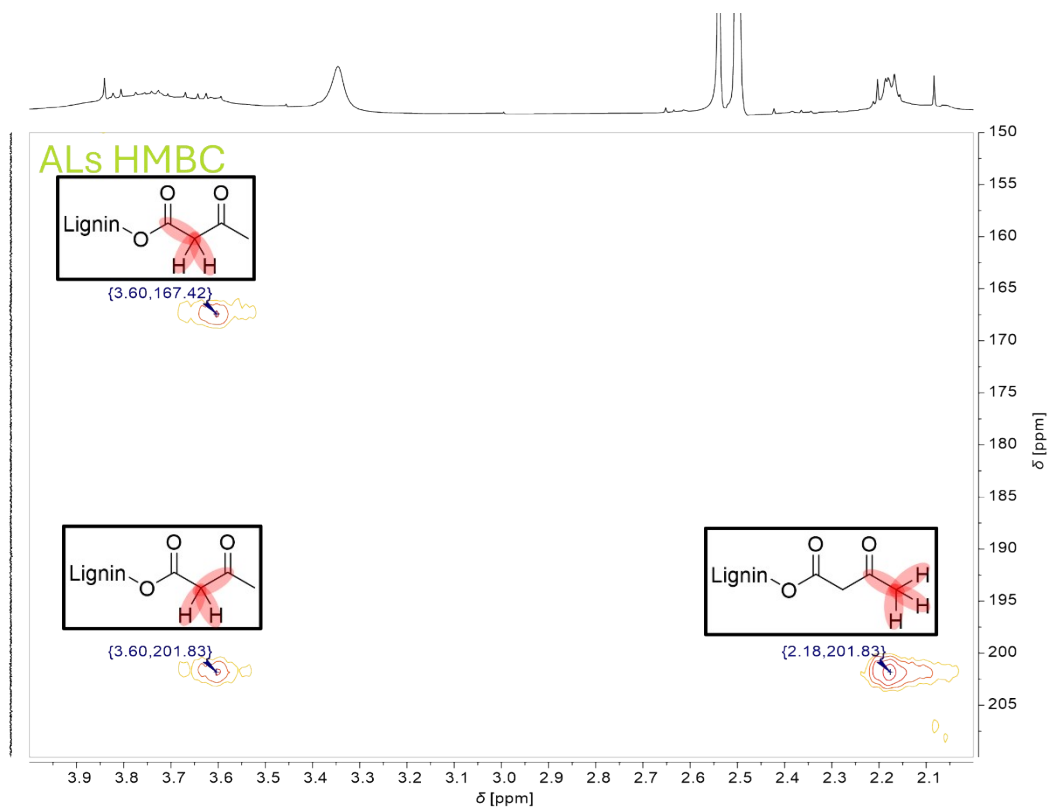


Figure S12: HMBC spectrum of ALs. The respective  $^2J$  couplings of acetoacetate moieties indicated in the structure above respective signals are presented. Measured with an AVIII600 600 MHz spectrometer in  $\text{DMSO-}d_6$ .

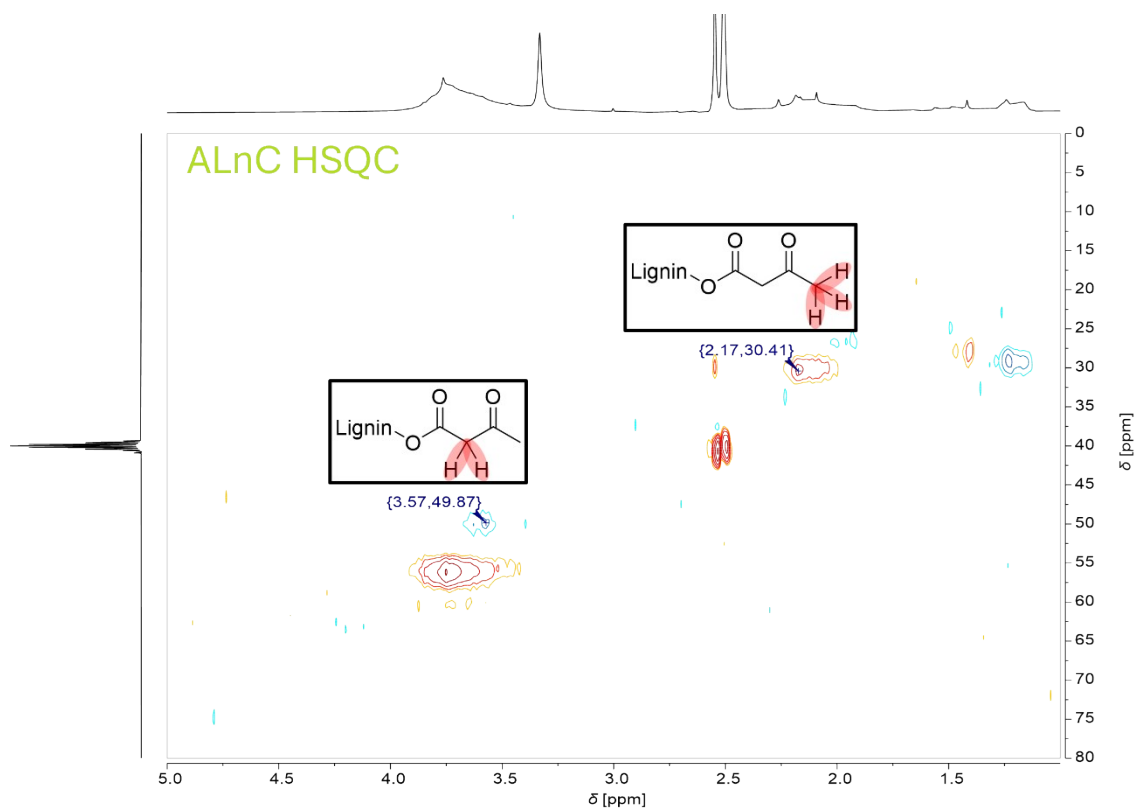


Figure S13: HSQC spectrum of ALnC. The  $^1J$  couplings of the terminal methyl group and the  $^1J$  of the methylene group of the acetoacetate functionalities are presented. Measured with an AVIII 400 MHz NMR spectrometer in DMSO- $d_6$ .

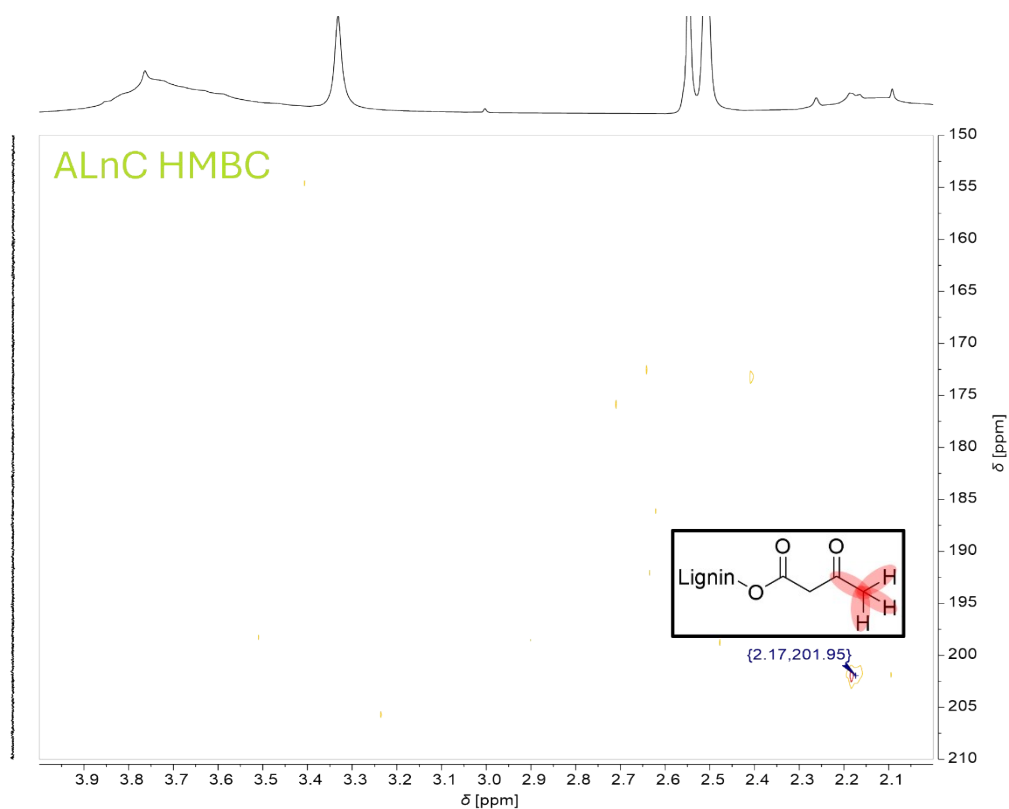


Figure S14: HMBC spectrum of ALnC. The corresponding  $^2J$  coupling of the acetoacetate moieties is indicated in the structure above the respective signal. Measured with an AVIII 400 MHz NMR spectrometer in DMSO- $d_6$ .

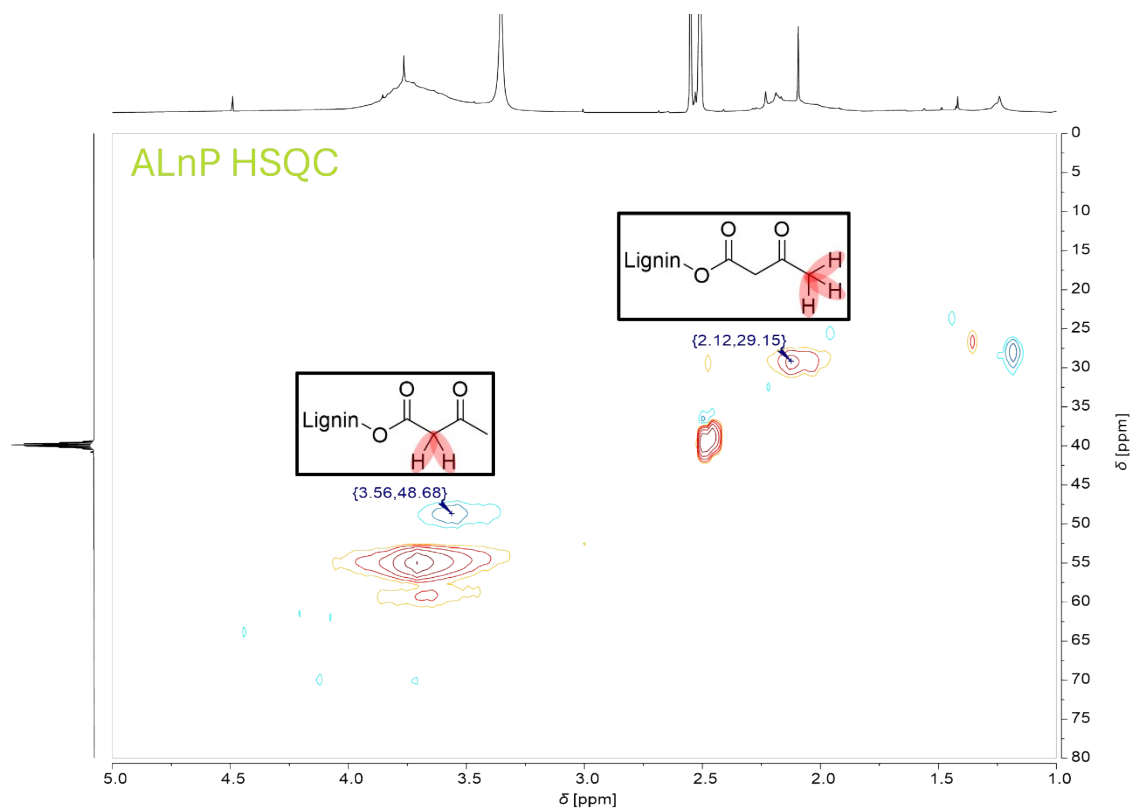


Figure S15: HSQC spectrum of ALnP. The  $^1J$  couplings of the terminal methyl group and the  $^1J$  of the methylene group of the acetoacetate functionalities are presented. Measured with an AV500 NMR spectrometer at 500 MHz in DMSO- $d_6$ .

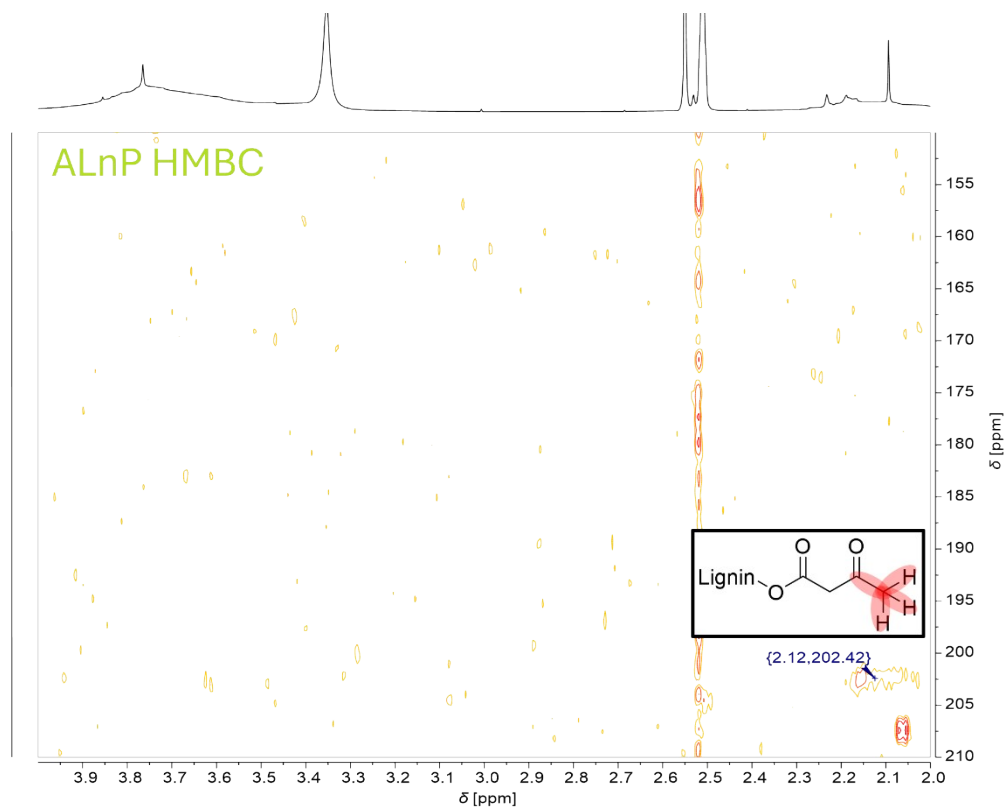


Figure S16: HMBC spectrum of ALnP. The corresponding  $^2J$  coupling of the acetoacetate moieties is indicated in the structure above the respective signal. Measured with an AV500 NMR spectrometer at 500 MHz in DMSO- $d_6$ .

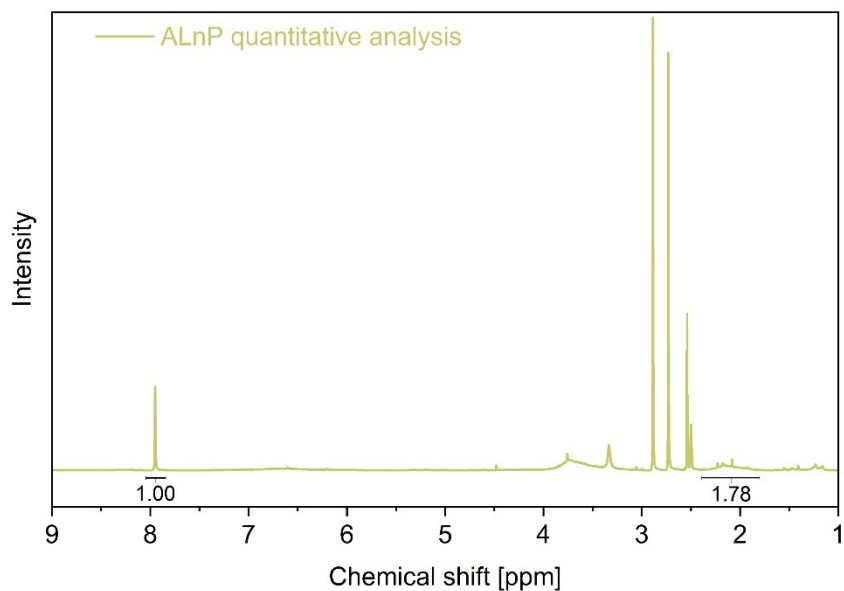


Figure S17: Quantitative determination of the acetoacetate moieties of ALnP by <sup>1</sup>H NMR spectroscopy with DMF as an internal standard in DMSO-*d*<sub>6</sub>. Integrals of the amide proton of DMF (8.5 mg) at 7.95 ppm and the methyl group of acetoacetate moieties of ALnP (30.2 mg) at 2.4 – 1.8 ppm are shown below the respective signal. Calculations result in a content of 2.28 mmol/g of acetoacetate functionalities in ALnP.

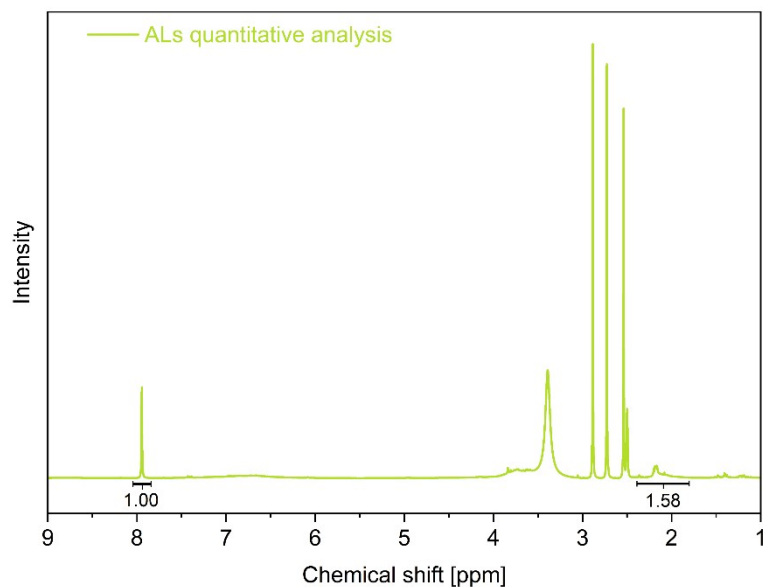


Figure S18: Quantitative determination of the acetoacetate moieties of ALs by  $^1\text{H}$  NMR spectroscopy with DMF as an internal standard in  $\text{DMSO-}d_6$ . Integrals of the amide proton of DMF (6.8 mg) at 7.95 ppm and the methyl group of acetoacetate moieties of ALs (30.1 mg) at 2.4 – 1.8 ppm are shown below the respective signal. Calculations result in a content of 1.63 mmol/g of acetoacetate functionalities in ALs.

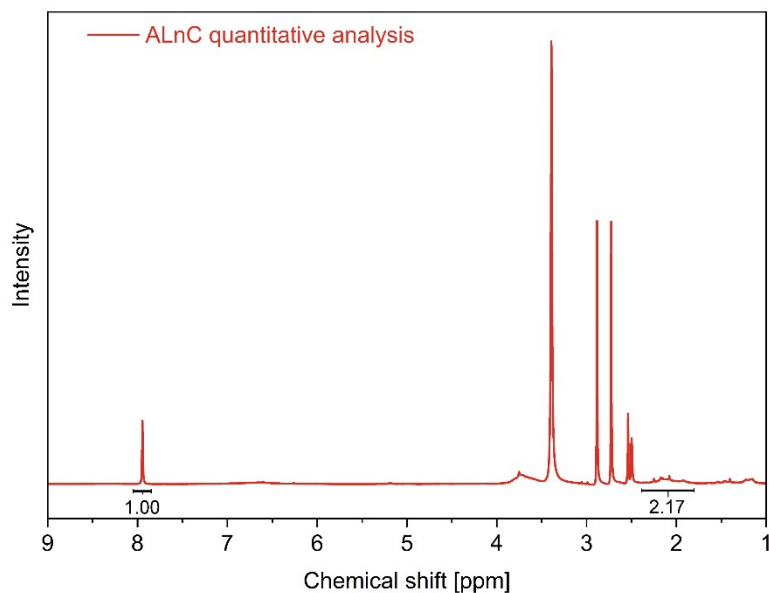


Figure S19: Quantitative determination of the acetoacetate moieties of ALnC by  $^1\text{H}$  NMR spectroscopy with DMF as an internal standard in  $\text{DMSO-}d_6$ . Integrals of the amide proton of DMF (7.4 mg) at 7.95 ppm and the methyl group of acetoacetate moieties of ALnC (28.6 mg) at 2.4 – 1.8 ppm are shown below the respective signal. Calculations result in a content of 2.57 mmol/g of acetoacetate functionalities in ALnC.

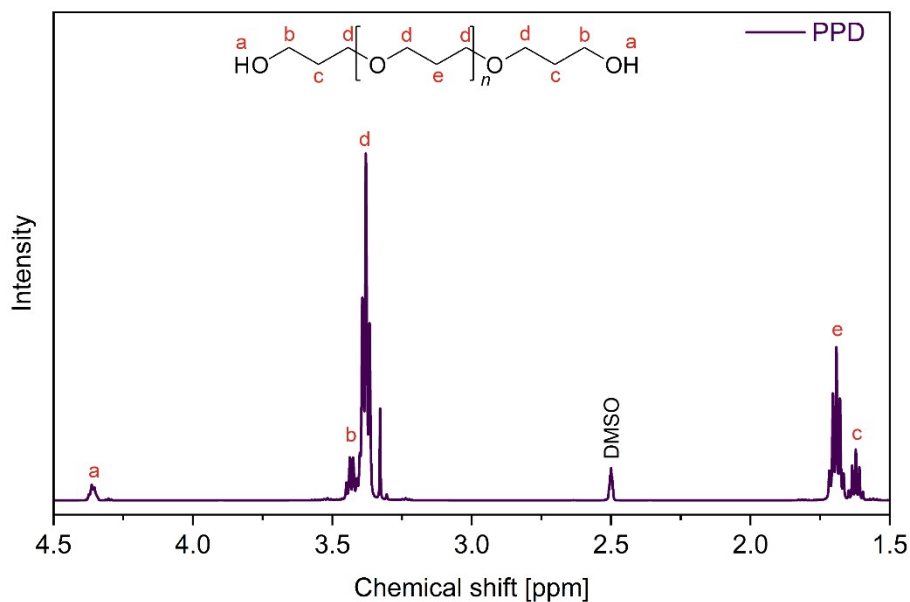


Figure S20: The  $^1\text{H}$  NMR spectrum of Poly(oxy-1,3-propanediyl) displays the characteristic signals and intensities.  $^1\text{H}$  NMR (400 MHz,  $\text{DMSO}-d_6$ , 298 K): 4.36 (2H, m, OH), 3.50 – 3.34 (42H, m, CH<sub>2</sub>), 1.77 – 1.53 (22H, m, CH<sub>2</sub>).

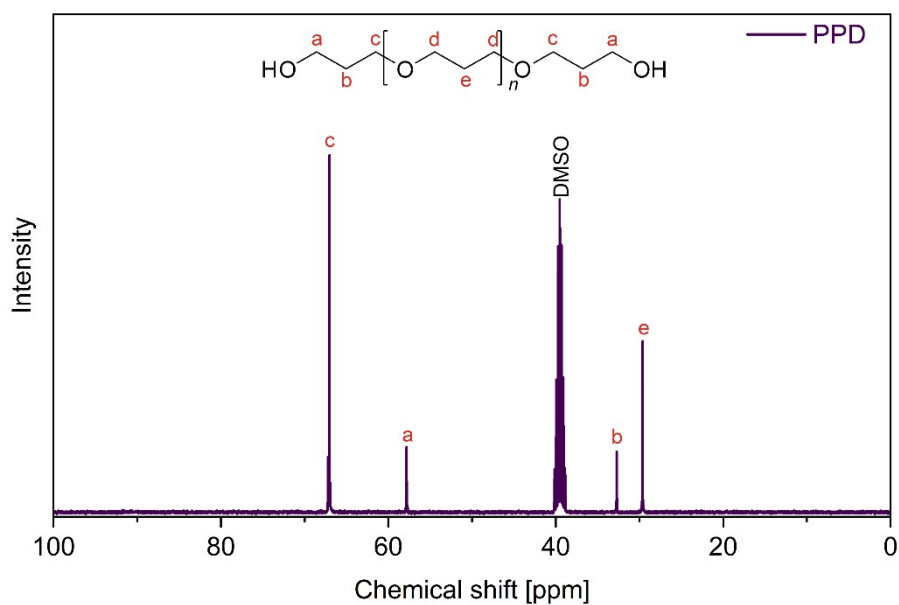


Figure S21: The  $^{13}\text{C}$  NMR spectrum of Poly(oxy-1,3-propanediyl) displays the characteristic signals and intensities.  $^{13}\text{C}$  NMR (100 MHz,  $\text{DMSO}-d_6$ , 298 K): 67.3 – 66.9 (m, CH<sub>2</sub>), 58.0 – 57.6 (m, CH<sub>2</sub>), 32.8 – 32.6 (m, CH<sub>2</sub>), 30.0 – 29.3 (m, CH<sub>2</sub>).

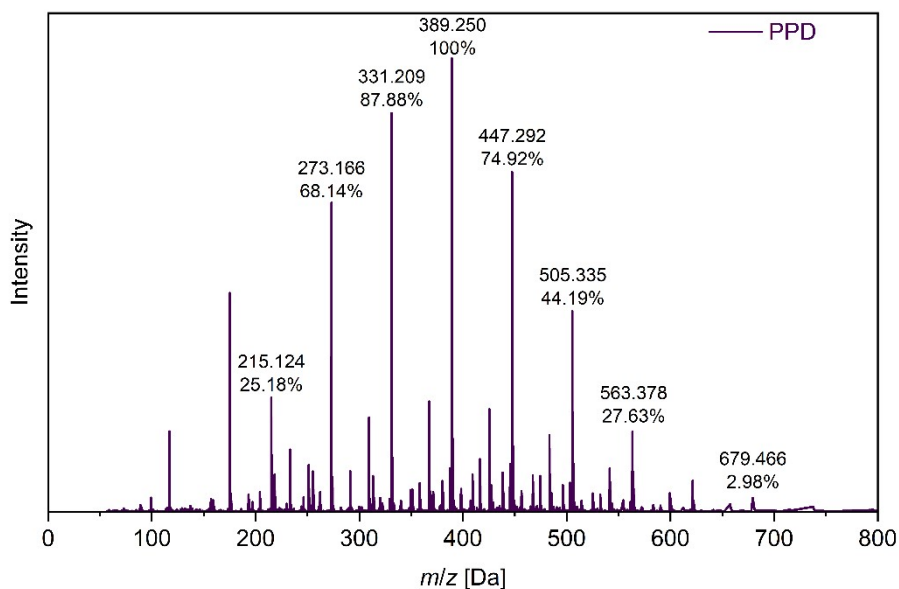


Figure S22: The ESI-MS (+) spectrum displays the characteristic peaks of  $[M+Na]^+$  of Poly(oxy-1,3-propanediyl) with 3, 4, 5, 6, 7, 8, 9, and 11 repeating units ( $m/z$ : 215.124, 273.166, 33.209, 389.250, 447.292, 505.335, 563.378, 679.466, respectively).

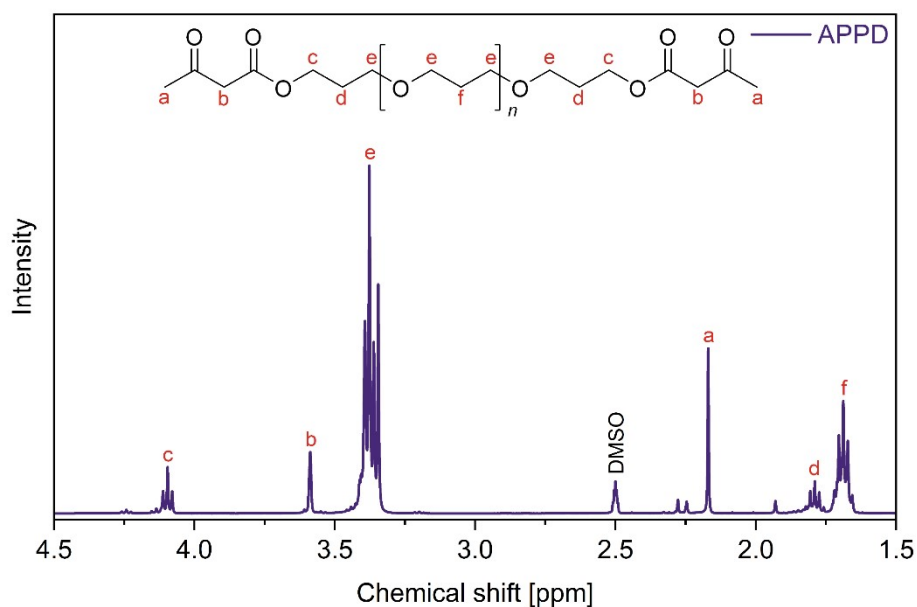


Figure S23: The  $^1H$  NMR spectrum of acetoacetylated Poly(oxy-1,3-propanediyl) displays the characteristic signals and intensities.  $^1H$  NMR (400 MHz,  $DMSO-d_6$ , 298 K): 4.10 (4H, t,  $CH_2$ ), 3.59 (4H, s,  $CH_2$ ), 3.50 – 3.34 (41H, m,  $CH_2$ ), 2.17 (6H, s,  $CH_3$ ), 1.90 – 1.61 (23H, m,  $CH_2$ ).

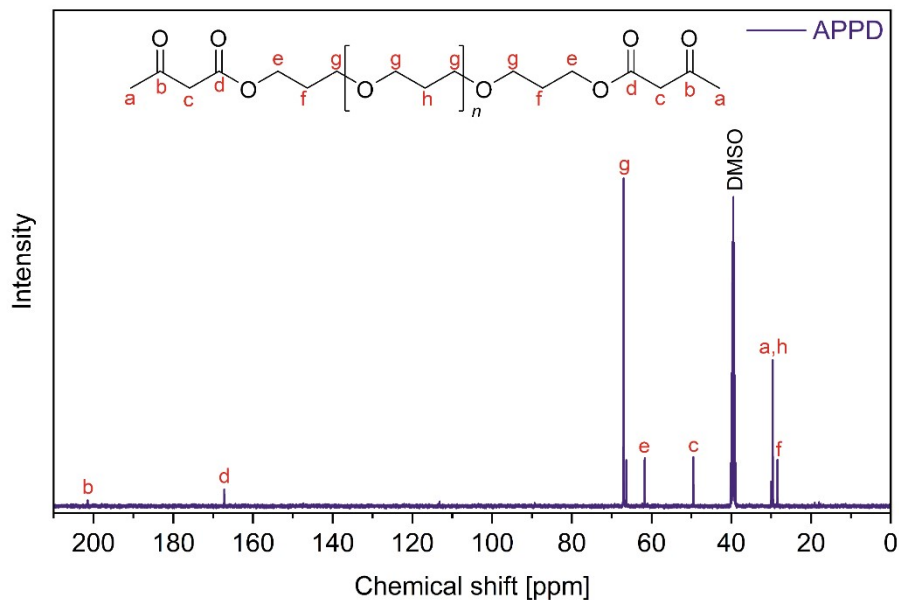


Figure S24: The  $^{13}\text{C}$  NMR spectrum of acetoacetylated Poly(oxy-1,3-propanediyl) displays the characteristic signals and intensities.  $^{13}\text{C}$  NMR (100 MHz,  $\text{DMSO-}d_6$ , 298 K): 201.4 (s,  $\text{C}_{\text{Carbonyl}}$ ), 167.2 (s,  $\text{C}_{\text{Carboxyl}}$ ), 67.2 – 66.7 (m,  $\text{CH}_2$ ), 66.4 (s,  $\text{CH}_2$ ), 61.7 (s,  $\text{CH}_2$ ), 49.5 (s,  $\text{CH}_2$ ), 30.1 – 29.5 (m,  $\text{CH}_3$ ,  $\text{CH}_2$ ), 28.4 (s,  $\text{CH}_2$ ).

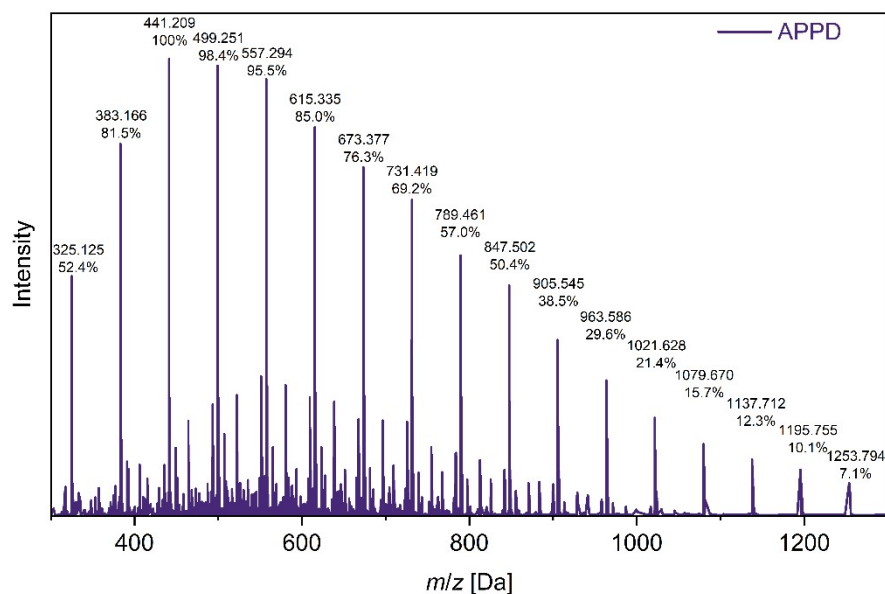


Figure S25: The ESI-MS (+) spectrum showing displays the characteristic peaks of  $[\text{M}+\text{Na}]^+$  of acetoacetylated Poly(oxy-1,3-propanediyl) with 2, 3, 4, 5, 6, 7, 8, 9, 10, 11, 12, 13, 14, 15, 16, 17, and 18 repeating units ( $m/z$ : 325.125, 383.166, 441.209, 499.251, 557.294, 615.335, 673.377, 731.419, 789.461, 847.502, 905.545, 963.586, 1021.628, 1079.670, 1137.712, 1195.755, and 1253.794, respectively).

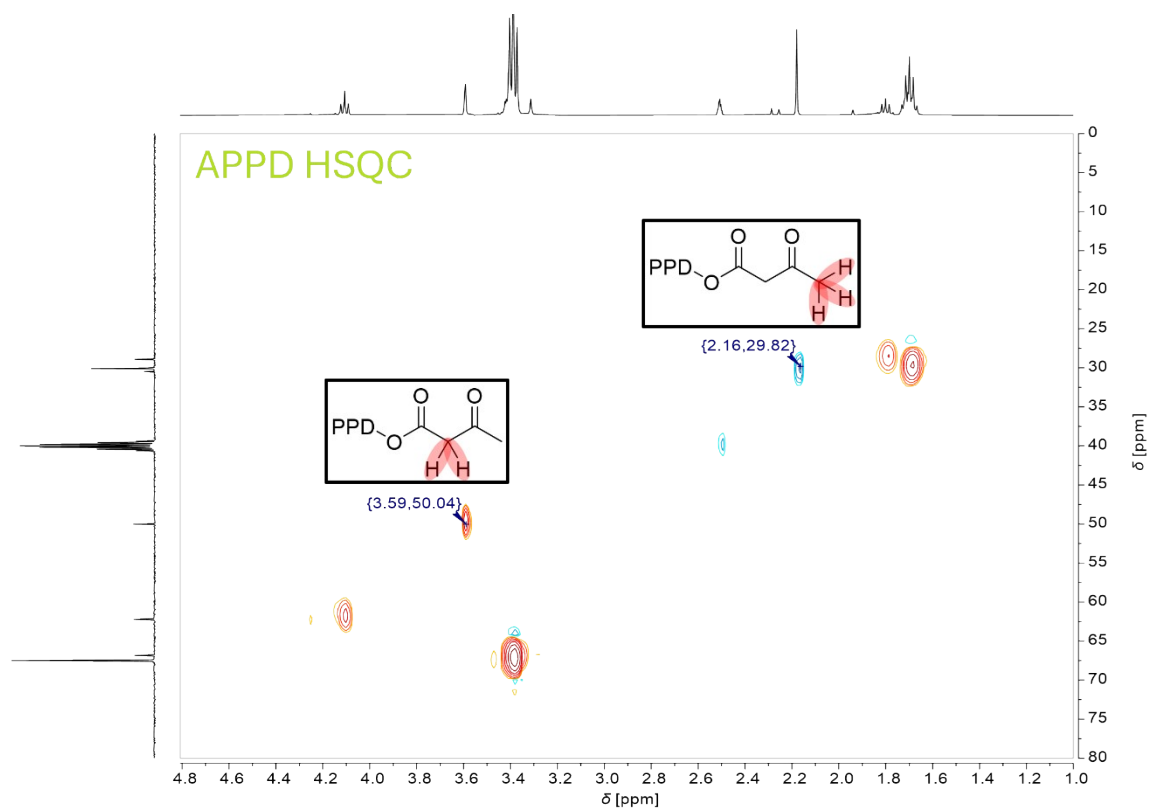


Figure S26: HSQC spectrum of APPD. The  $^1J$  couplings of the terminal methyl group and the  $^1J$  of the methylene group of the acetoacetate functionalities are presented. Measured with an AVIII 400 MHz NMR spectrometer in DMSO- $d_6$ .

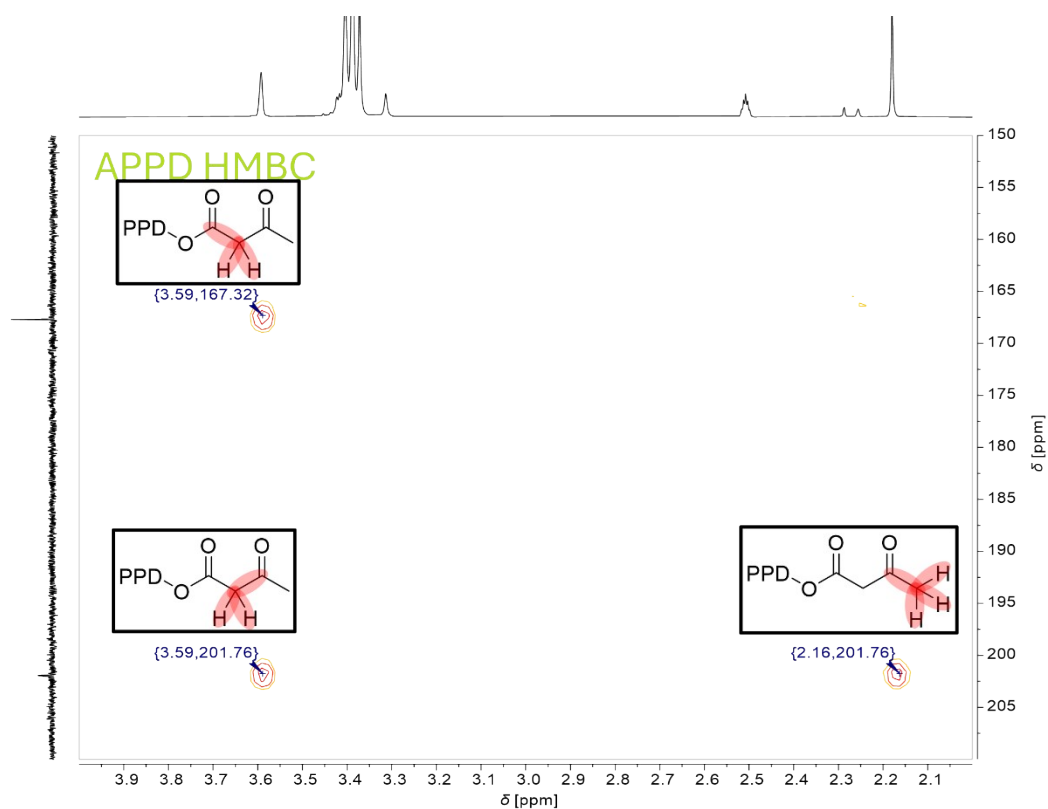


Figure S27: HMBC spectrum of APPD. The corresponding  $^2J$  coupling of the acetoacetate moieties is indicated in the structure above the respective signal. Measured with an AVIII 400 MHz NMR spectrometer in DMSO- $d_6$ .

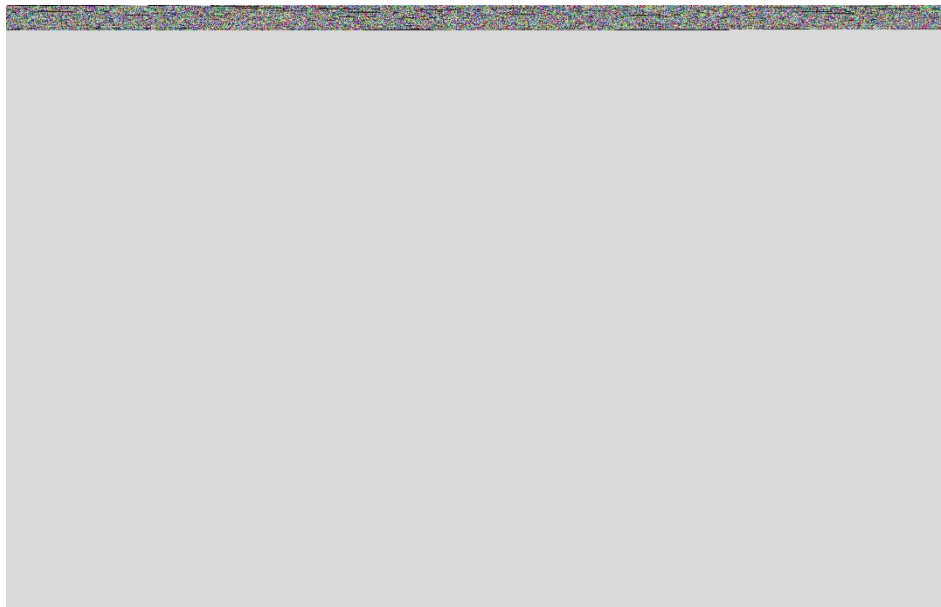


Figure S28: ESI-MS (+) spectrum showing the characteristic peaks of  $[M+Na]^+$  of acetoacetylated Poly(oxy-1,3-propanediyl) with 2, 3, 4, 5, 6, 7, 8, 9, 10, 11, 12, 13, 14, 15, 16, 17, and 18 repeating units ( $m/z$ : 325.125, 383.166, 441.209, 499.251, 557.294, 615.335, 673.377, 731.419, 789.461, 847.502, 905.545, 963.586, 1021.628, 1079.670, 1137.712, 1195.755, and 1253.794 respectively).

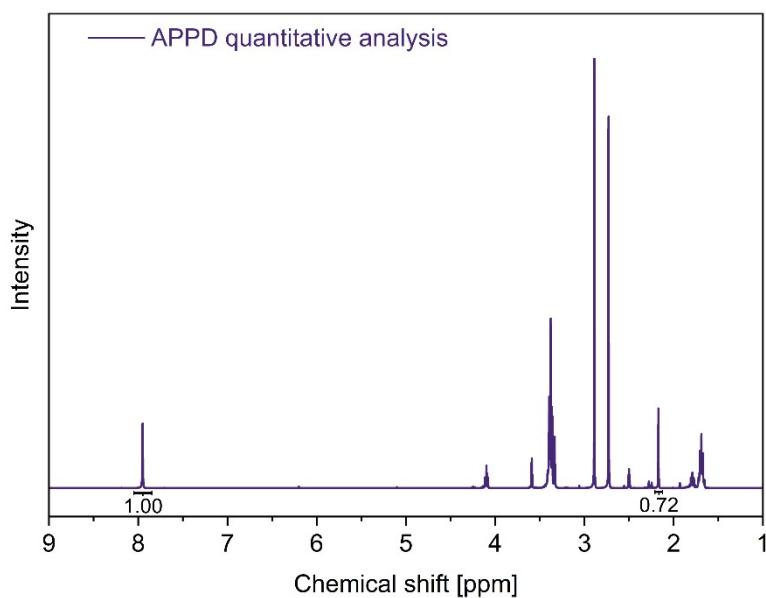


Figure S29: Quantitative determination of the acetoacetate moieties of APPD by <sup>1</sup>H NMR spectroscopy with DMF as an internal standard in DMSO-*d*<sub>6</sub>. Integrals of the amide proton of DMF (19.4 mg) at 7.95 ppm and the methyl group of acetoacetate moieties of APPD (25.5 mg) at 2.17 ppm are shown below the respective signal. Calculations result in a content of 2.49 mmol/g of acetoacetate functionalities in APPD.



Figure S30: Lignosulfonate-based vinyl urethane vitrimer crosslinked with Priamine™ 1073. Weight ratio of lignosulfonate exceeds 55 wt.% and therefore the inhomogeneous sample is too brittle to be processed. Cutting out the samples for tensile testing and DMA only led to the shattering of the film into smaller pieces.

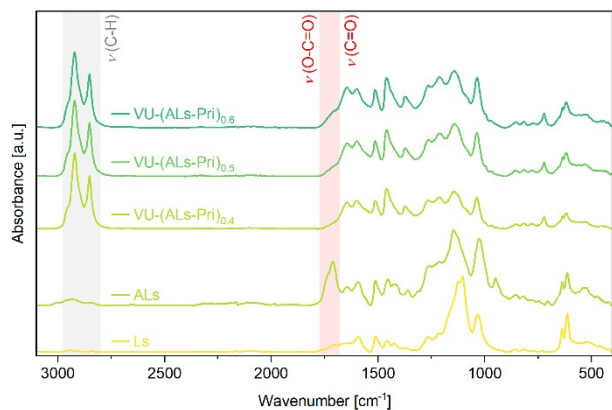


Figure S31: ATR-FT-IR spectra of the lignosulfonate-based (Ls) lignin vitrimers, showing the acetoacetylated ALs with the characteristic acetoacetate bands of the ester ( $1740\text{ cm}^{-1}$ ) and ketone stretching vibrations ( $1711\text{ cm}^{-1}$ ). After the conversion with Priamine™ 1073, the characteristic acetoacetate bands disappear, while the conjugated C=C ( $1593\text{ cm}^{-1}$ ) and C=O ester ( $1644\text{ cm}^{-1}$ ) display the stretching vibration bands of the vinylogous urethanes.

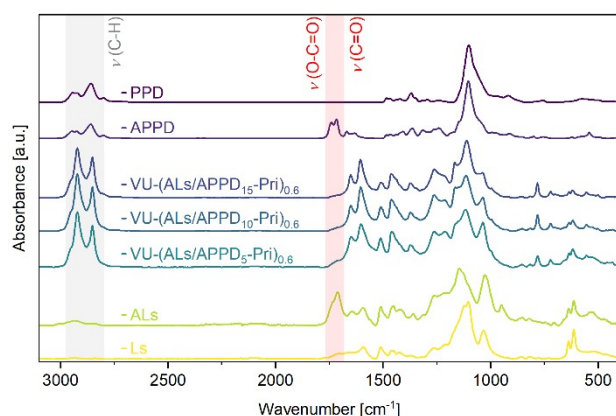


Figure S32: ATR-FT-IR spectra of the lignosulfonate-based (Ls) lignin vitrimers combined with poly(oxypropylene-1,3-diyl) (PPD), showing the acetoacetylated ALs and APPD with the characteristic acetoacetate bands of the ester ( $1740\text{ cm}^{-1}$ ) and ketone stretching vibrations ( $1711\text{ cm}^{-1}$ ). After the conversion with Priamine™ 1073, the characteristic acetoacetate bands disappear, while the conjugated C=C ( $1593\text{ cm}^{-1}$ ) and C=O ester ( $1644\text{ cm}^{-1}$ ) display the stretching vibration bands of the vinylogous urethanes.

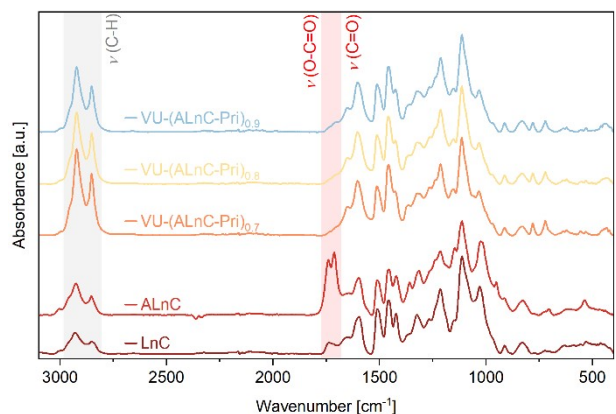


Figure S33: ATR-FT-IR spectra of the Lignova Crude™-based (LnC) lignin vitrimers, showing the acetoacetylated ALnC with the characteristic acetoacetate bands of the ester ( $1740\text{ cm}^{-1}$ ) and ketone stretching vibrations ( $1711\text{ cm}^{-1}$ ). After the conversion with Priamine™ 1073, the characteristic acetoacetate bands disappear, while the conjugated C=C ( $1593\text{ cm}^{-1}$ ) and C=O ester ( $1644\text{ cm}^{-1}$ ) display the stretching vibration bands of the vinylogous urethanes.

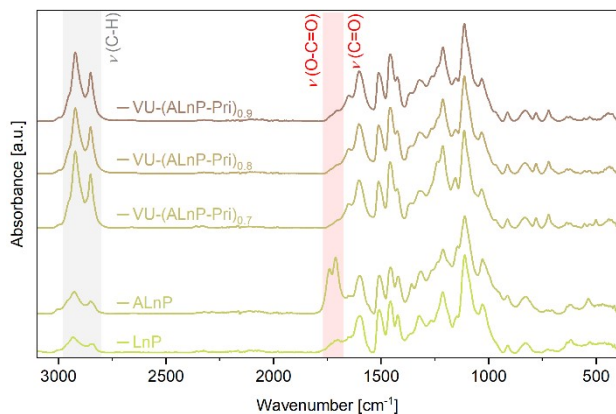


Figure S34: ATR-FT-IR spectra of the Lignova Pure™-based (LnP) lignin vitrimers, showing the acetoacetylated ALnP with the characteristic acetoacetate bands of the ester (1740  $\text{cm}^{-1}$ ) and ketone stretching vibrations (1711  $\text{cm}^{-1}$ ). After the conversion with Priamine™ 1073, the characteristic acetoacetate bands disappear, while the conjugated C=C (1593  $\text{cm}^{-1}$ ) and C=O ester (1644  $\text{cm}^{-1}$ ) display the stretching vibration bands of the vinylogous urethanes.

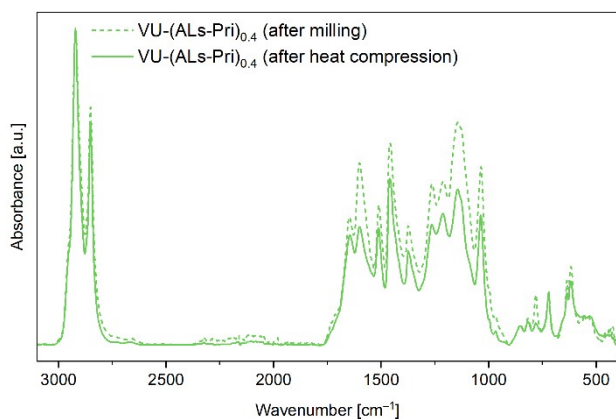


Figure S35: ATR-FT-IR spectra of the lignosulfonate-based lignin vitrimer VU-(ALs-Pri)<sub>0.4</sub> after ball milling and after the film formation by heat compression, showing a similar absorption pattern. The conjugated C=C (1593  $\text{cm}^{-1}$ ) band and the C=O ester (1644  $\text{cm}^{-1}$ ) band display the stretching vibration bands of the vinylogous urethanes.

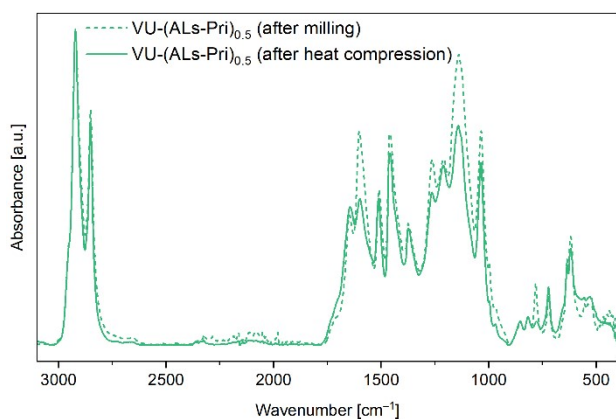


Figure S36: ATR-FT-IR spectra of the lignosulfonate-based lignin vitrimer VU-(ALs-Pri)<sub>0.5</sub> after ball milling and after the film formation by heat compression, showing a similar absorption pattern. The conjugated C=C (1593  $\text{cm}^{-1}$ ) band and the C=O ester (1644  $\text{cm}^{-1}$ ) band display the stretching vibration bands of the vinylogous urethanes.

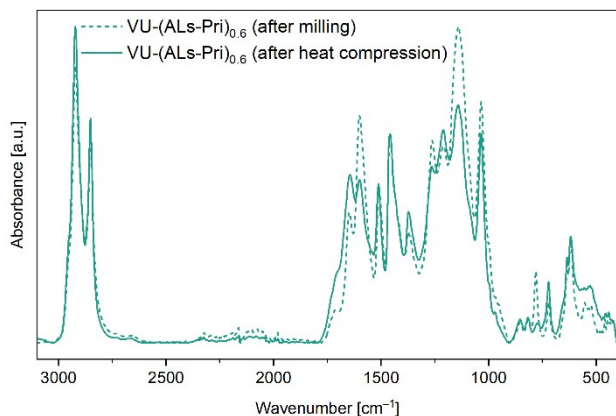


Figure S37: ATR-FT-IR spectra of the lignosulfonate-based lignin vitrimer VU-(ALs-Pri)<sub>0.6</sub> after ball milling and after the film formation by heat compression, showing a similar absorption pattern. The conjugated C=C (1593 cm<sup>-1</sup>) band and the C=O ester (1644 cm<sup>-1</sup>) band display the stretching vibration bands of the vinylogous urethanes.

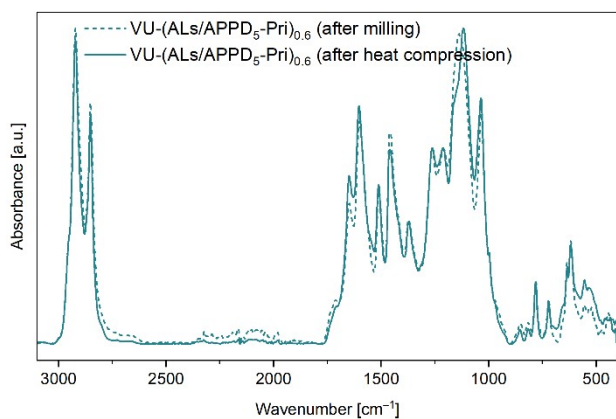


Figure S38: ATR-FT-IR spectra of the lignosulfonate-based lignin vitrimer VU-(ALs/APPD<sub>5</sub>-Pri)<sub>0.6</sub> after ball milling and after the film formation by heat compression, showing a similar absorption pattern. The conjugated C=C (1593 cm<sup>-1</sup>) band and the C=O ester (1644 cm<sup>-1</sup>) band display the stretching vibration bands of the vinylogous urethanes.

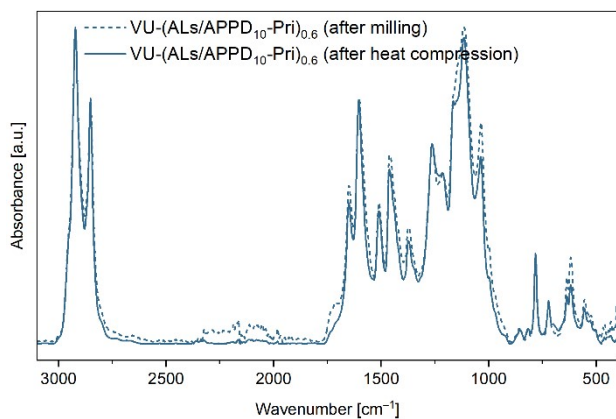


Figure S39: ATR-FT-IR spectra of the lignosulfonate-based lignin vitrimer VU-(ALs/APPD<sub>10</sub>-Pri)<sub>0.6</sub> after ball milling and after the film formation by heat compression, showing a similar absorption pattern. The conjugated C=C (1593 cm<sup>-1</sup>) band and the C=O ester (1644 cm<sup>-1</sup>) band display the stretching vibration bands of the vinylogous urethanes.

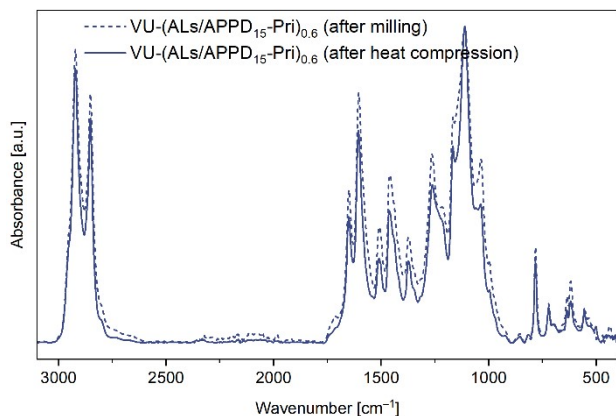


Figure S40: ATR-FT-IR spectra of the lignin vitrimer VU-(ALs/APPD<sub>15</sub>-Pri)<sub>0.6</sub> after ball milling and after the film formation by heat compression, showing a similar absorption pattern. The conjugated C=C (1593 cm<sup>-1</sup>) band and the C=O ester (1644 cm<sup>-1</sup>) band display the stretching vibration bands of the vinylogous urethanes.

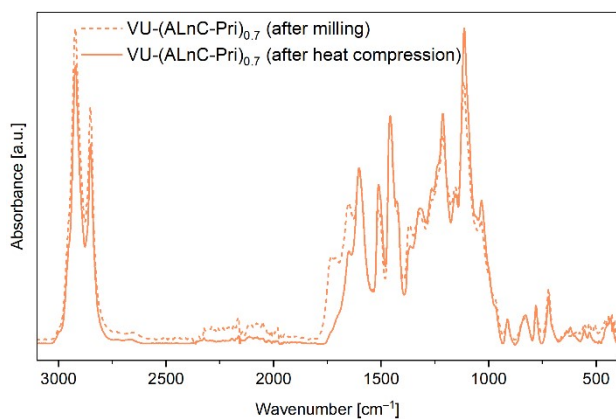


Figure S41: ATR-FT-IR spectra of the enzymatic-based lignin vitrimer VU-(ALnC-Pri)<sub>0.7</sub> after ball milling and after the film formation by heat compression. After the heat compression, the characteristic acetoacetate bands disappear completely, while the conjugated C=C (1593 cm<sup>-1</sup>) and C=O ester (1644 cm<sup>-1</sup>) display the stretching vibration bands of the vinylogous urethanes.

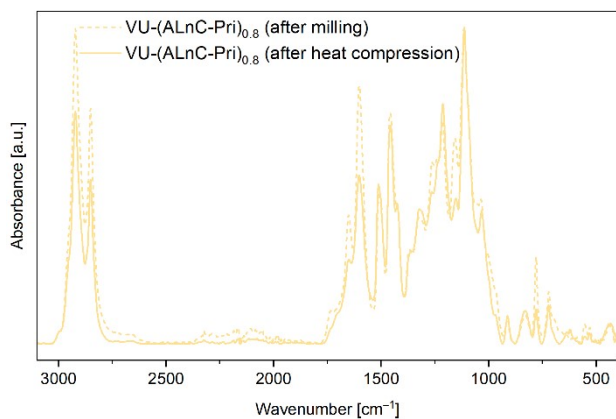


Figure S42: ATR-FT-IR spectra of the enzymatic-based lignin vitrimer VU-(ALnC-Pri)<sub>0.8</sub> after ball milling and after the film formation by heat compression. After the heat compression, the characteristic acetoacetate bands disappear completely, while the conjugated C=C (1593 cm<sup>-1</sup>) and C=O ester (1644 cm<sup>-1</sup>) display the stretching vibration bands of the vinylogous urethanes.

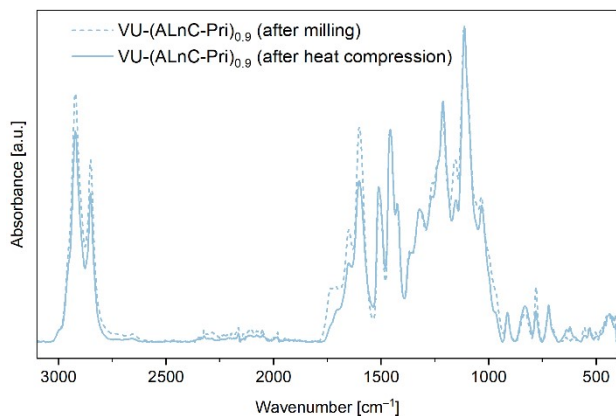


Figure S43: ATR-FT-IR spectra of the enzymatic-based lignin vitrimer VU-(ALnC-Pri)<sub>0.9</sub> after ball milling and after the film formation by heat compression. After the heat compression, the characteristic acetoacetate bands disappear completely, while the conjugated C=C (1593 cm<sup>-1</sup>) and C=O ester (1644 cm<sup>-1</sup>) display the stretching vibration bands of the vinylogous urethanes.

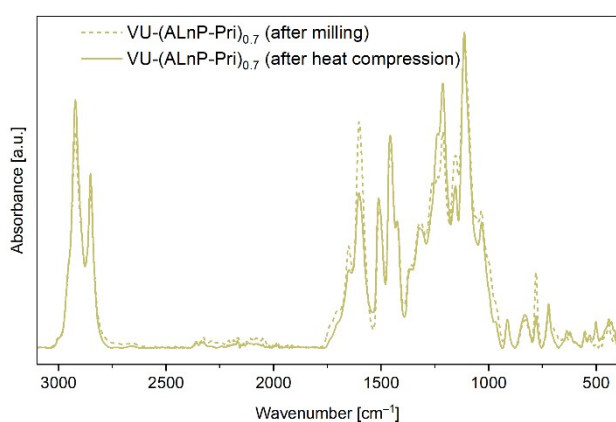


Figure S44: ATR-FT-IR spectra of the enzymatic-based lignin vitrimer VU-(ALnP-Pri)<sub>0.7</sub> after ball milling and after the film formation by heat compression, showing a similar absorption pattern. The conjugated C=C (1593 cm<sup>-1</sup>) band and the C=O ester (1644 cm<sup>-1</sup>) band display the stretching vibration bands of the vinylogous urethanes.

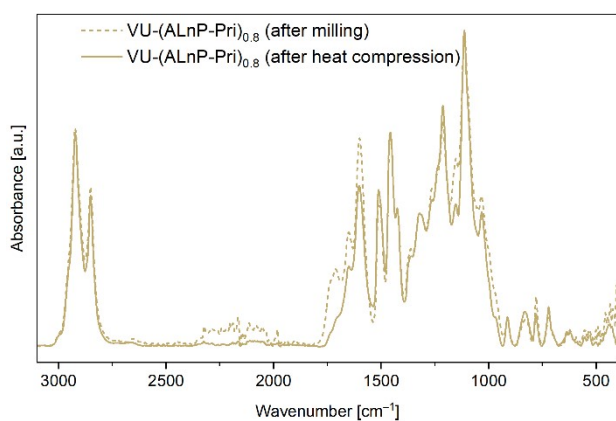


Figure S45: ATR-FT-IR spectra of the enzymatic-based lignin vitrimer VU-(ALnP-Pri)<sub>0.8</sub> after ball milling and after the film formation by heat compression. After the heat compression, the characteristic acetoacetate bands disappear completely, while the conjugated C=C (1593 cm<sup>-1</sup>) and C=O ester (1644 cm<sup>-1</sup>) display the stretching vibration bands of the vinylogous urethanes.

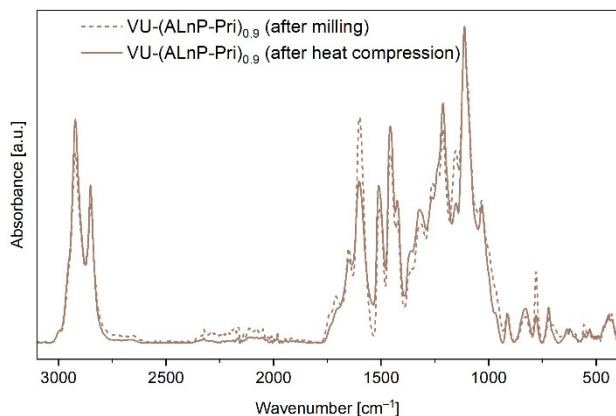


Figure S46: ATR-FT-IR spectra of the enzymatic-based lignin vitrimer VU-(ALnP-Pri)<sub>0.9</sub> after ball milling and after the film formation by heat compression. After the heat compression, the characteristic acetoacetate bands disappear completely, while the conjugated C=C (1593 cm<sup>-1</sup>) and C=O ester (1644 cm<sup>-1</sup>) display the stretching vibration bands of the vinylogous urethanes.

### Equation S2

$$S = \frac{m_1 - m_0}{m_0} \cdot 100$$

- S** : Swelling ratio [%]  
**m<sub>0</sub>** : Weight of the sample before swelling [g]  
**m<sub>1</sub>** : Weight of the sample after swelling [g]

### Equation S3

$$SF = \frac{m_0 - m_2}{m_0} \cdot 100$$

- SF** : Soluble fraction [%]  
**m<sub>0</sub>** : Weight of the sample before swelling [g]  
**m<sub>2</sub>** : Weight of the sample after drying [g]

Table S2: Results of the swelling tests performed by addition of 1 mL of solvent (deionized water, acetone) to approximately 50 mg (*m*<sub>0</sub>) of the respective sample. The vials were subsequently sealed and stored for 24 h at 25 °C. Afterwards, the supernatant was decanted, and the sample was weighed (*m*<sub>1</sub>) and stored at 80 °C under vacuum for at least 24 h until a constant mass was measured (*m*<sub>2</sub>). The swelling ratio was calculated via (*m*<sub>1</sub>-*m*<sub>0</sub>)/*m*<sub>0</sub>; the soluble fraction was calculated via (*m*<sub>0</sub>-*m*<sub>2</sub>)/*m*<sub>0</sub>.

Sample	H <sub>2</sub> O		Acetone	
	S [wt.%]	SF [wt.%]	S [wt.%]	SF [wt.%]
VU-(ALs-Pri) <sub>0.4</sub>	15	1.6	24	3.7
VU-(ALs-Pri) <sub>0.5</sub>	19	2.7	25	1.8
VU-(ALs-Pri) <sub>0.6</sub>	28	2.8	30	4.7
VU-(ALs/APPD <sub>5</sub> -Pri) <sub>0.6</sub>	39	4.4	29	5.9
VU-(ALs/APPD <sub>10</sub> -Pri) <sub>0.6</sub>	24	2.8	30	5.9
VU-(ALs/APPD <sub>15</sub> -Pri) <sub>0.6</sub>	25	1.9	34	9.0
VU-(ALnC-Pri) <sub>0.7</sub>	2.5	0.3	31	6.3
VU-(ALnC-Pri) <sub>0.8</sub>	5.1	0	30	7.2
VU-(ALnC-Pri) <sub>0.9</sub>	1.6	0.2	34	7.0
VU-(ALnP-Pri) <sub>0.7</sub>	3.6	0	41	6.1
VU-(ALnP-Pri) <sub>0.8</sub>	2.4	0	36	9.6
VU-(ALnP-Pri) <sub>0.9</sub>	3.1	0	34	12

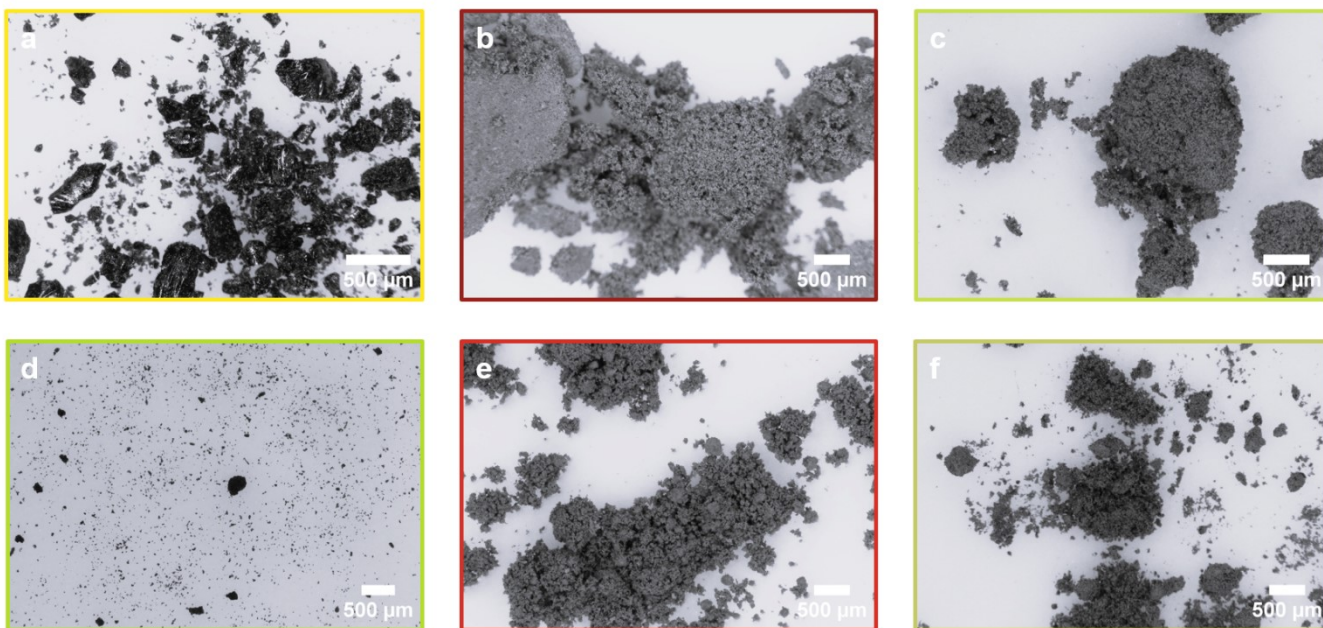


Figure S47: OM images of the different lignin sources Ls (a), LnC (b), and LnP (c), and the acetoacetylated lignin sources ALs (d), ALnC (e), and ALnP (f), showing similar powders with granules and agglomerates in all images.

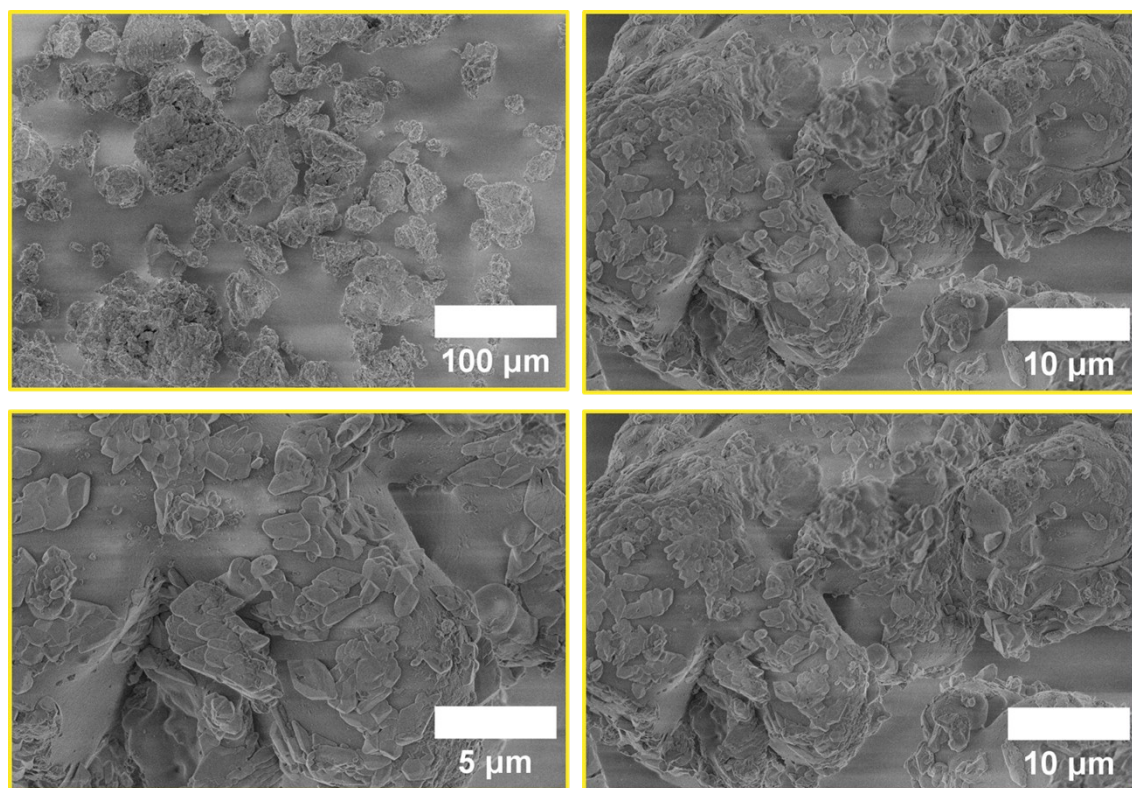


Figure S48: SEM images of the raw lignosulfonate Ls with different magnifications.

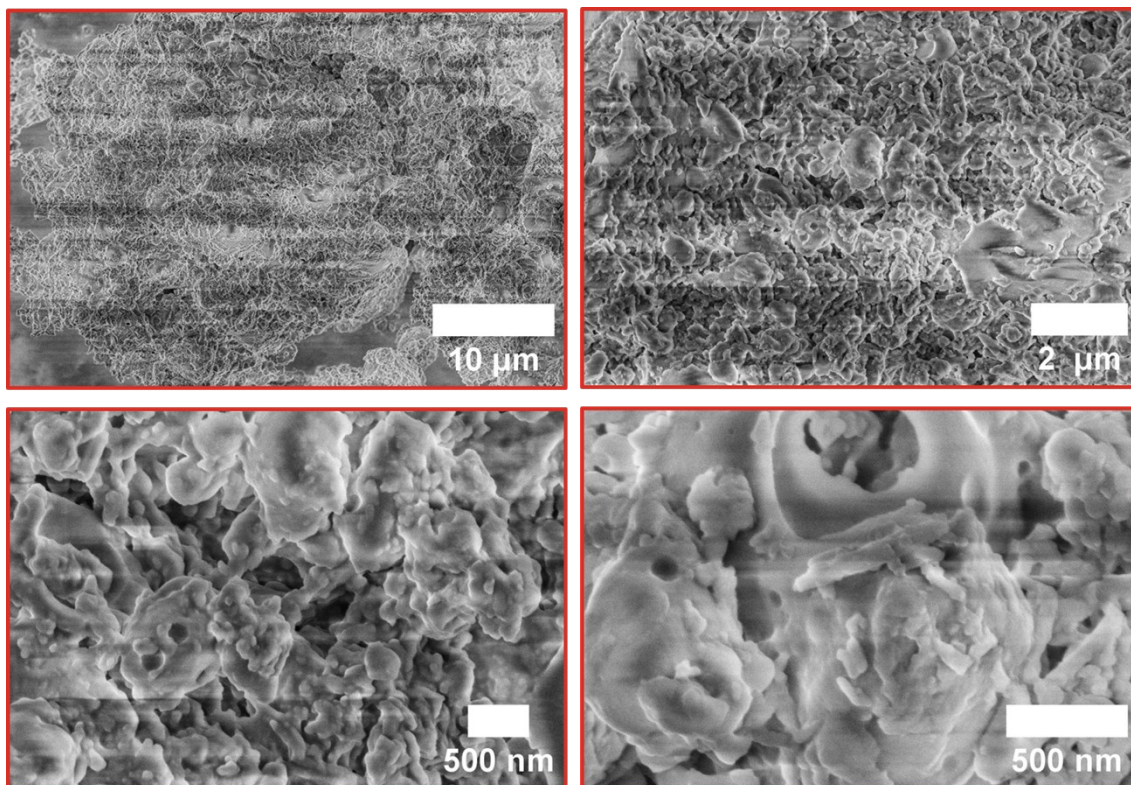


Figure S49: SEM images of the raw enzymatic LnC with different magnifications.

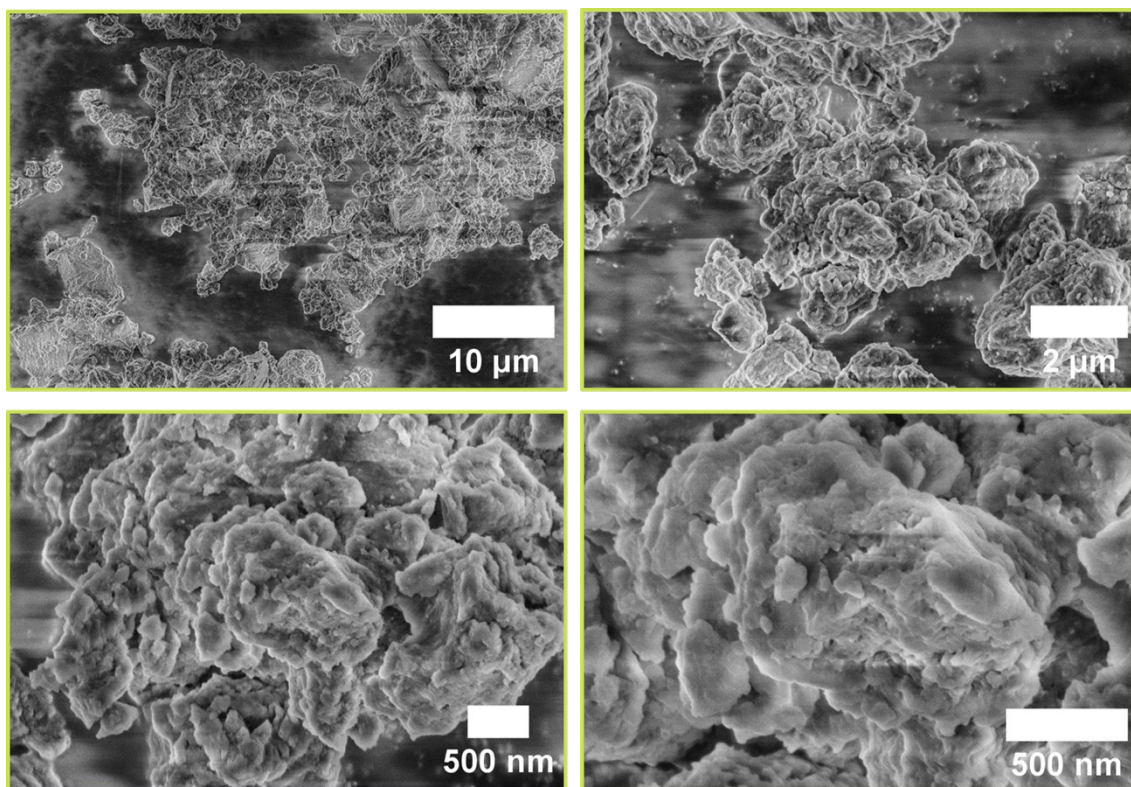


Figure S50: SEM images of the raw enzymatic LnP with different magnifications.

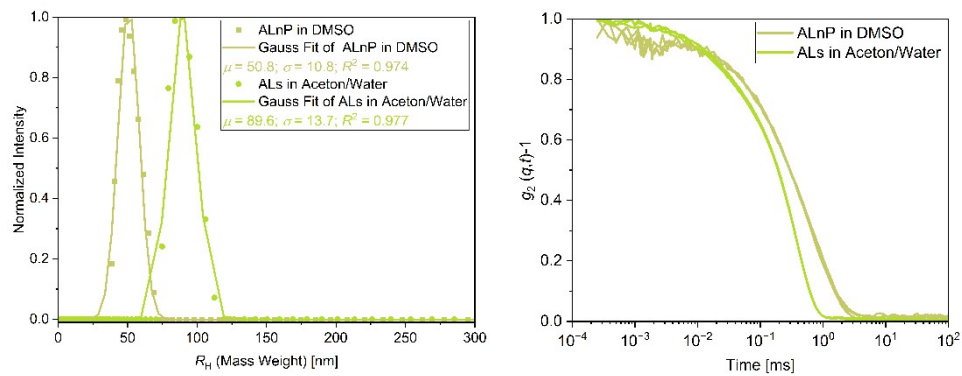


Figure S51: DLS measurements of ALs and ALnP. Shown are the distributions of the hydrodynamic radii of the particles (left) and the correlation curves of respective samples (right). A Gaussian fit was used to determine the expected value and standard deviation of the distributions. Measured at a temperature of 30 °C and an angle of 90°.

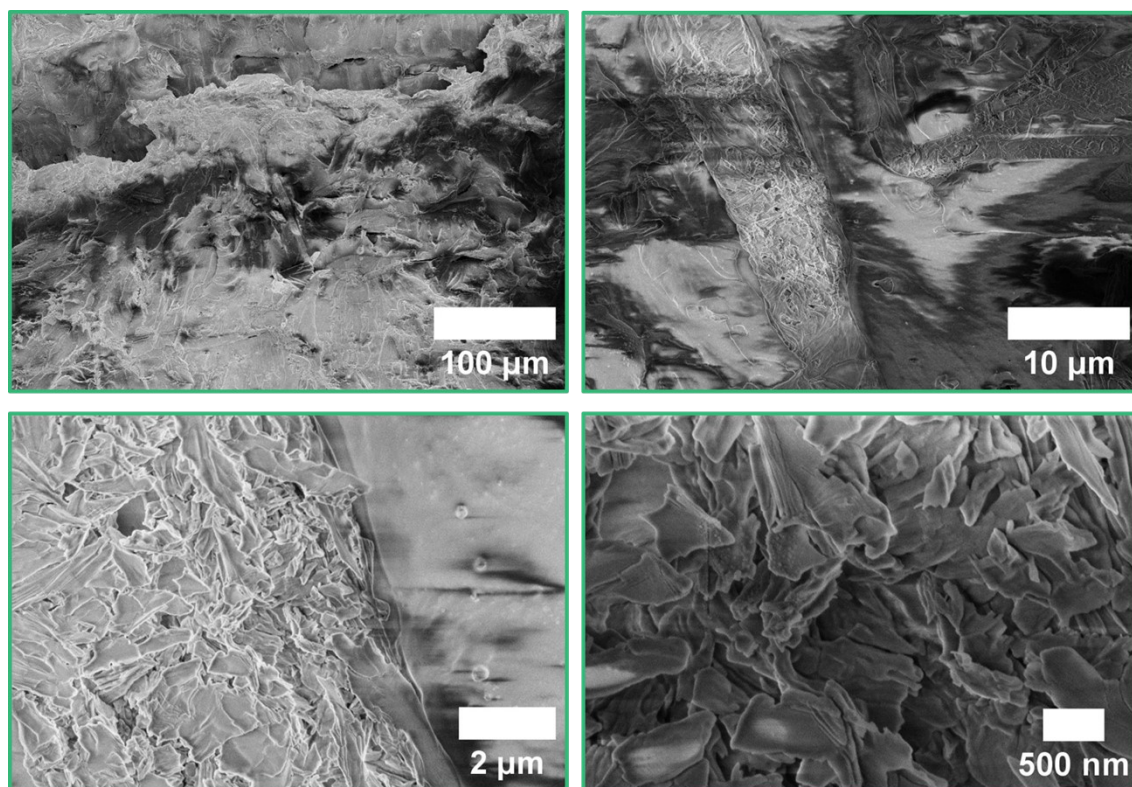


Figure S52: SEM images of VU-(Als-Pri)<sub>0.5</sub> with different magnifications.

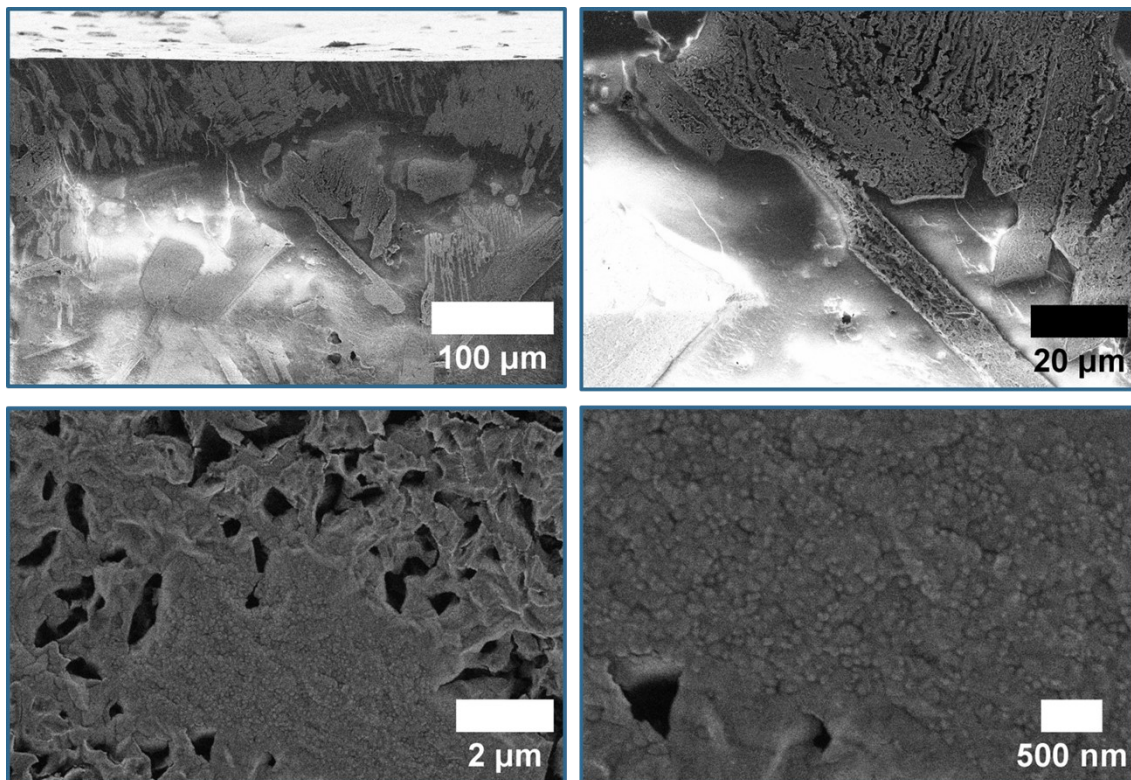
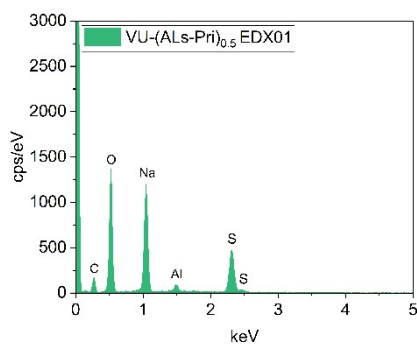
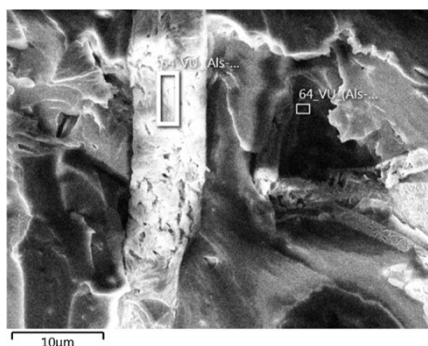


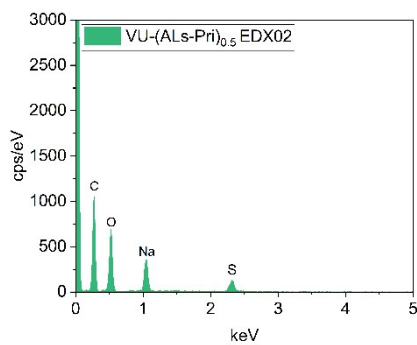
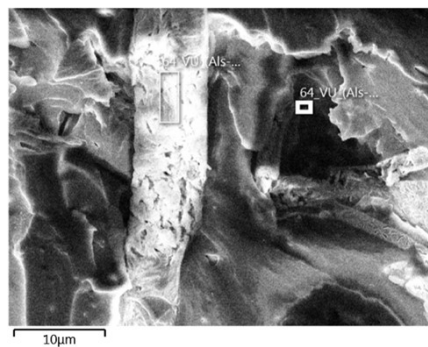
Figure S53: SEM images of VU-(AlS/APPD<sub>10</sub>-Pri)<sub>0.6</sub> with different magnifications.

Table S3: EDX-measurements of VU-(AlS-Pri)<sub>0.5</sub>, showing the irradiated area (left), the EDX spectra (middle) and a table with the relative intensity of respective elements in % (right).

### VU-(AlS-Pri)<sub>0.5</sub>



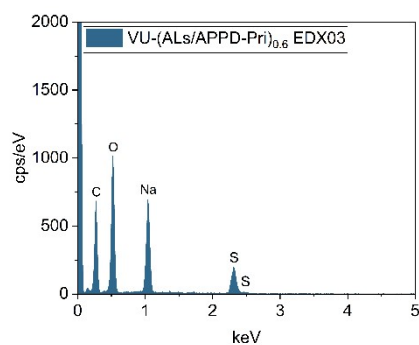
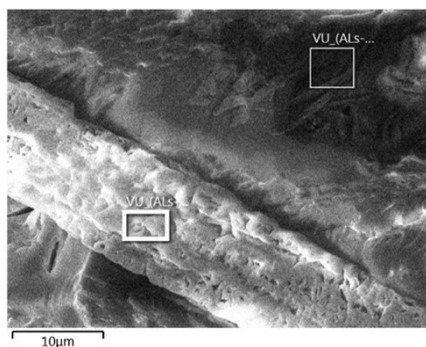
Element	Atom%
C	25.44
N	-
O	42.32
Na	19.84
Al	1.25
S	11.15



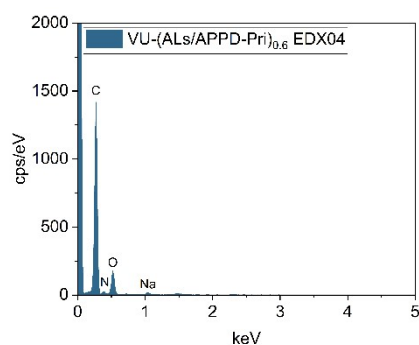
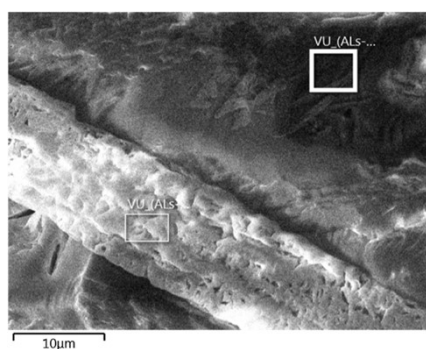
Element	Atom%
C	67.10
N	-
O	24.99
Na	5.47
Al	-
S	2.45

Table S4: EDX-measurements of VU-(ALs/APPD<sub>10</sub>-Pri)<sub>0.6</sub>, showing the irradiated area (left), the EDX spectra (middle) and a table with the relative intensity of respective elements in % (right).

**VU-(ALs/APPD<sub>10</sub>-Pri)<sub>0.6</sub>**



Element	Atom%
C	53.73
N	-
O	31.90
Na	10.35
Al	-
S	4.03



Element	Atom%
C	76.58
N	8.56
O	14.49
Na	0.37
Al	-
S	-

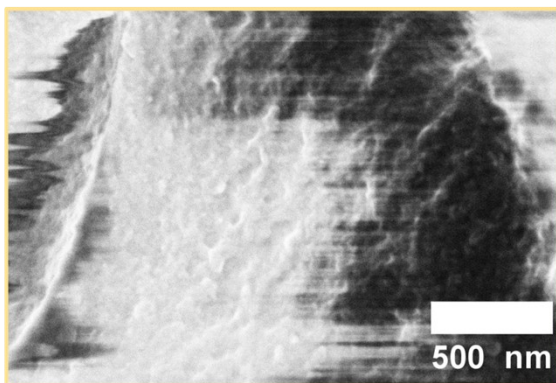
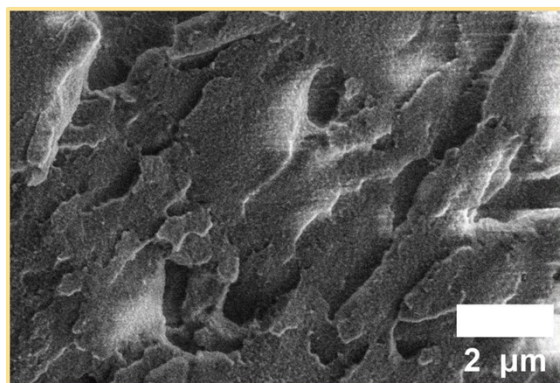
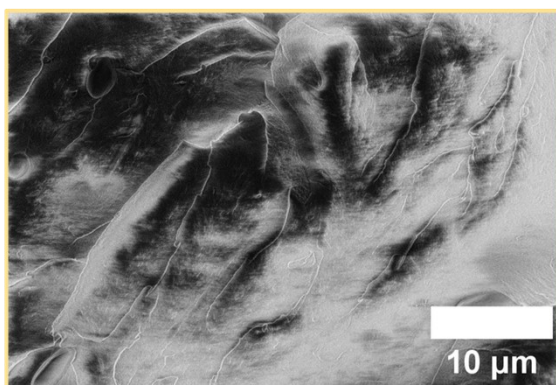
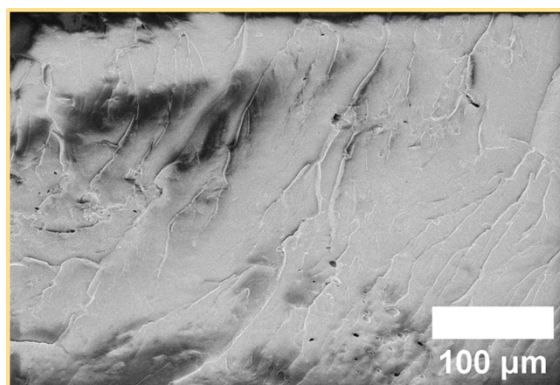


Figure S54: SEM images of VU-(AlnC-Pri)<sub>0.8</sub> with different magnifications.

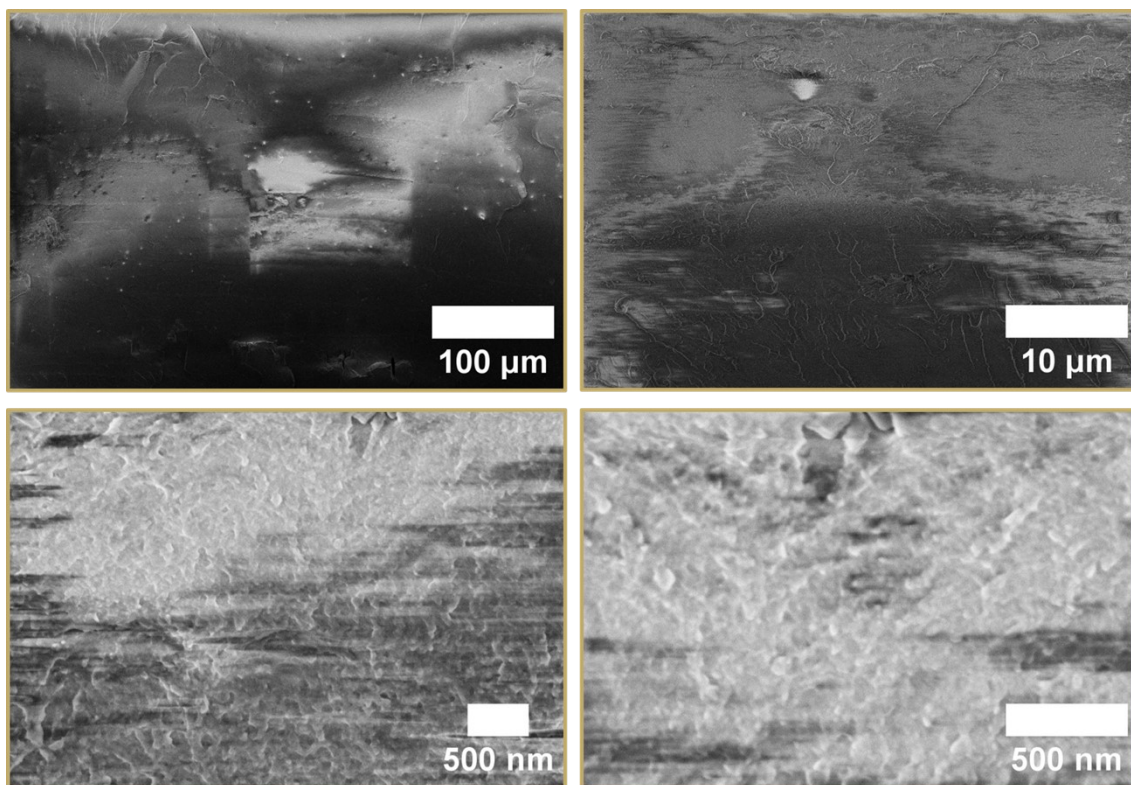
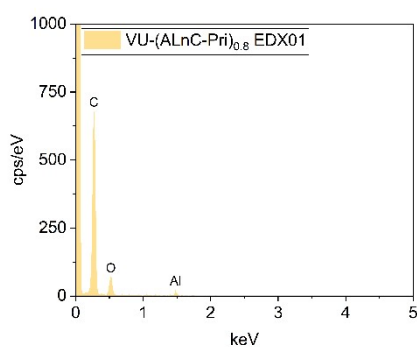
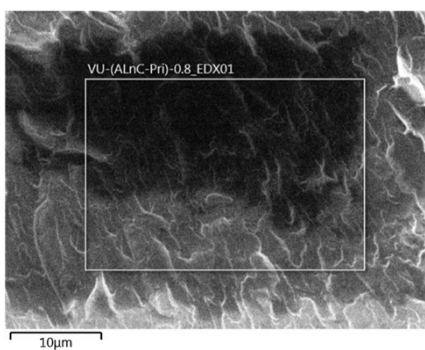


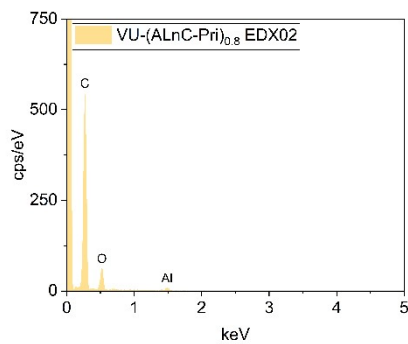
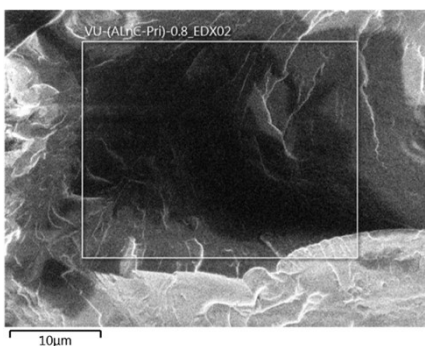
Figure S55: SEM images of VU-(AlnP-Pri)<sub>0.8</sub> with different magnifications.

Table S5: EDX-measurements of VU-(AlnC-Pri)<sub>0.8</sub>, showing the irradiated area (left), the EDX spectra (middle) and a table with the relative intensity of respective elements in % (right).

**VU-(AlnC-Pri)<sub>0.8</sub>**



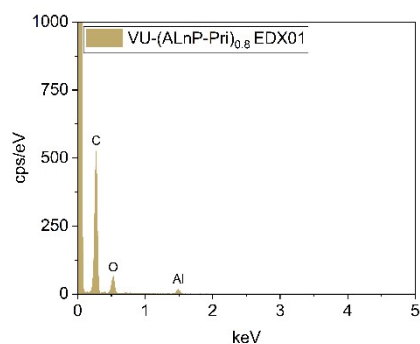
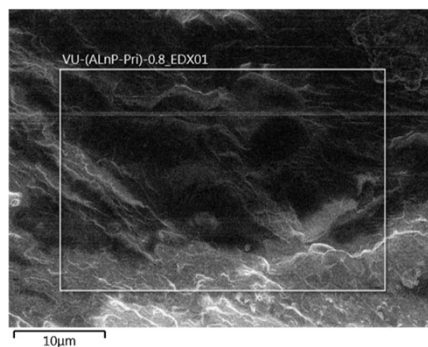
Element	Atom%
C	86.06
N	-
O	13.22
Na	-
Al	0.72
S	-



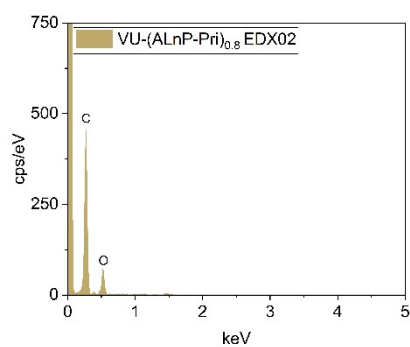
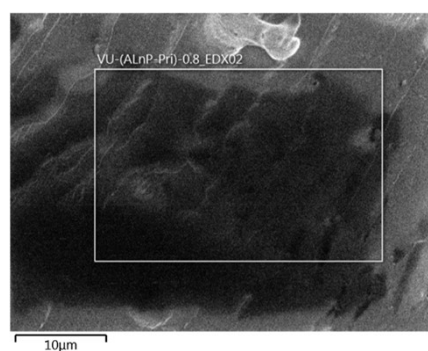
Element	Atom%
C	84.69
N	-
O	14.72
Na	-
Al	0.60
S	-

Table S6: EDX-measurements of VU-(ALnP-Pri)<sub>0.8</sub>, showing the irradiated area (left), the EDX spectra (middle) and a table with the relative intensity of respective elements in % (right).

### VU-(ALnP-Pri)<sub>0.8</sub>



Element	Atom%
C	84.69
N	-
O	14.17
Na	-
Al	1.14
S	-



Element	Atom%
C	80.86
N	-
O	19.14
Na	-
Al	-
S	-

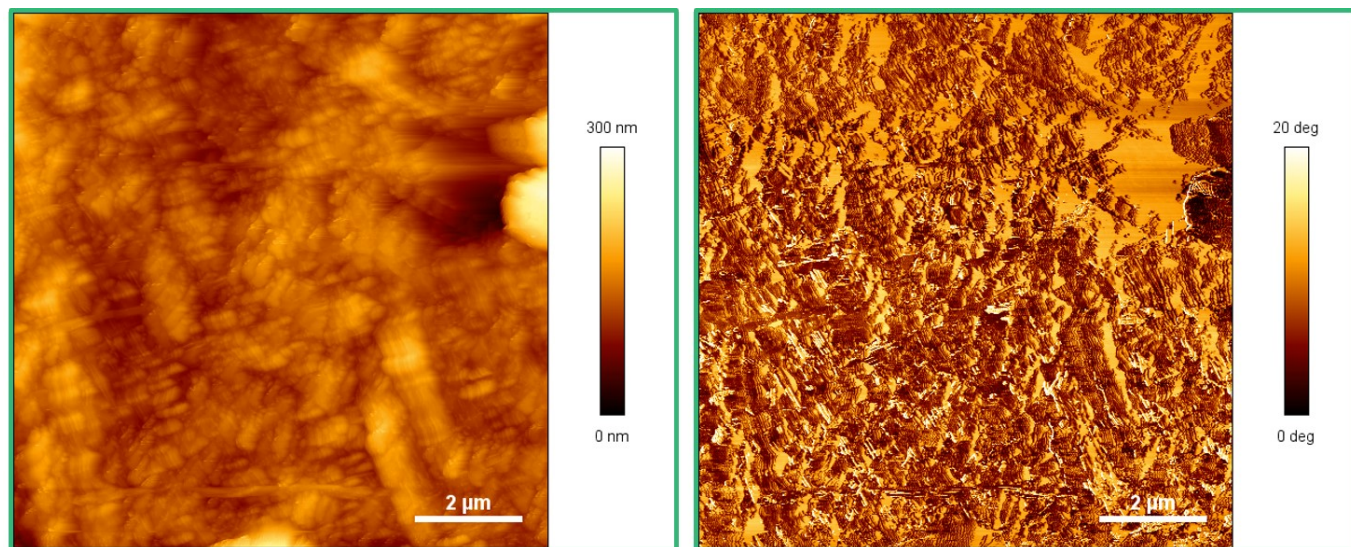


Figure S56: AFM image of VU-(ALS-Pri)<sub>0.5</sub> showing the height plot (left) and the phase plot (right).

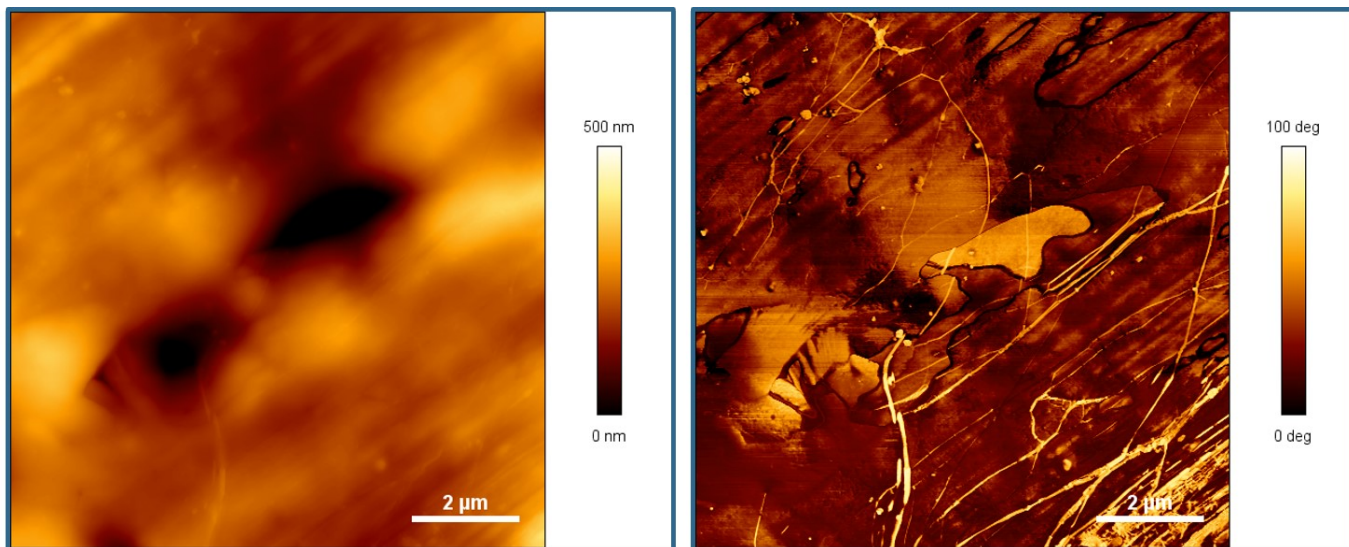


Figure S57: AFM image of VU-(ALs/APPD<sub>10</sub>-Pri)<sub>0.5</sub> showing the height plot (left) and the phase plot (right).

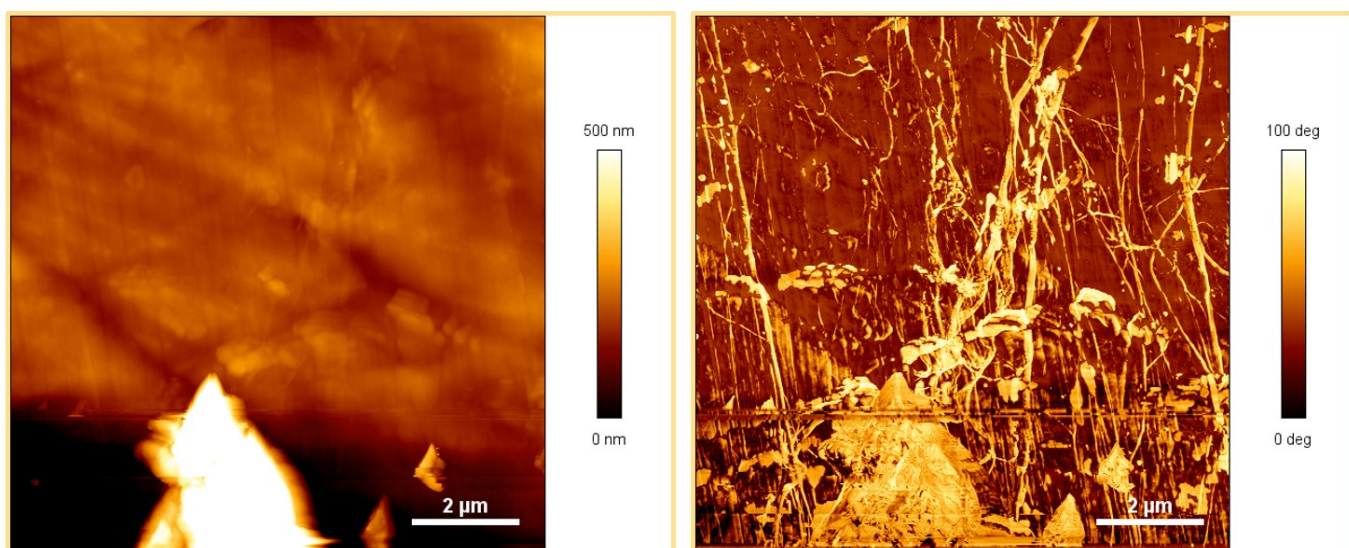


Figure S58: AFM image of VU-(ALnC-Pri)<sub>0.8</sub> showing the height plot (left) and the phase plot (right).

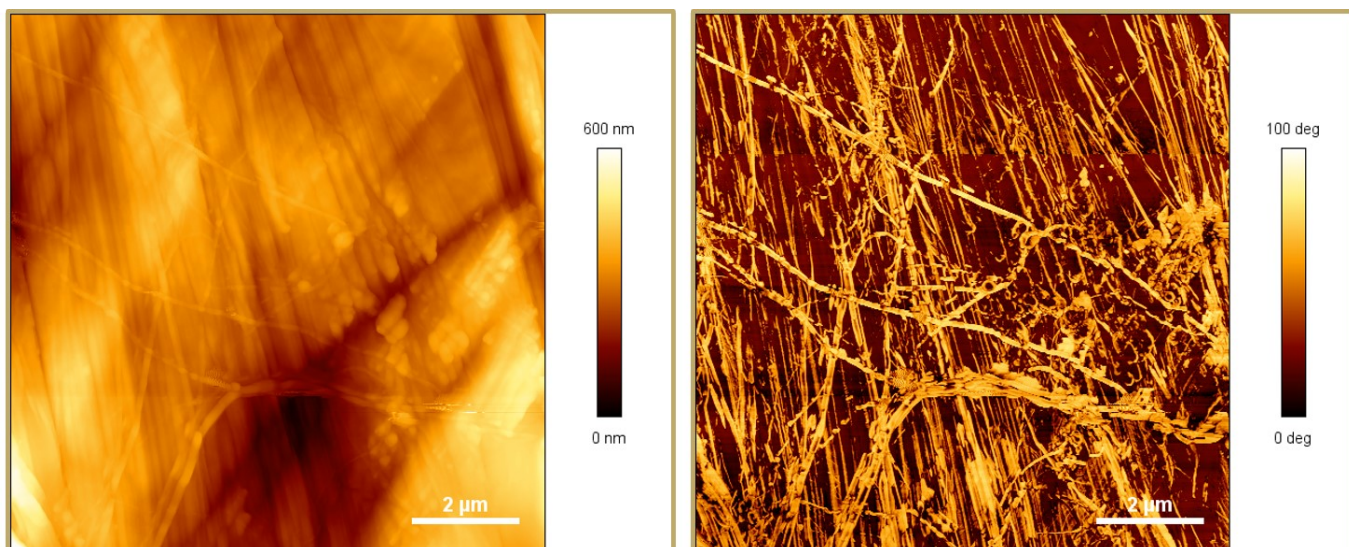


Figure S59: AFM image of VU-(ALnP-Pri)<sub>0.8</sub> showing the height plot (left) and the phase plot (right).

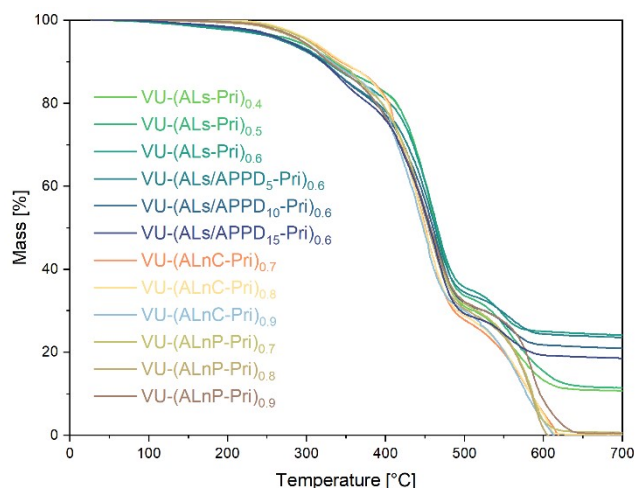


Figure S60: Thermogravimetric analysis measurements of the lignin vitrimers carried out in the range of 25 °C to 800 °C (10 K min<sup>-1</sup>) under ambient (oxygen) atmosphere, showing thermal degradation temperatures  $T_{5\%}$  of 272 °C to 307 °C.

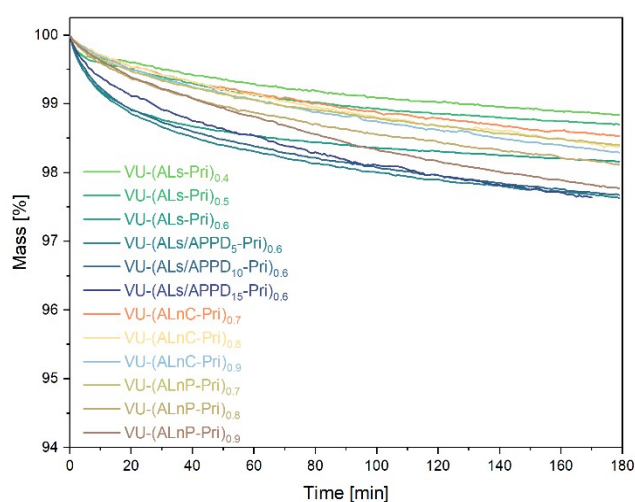


Figure S61: Isothermal thermogravimetric analysis measurements under oxygen atmosphere of the lignin vitrimers carried out at a temperature of 180 °C for 3 h, showing no thermal degradation.

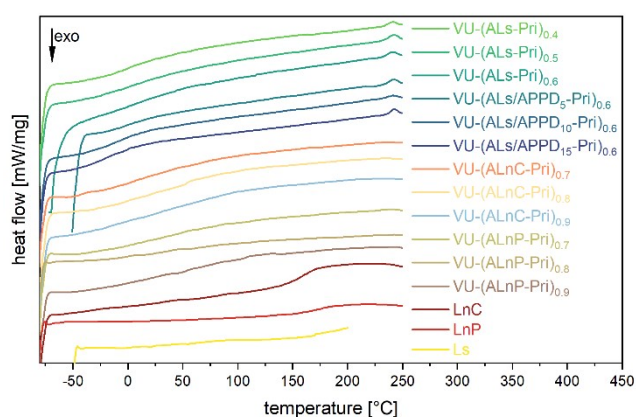


Figure S62: DSC-heating curves (-50 °C to 250 °C, 10 K min<sup>-1</sup>, N<sub>2</sub> atmosphere, second heating cycle) of the lignin vitrimers.

Table S7: Overview of the synthesized Lignin vitrimers and their characteristic properties measured by DSC, DMA, TGA, and tensile testing.

Sample	$T_{g,DSC}^a$ [°C]	$T_{g,DMA}^b$ [°C]	$T_{5\%}^c$ [°C]	$G'_{20^\circ C}^d$ [MPa]	$G'_{110^\circ C}^e$ [MPa]	$E_{t,\theta,r,t}^f$ [MPa]	$\sigma_{m,\theta,r,t}^g$ [MPa]	$\epsilon_{m,\theta,r,t}^h$ [%]	$E_a^i$ [kJ mol <sup>-1</sup> ]
VU-(ALs-Pri) <sub>0.4</sub>	-	35	287	144.3	3.91	255 ± 19	13.5 ± 0.2	13.3 ± 2.0	61.4 ± 1.7
VU-(ALs-Pri) <sub>0.5</sub>	-	40	287	173.7	6.61	383 ± 20	17.5 ± 1.3	8.3 ± 0.4	63.8 ± 3.1
VU-(ALs-Pri) <sub>0.6</sub>	-	45	272	192.7	11.5	489 ± 8.8	10.6 ± 1.6	2.1 ± 0.3	123 ± 3.6
VU-(ALs/APPD <sub>5</sub> -Pri) <sub>0.6</sub>	-	-	271	253.2	16.5	360 ± 19	11.5 ± 2.8	3.7 ± 1.1	81.3 ± 3.0
VU-(ALs/APPD <sub>10</sub> -Pri) <sub>0.6</sub>	-	-	274	100.0	6.86	230 ± 6.0	13.0 ± 0.3	20.1 ± 1.7	64.1 ± 1.9
VU-(ALs/APPD <sub>15</sub> -Pri) <sub>0.6</sub>	-	-	275	85.2	8.75	108 ± 12	6.0 ± 1.8	11.5 ± 4.4	79.3 ± 1.8
VU-(ALnC-Pri) <sub>0.7</sub>	-	85	305	340.8	5.1	479 ± 53	24.3 ± 3.0	10.6 ± 1.5	219 ± 11 <sup>j</sup>
VU-(ALnC-Pri) <sub>0.8</sub>	-	95	307	347.1	6.5	594 ± 14	29.4 ± 1.1	8.9 ± 1.0	170 ± 4.5 <sup>j</sup>
VU-(ALnC-Pri) <sub>0.9</sub>	-	110	295	440.7	10.3	672 ± 25	30.3 ± 1.0	6.8 ± 1.2	290 ± 16 <sup>j</sup>
VU-(ALnP-Pri) <sub>0.7</sub>	-	115	302	487.1	12.1	704 ± 17	24.5 ± 1.0	3.7 ± 0.2	312 ± 6.4 <sup>j</sup>
VU-(ALnP-Pri) <sub>0.8</sub>	-	125	294	370.9	18.5	798 ± 27	21.0 ± 0.6	2.7 ± 0.1	465 ± 2.3 <sup>j</sup>
VU-(ALnP-Pri) <sub>0.9</sub>	-	135	295	430.2	25.9	837 ± 114	17.1 ± 6.5	2.1 ± 0.5	773 ± 53 <sup>j</sup>

a) The  $T_{g,DSC}$  was determined using the mid-point of the step in the DSC-curves of the second heating cycle. b) The  $T_{g,DMA}$  was determined by the maximum of the  $\tan \delta$  curve of the temperature-sweep measurements, if applicable, which were also used to determine the values of  $G'$  ( $\omega = 6.28 \text{ rad s}^{-1}$ ,  $\gamma = 0.01\%$ ,  $T = 150 - 0^\circ \text{C}$ ) at  $20^\circ \text{C}$  d) and  $110^\circ \text{C}$ . c) The temperature of 5% mass loss was determined by TGA-measurements ( $T = 25 - 700^\circ \text{C}$ ,  $10 \text{ K min}^{-1}$ ). f) The elastic modulus was determined at the start of the stress strain measurement ( $1 \text{ mm min}^{-1}$ ,  $\epsilon = 0.05\% - 0.25\%$ ,  $23^\circ \text{C}$ ). g,h) The stress, strain, and elongation values were determined in a stress-strain measurement ( $1 \text{ mm min}^{-1}$  between 0.05% and 0.25% elongation and the rest of the test was carried out at  $10 \text{ mm min}^{-1}$ ,  $T = 23^\circ \text{C}$ ) i) The activation energy was determined by linearization of the characteristic averaged stress-relaxation times from KWW-fitted stress-relaxation modulus data ( $\gamma = 1\%$ ,  $T = 180 - 110^\circ \text{C}$ ). j) The calculated values are strongly influenced by the  $T_g$  of the lignin source, thereby leading to significant error, showing influence of segmental relaxation and movement.

Table S8: Overview of vinylogous urethane lignin vitrimers from the literature and their characteristic properties measured by DSC, DMA, TGA, and tensile stress.

Sample	Lignin	Lignin [wt.%]	$E$ (MPa)	$\sigma$ (MPa)	$\epsilon$ (%)	$T_g$ (°C)	$T_{5\%}$ (°C)	$E_a$ [kJ mol <sup>-1</sup> ]
Ph-VU-600 <sup>1</sup>	OOSL	46	2.4 ± 0.10	1.0 ± 0.05	115 ± 4	- 10	266	68 ± 5
VU-50-300 <sup>2</sup>	OSL	50	420 ± 30	17.2 ± 0.7	22 ± 3	18	270	72
Vitrimer-1 <sup>3</sup>	WSL	39.8	184 ± 7.1	15.1 ± 1.5	34.5 ± 7.6	87	309	134

1) L. Sougrati, A. Duval and L. Avérous, *Chem. Eng. J.*, **2025**, 511. 2) L. Sougrati, A. Duval and L. Avérous, *ChemSusChem*, **2023**, 16, e202300792. 3) J. Liu, A. Pich and K. V. Bernaerts, *Green Chem.*, **2024**, 26, 1414-1429.

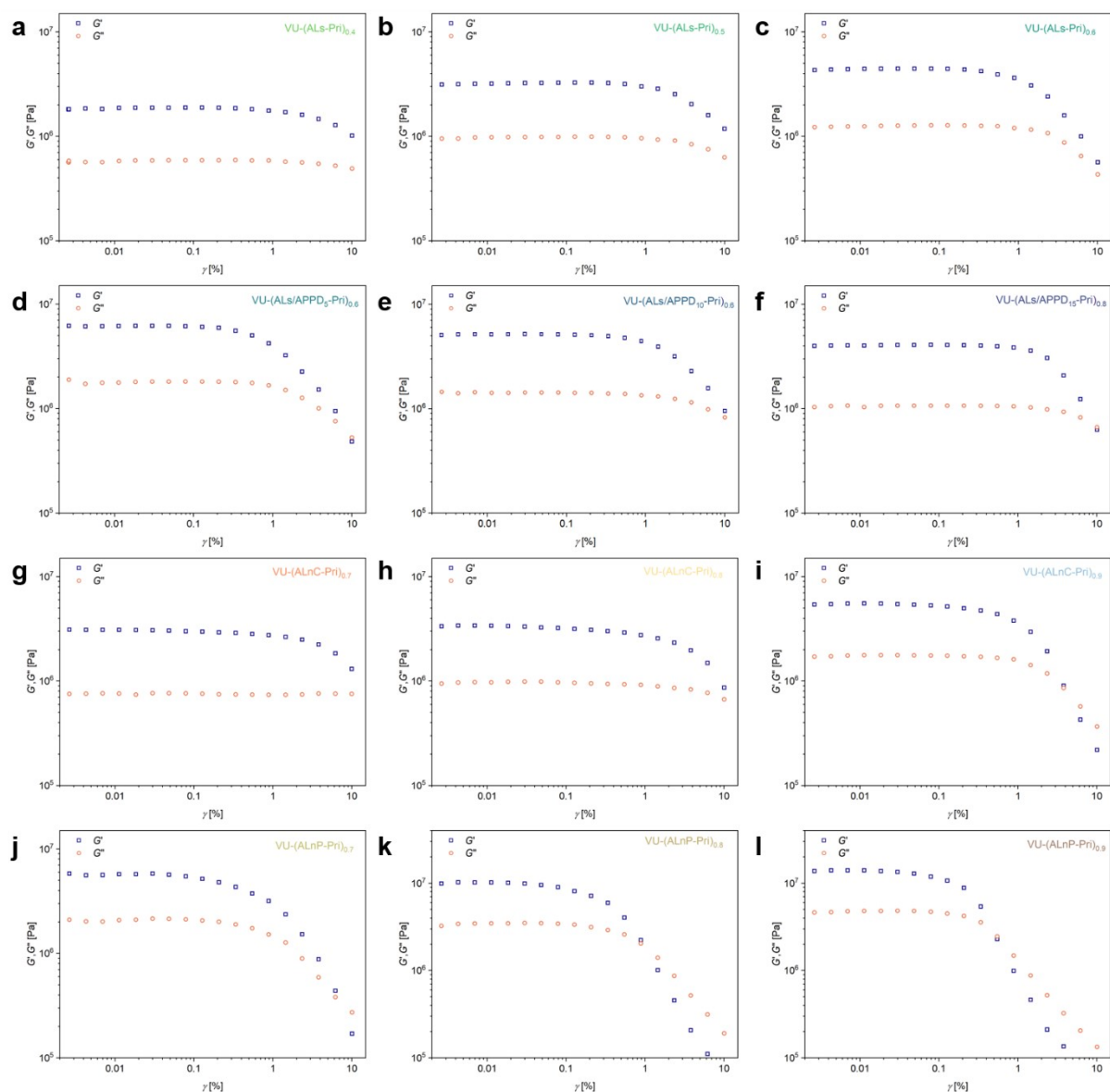


Figure S63: Amplitude sweep measurements of the produced lignin vitrimers between 0.001% and 10% shear strain  $\gamma$  performed at a constant angular frequency of  $6.28 \text{ rad s}^{-1}$ .

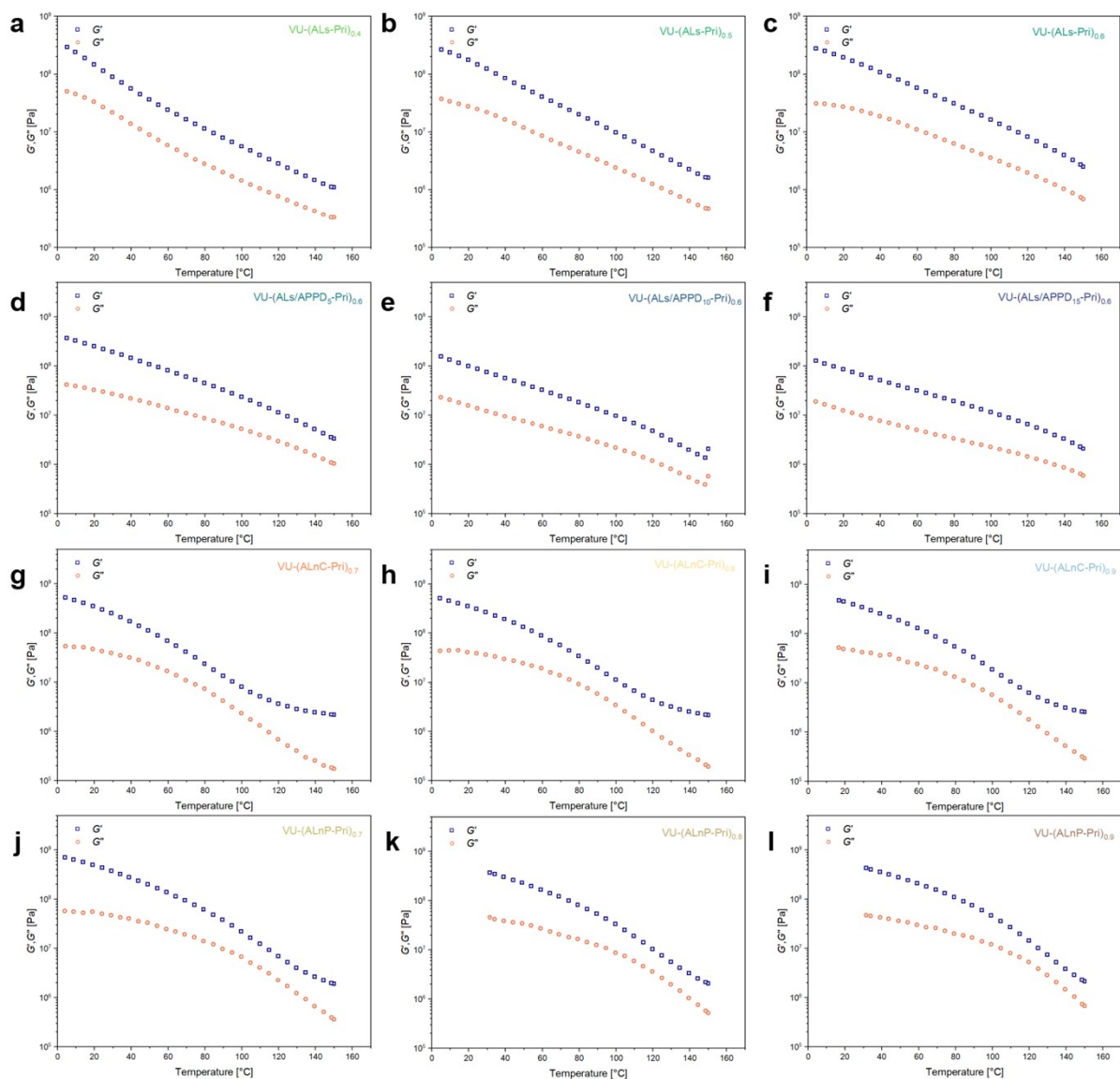


Figure S64: Temperature sweep measurements of the produced lignin vitrimers in the temperature range of 150 °C – 0 °C performed at a constant angular frequency of 6.28 rad s<sup>-1</sup> and a constant shear strain amplitude of 0.01%.

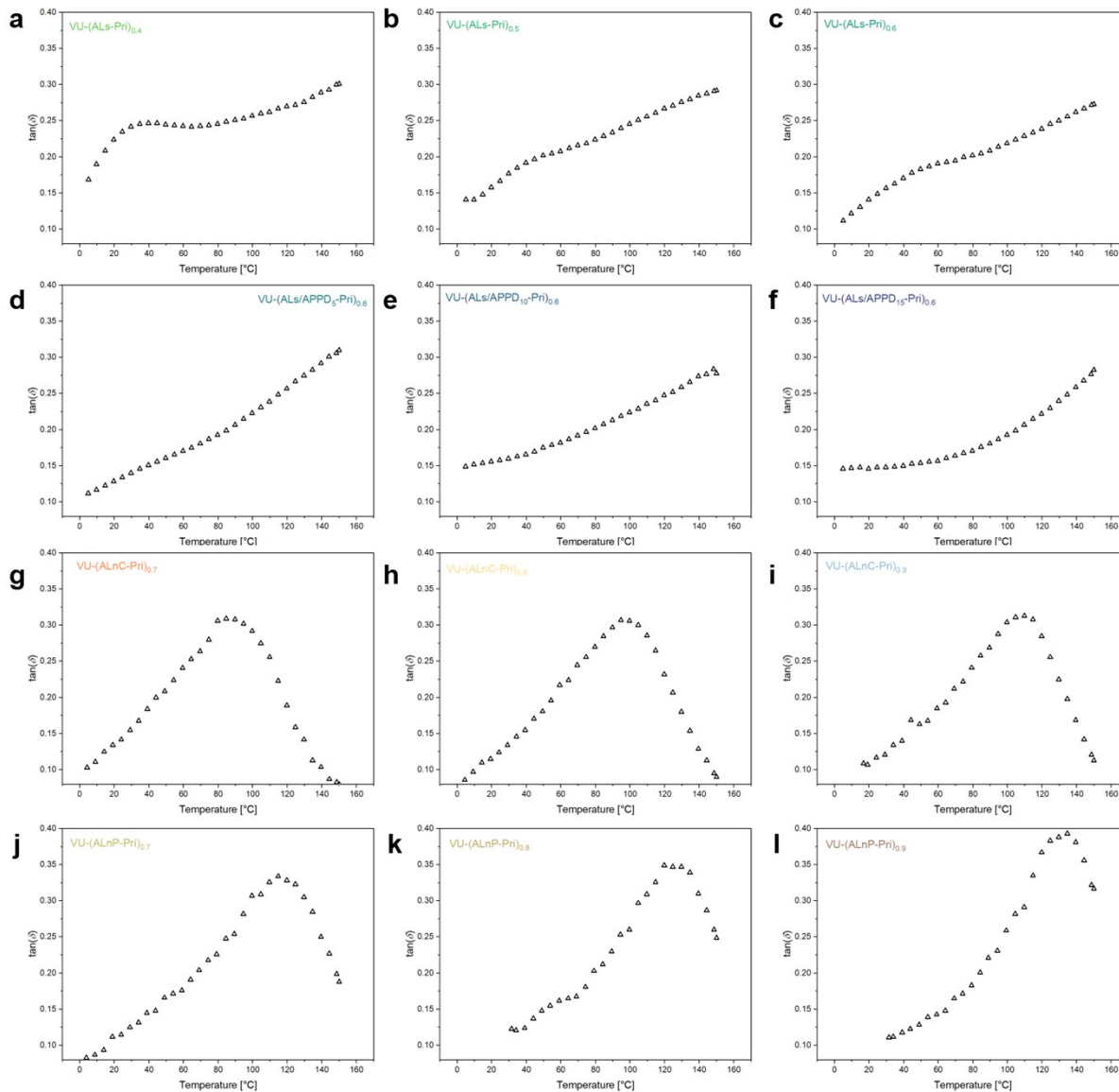


Figure S65:  $\tan(\delta)$  values calculated from the storage and loss moduli of the temperature sweep measurements of the produced lignin vitrimer materials in the temperature range of 150 °C – 0 °C performed at a constant angular frequency of 6.28 rad s<sup>-1</sup> and a shear strain amplitude of 0.01%.

Equation S4

$$G(t) = G_0 e^{\left(\frac{-t}{\tau_r}\right)^\beta}$$

- $G(t)$  : stress modulus at relaxation time [Pa]
- $G_0$  : initial stress modulus [Pa]
- $t$  : time [s]
- $\tau_r$  : characteristic relaxation time [s]
- $\beta$  : stretch parameter ( $0 \leq \beta \leq 1$ ) [-]

Supporting Information:  
Bio-Based Vinylogous Urethane Vitrimers from Waste-Wood Lignosulfonate and Enzymatic Lignin:  
Explorations in Stress Relaxation Behavior and Mechanical Strength

Equation S5

$$\langle \tau_r \rangle = \frac{\tau_r \Gamma\left(\frac{1}{\beta}\right)}{\beta}$$

$\langle \tau_r \rangle$  : average stress relaxation time [s]  
 $\Gamma$  : gamma function [-]

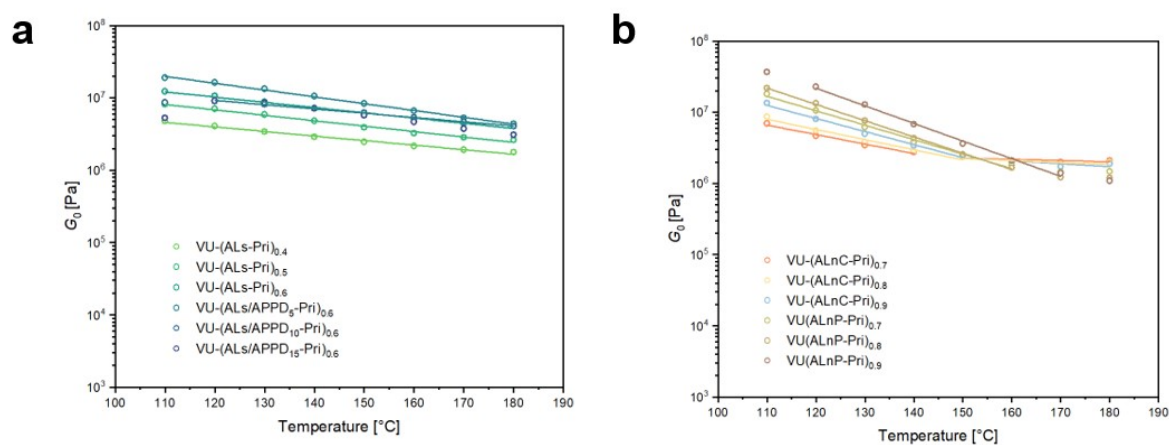


Figure S66: Initial relaxation moduli  $G_0$  of the lignin vitrimers VU-(ALs-Pri) and VU-(ALs/APPD-Pri) (a) and the vitrimers VU-(ALnC-Pri) and VU-(ALnP-Pri) (b) as a function of temperature from the stress-relaxation measurement ( $\gamma = 1\%$ ,  $F_N = 1\text{ N}$ ) between 110 °C and 180 °C. The straight lines connecting the dots serve as an orientation guide for the eye. The materials VU-(ALnC-Pri) and VU-(ALnP-Pri) (b) show two different slopes of these straight lines above and under 160 °C.

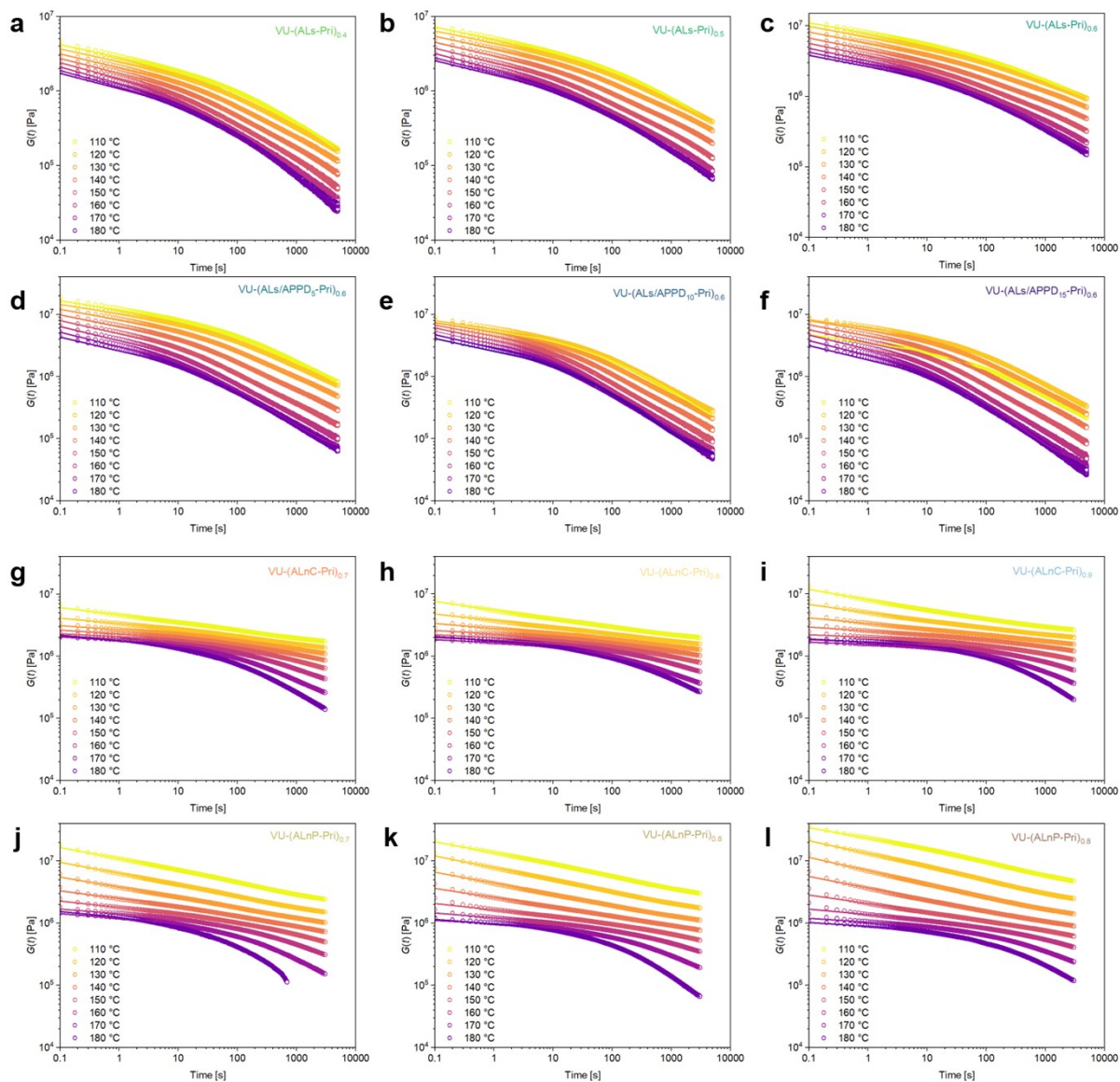


Figure S67: Stress-relaxation measurement of the lignin vitrimers, plotting the stress-relaxation modulus  $G(t)$  versus the stress-relaxation time measured at temperatures in the range of 110 to 180 °C while applying a shear strain of 1%. The lines display the stretched exponential fit functions for the respective temperatures, calculated from the stress-relaxation data.

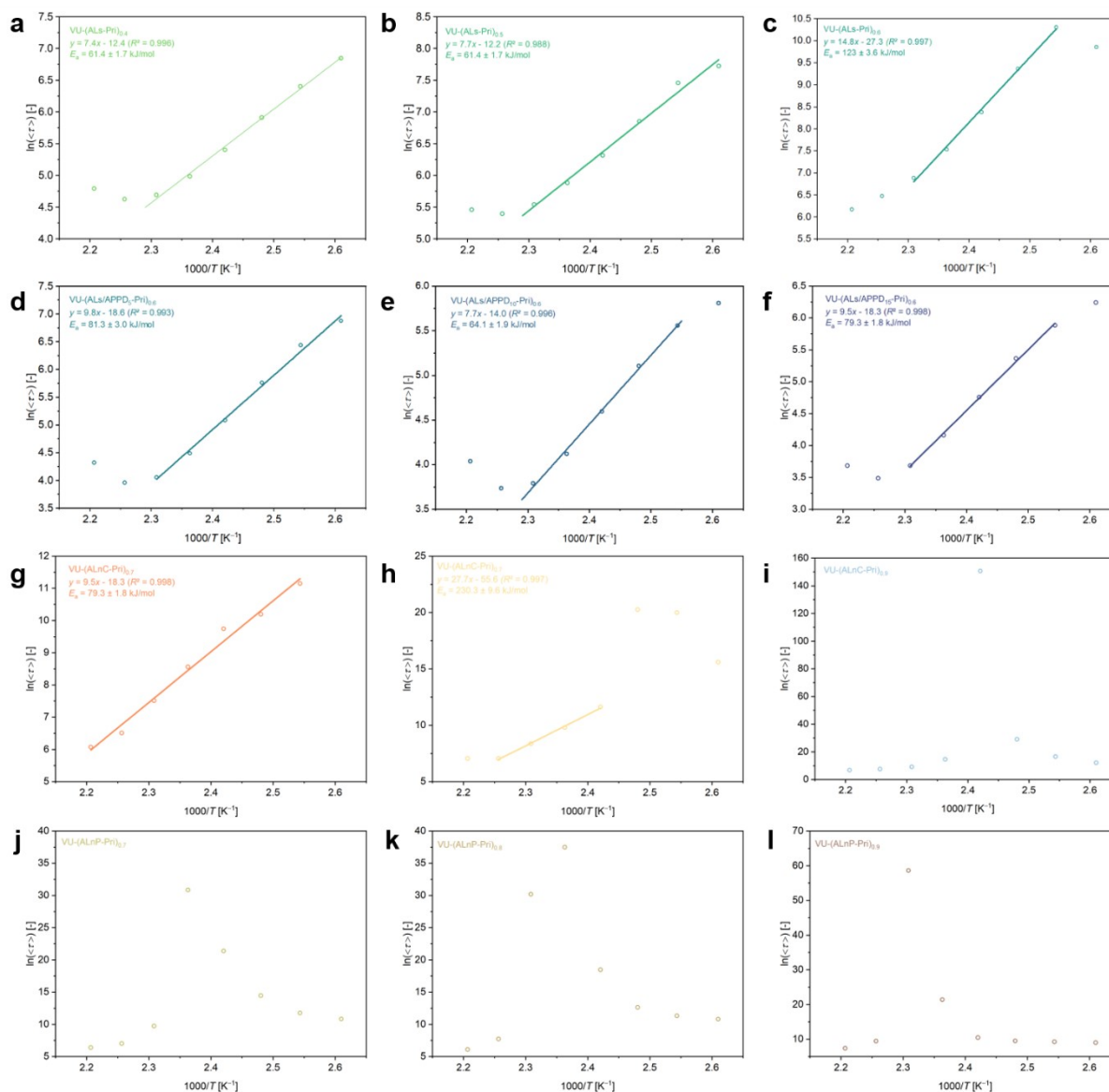


Figure S68: Plot of  $\ln \langle \tau \rangle$  versus  $1000/T$  of the lignin vitrimers to calculate the activation energies (a – h) from the slope of the linear fit of the calculated  $\langle \tau \rangle$  values from the stretched exponential fit in the temperature range of the stress-relaxation measurements ( $\gamma = 1\%$ ,  $F_N = 1N$ ) between 110 °C and 180 °C of the lignin vitrimers. The stress relaxation times of the materials VU-(ALnC-Pri)<sub>0.8</sub>, VU-(ALnC-Pri)<sub>0.9</sub>, VU-(ALnC-Pri)<sub>0.7</sub>, VU-(ALnC-Pri)<sub>0.8</sub>, and VU-(ALnC-Pri)<sub>0.9</sub> are influenced by the  $T_g$  of the lignin particles and show deviations from the expected values, and the diagrams cannot be used to calculate the activation energy of the transamination reaction under 160 °C.

Table S9: Summary of the values of the stretch factor  $\beta$  and the calculated average values of the characteristic stress relaxation time  $\langle \tau \rangle$  for the KWW fit of the stress-relaxation measurements ( $\gamma = 1\%$ ,  $F_N = 1N$ ) between 110 °C and 180 °C of the lignin vitrimers. The orange markings are used to highlight the relaxation times, which are influenced by the  $T_g$  of the respective materials (VU-(ALnC-Pri) and VU-(ALnP-Pri)) and show deviations from the expected values.

Sample	$\beta_{110^\circ\text{C}}$ [-]	$\beta_{120^\circ\text{C}}$ [-]	$\beta_{130^\circ\text{C}}$ [-]	$\beta_{140^\circ\text{C}}$ [-]	$\beta_{150^\circ\text{C}}$ [-]	$\beta_{160^\circ\text{C}}$ [-]	$\beta_{170^\circ\text{C}}$ [-]	$\beta_{180^\circ\text{C}}$ [-]	$\langle \tau \rangle_{110^\circ\text{C}}$ [s]	$\langle \tau \rangle_{120^\circ\text{C}}$ [s]	$\langle \tau \rangle_{130^\circ\text{C}}$ [s]	$\langle \tau \rangle_{140^\circ\text{C}}$ [s]	$\langle \tau \rangle_{150^\circ\text{C}}$ [s]	$\langle \tau \rangle_{160^\circ\text{C}}$ [s]	$\langle \tau \rangle_{170^\circ\text{C}}$ [s]	$\langle \tau \rangle_{180^\circ\text{C}}$ [s]
VU-(ALs-Pri) <sub>0.4</sub>	0.151	0.156	0.157	0.159	0.158	0.160	0.160	0.174	940	603	369	221	146	109	102	120
VU-(ALs-Pri) <sub>0.5</sub>	0.138	0.140	0.144	0.146	0.145	0.146	0.151	0.167	2263	1729	945	552	358	254	221	235
VU-(ALs-Pri) <sub>0.6</sub>	0.111	0.103	0.108	0.116	0.126	0.136	0.150	0.176	19130	29962	11618	4363	1871	980	651	480
VU-(ALs/APPD <sub>10</sub> -Pri) <sub>0.6</sub>	0.170	0.175	0.180	0.181	0.182	0.182	0.179	0.179	966	623	317	161	89	57	52	75
VU-(ALs/APPD <sub>10</sub> -Pri) <sub>0.6</sub>	0.218	0.227	0.227	0.226	0.225	0.224	0.223	0.222	333	259	165	99	62	44	42	57
VU-(ALs/APPD <sub>15</sub> -Pri) <sub>0.6</sub>	0.209	0.217	0.211	0.208	0.207	0.210	0.210	0.208	513	359	213	116	64	40	33	40
VU-(ALnC-Pri) <sub>0.7</sub>	0.069	0.120	0.165	0.201	0.248	0.287	0.315	0.281	2.5·10 <sup>6</sup>	6.9·10 <sup>4</sup>	2.7·10 <sup>4</sup>	1.7·10 <sup>4</sup>	5216	1837	673	435
VU-(ALnC-Pri) <sub>0.8</sub>	0.051	0.053	0.166	0.229	0.286	0.229	0.324	0.280	5.9·10 <sup>6</sup>	4.8·10 <sup>8</sup>	6.2·10 <sup>8</sup>	1.1·10 <sup>5</sup>	1.8·10 <sup>4</sup>	4264	1164	1167
VU-(ALnC-Pri) <sub>0.9</sub>	0.052	0.048	0.043	0.022	0.172	0.287	0.344	0.360	1.7·10 <sup>5</sup>	1.7·10 <sup>7</sup>	4.1·10 <sup>12</sup>	2.7·10 <sup>65</sup>	2.0·10 <sup>6</sup>	9185	1990	819
VU-(ALnP-Pri) <sub>0.7</sub>	0.067	0.060	0.056	0.053	0.055	0.194	0.277	0.244	5.1·10 <sup>4</sup>	1.3·10 <sup>5</sup>	1.9·10 <sup>8</sup>	1.9·10 <sup>9</sup>	2.5·10 <sup>13</sup>	1.7·10 <sup>4</sup>	1128	597
VU-(ALnP-Pri) <sub>0.8</sub>	0.068	0.056	0.051	0.047	0.041	0.079	0.289	0.328	4.9·10 <sup>4</sup>	8.3·10 <sup>4</sup>	3.1·10 <sup>5</sup>	1.1·10 <sup>8</sup>	1.9·10 <sup>16</sup>	1.3·10 <sup>13</sup>	2273	443
VU-(ALnP-Pri) <sub>0.9</sub>	0.092	0.067	0.054	0.056	0.045	0.038	0.223	0.278	7922	1.1·10 <sup>4</sup>	1.3·10 <sup>4</sup>	3.5·10 <sup>4</sup>	1.9·10 <sup>9</sup>	2.8·10 <sup>25</sup>	1.3·10 <sup>4</sup>	1630

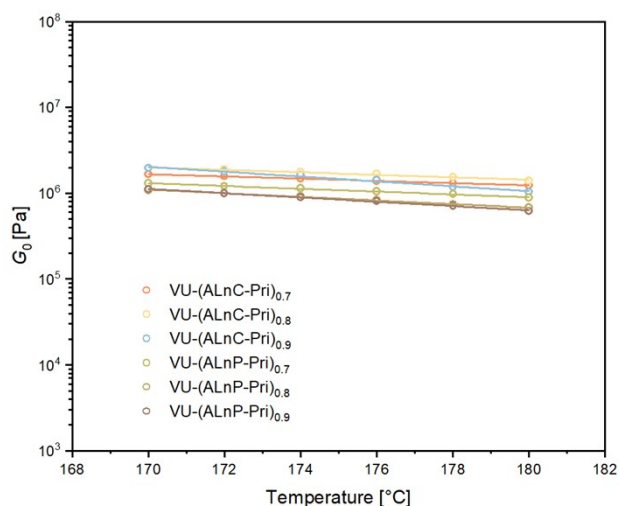


Figure S69: Initial relaxation moduli  $G_0$  of the lignin vitrimers VU-(ALnC-Pri) and VU-(ALnP-Pri) as a function of temperature of the stress-relaxation measurements ( $\gamma = 1\%$ ,  $F_N = 1N$ ) between 170 °C and 180 °C of the indicated lignin vitrimers. The straight lines connecting the dots serve as an orientation guide for the eye.

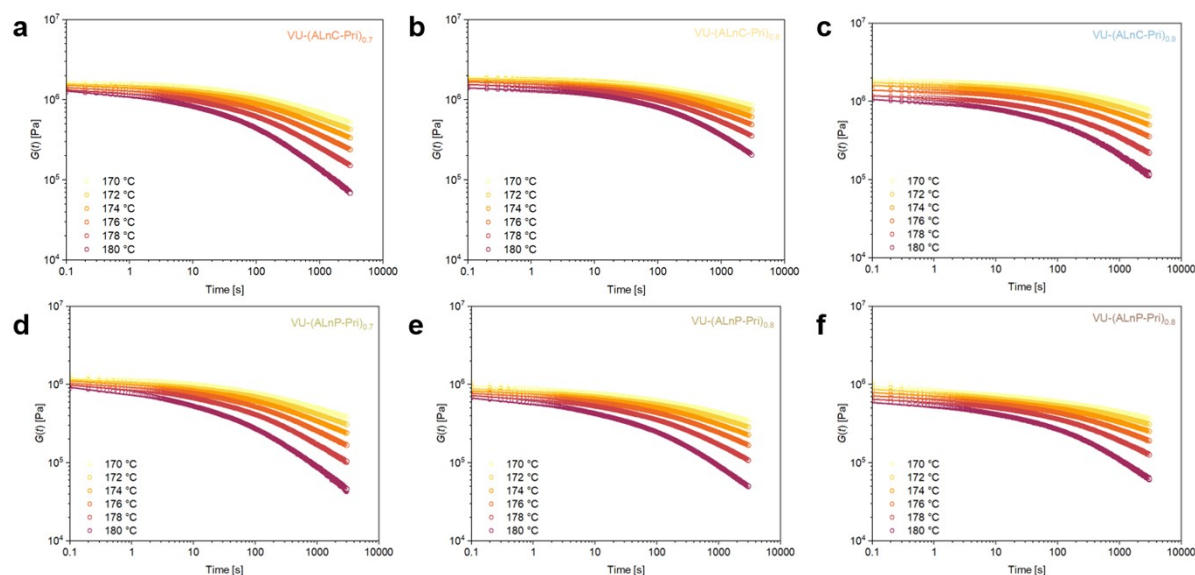


Figure S70: Stress-relaxation measurement of the lignin vitrimers VU-(ALnC-Pri) and VU-(ALnP-Pri), plotting the stress-relaxation modulus  $G(t)$  versus the stress-relaxation time measured at temperatures in the range of 170 to 180 °C while applying a shear strain of 1%. The lines display the stretched exponential fit functions for the respective temperatures, calculated from the stress-relaxation data.

Table S10: Summary of the  $\beta \langle \tau \rangle$  values for the KWW fit of the stress-relaxation measurements of the lignin vitrimer materials VU-(ALnC-Pri) and VU-(ALnP-Pri) in the temperature range of 170 °C to 180 °C while applying a shear strain of 1%.

Sample	$\beta_{170^\circ\text{C}}$ [-]	$\beta_{172^\circ\text{C}}$ [-]	$\beta_{174^\circ\text{C}}$ [-]	$\beta_{176^\circ\text{C}}$ [-]	$\beta_{178^\circ\text{C}}$ [-]	$\beta_{180^\circ\text{C}}$ [-]	$\langle \tau \rangle_{170^\circ\text{C}}$ [s]	$\langle \tau \rangle_{172^\circ\text{C}}$ [s]	$\langle \tau \rangle_{174^\circ\text{C}}$ [s]	$\langle \tau \rangle_{176^\circ\text{C}}$ [s]	$\langle \tau \rangle_{178^\circ\text{C}}$ [s]	$\langle \tau \rangle_{180^\circ\text{C}}$ [s]
VU-(ALnC-Pri) <sub>0.7</sub>	0.363	0.364	0.364	0.357	0.347	0.334	1668	1325	1032	809	570	289
VU-(ALnC-Pri) <sub>0.8</sub>	0.373	0.383	0.389	0.394	0.391	0.396	2939	2350	1956	1543	1303	923
VU-(ALnC-Pri) <sub>0.9</sub>	0.347	0.361	0.368	0.381	0.363	0.344	5331	3439	2531	1667	1341	790
VU-(ALnP-Pri) <sub>0.7</sub>	0.305	0.312	0.320	0.316	0.300	0.275	3053	2163	1448	1029	678	312
VU-(ALnP-Pri) <sub>0.8</sub>	0.202	0.262	0.290	0.299	0.294	0.279	149858	10062	4094	2336	1353	597
VU-(ALnP-Pri) <sub>0.9</sub>	0.163	0.174	0.183	0.192	0.204	0.237	30662	20130	13835	9751	6599	3230

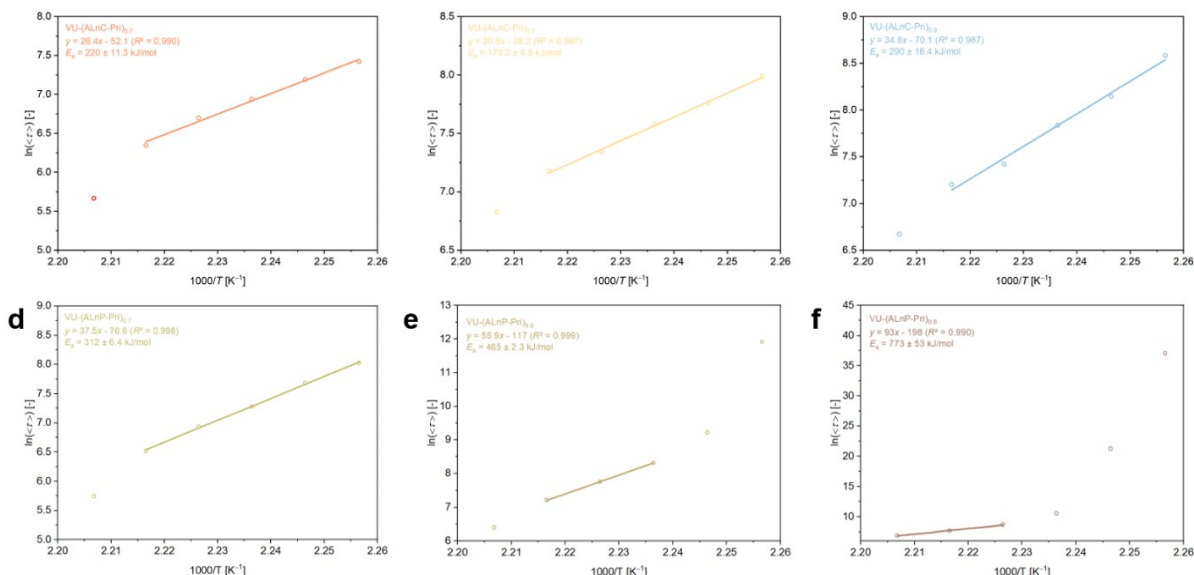


Figure S71: Plot of  $\ln\langle\tau\rangle$  versus  $1000/T$  of the lignin vitrimers VU-(ALnC-Pri) and VU-(ALnP-Pri) in the range of 170 to 180 °C while applying a shear strain of 1% to calculate the activation energies (a – f) from the slope of the linear fit of the calculated  $\langle\tau\rangle$  values from the stretched exponential fit. The stress relaxation times of the materials are still influenced by the  $T_g$  of the lignin particles and show high relaxation activation energies, which cannot be assigned solely to the transamination reaction of vinylogous urethanes but also involve other relaxation effects.

Table S11: Overview of the recycled lignin vitrimers and their characteristic properties measured by DSC, DMA, TGA, and tensile stress.

Sample	$T_{g,DMA}^a)$ [°C]	$G'_{20^\circ C}^b)$ [MPa]	$G'_{110^\circ C}^c)$ [MPa]	$E_{t,\theta,r,t.}^d)$ [MPa]	$\sigma_{m,\theta,r,t.}^e)$ [MPa]	$\epsilon_{m,\theta,r,t.}^f)$ [%]	$E_a^i)$ [kJ mol <sup>-1</sup> ]
VU-(ALs-Pri) <sub>0.5</sub> (5 recycles)	45	11.2	2.78	415 ± 26	18.3 ± 1.0	8.3 ± 0.4	-
VU-(ALs/APPD <sub>10</sub> -Pri) <sub>0.6</sub> (5 recycles)	35	31.8	4.36	133 ± 4.9	12.0 ± 0.8	19.3 ± 0.5	1171 ± 182 <sup>j)</sup>
VU-(ALnC-Pri) <sub>0.8</sub> (5 recycles)	95	43.4	1.15	598 ± 17	21.6 ± 2.6	4.0 ± 0.8	1797 ± 484.5 <sup>j)</sup>
VU-(ALnP-Pri) <sub>0.8</sub> (5 recycles)	140	95.8	3.45	418 ± 7.4	18.8 ± 1.3	5.1 ± 0.5	13902 ± 469 <sup>j)</sup>

a) The  $T_{g,DMA}$  was determined by the maximum of the  $\tan \delta$  curve of the temperature-sweep measurements, which were also used to determine the values of  $G'$  ( $\omega = 6.28$  rad s<sup>-1</sup>,  $\gamma = 0.01\%$ ,  $T = 150 - 0$  °C) at 20 °C b) and 110 °C c). The closest available data point to the respective temperature is listed. d) The elastic modulus was determined at the start of the stress strain measurement (1 mm min<sup>-1</sup>,  $\epsilon = 0.05\% - 0.25\%$ , 23 °C). e,f) The stress, strain, and elongation values were determined in a stress-strain measurement (1 mm min<sup>-1</sup> between 0.05% and 0.25% elongation and the rest of the test was carried out at 10 mm min<sup>-1</sup>,  $T = 23$  °C) i) The activation energy was determined by linearization of the characteristic averaged stress-relaxation times from KWW-fitted stress-relaxation modulus data ( $\gamma = 1\%$ ,  $T = 180 - 110$  °C) j) The calculated values are strongly influenced by the  $T_g$  of the lignin resource, thereby leading to significant error, showing influence of segmental relaxation and movement.

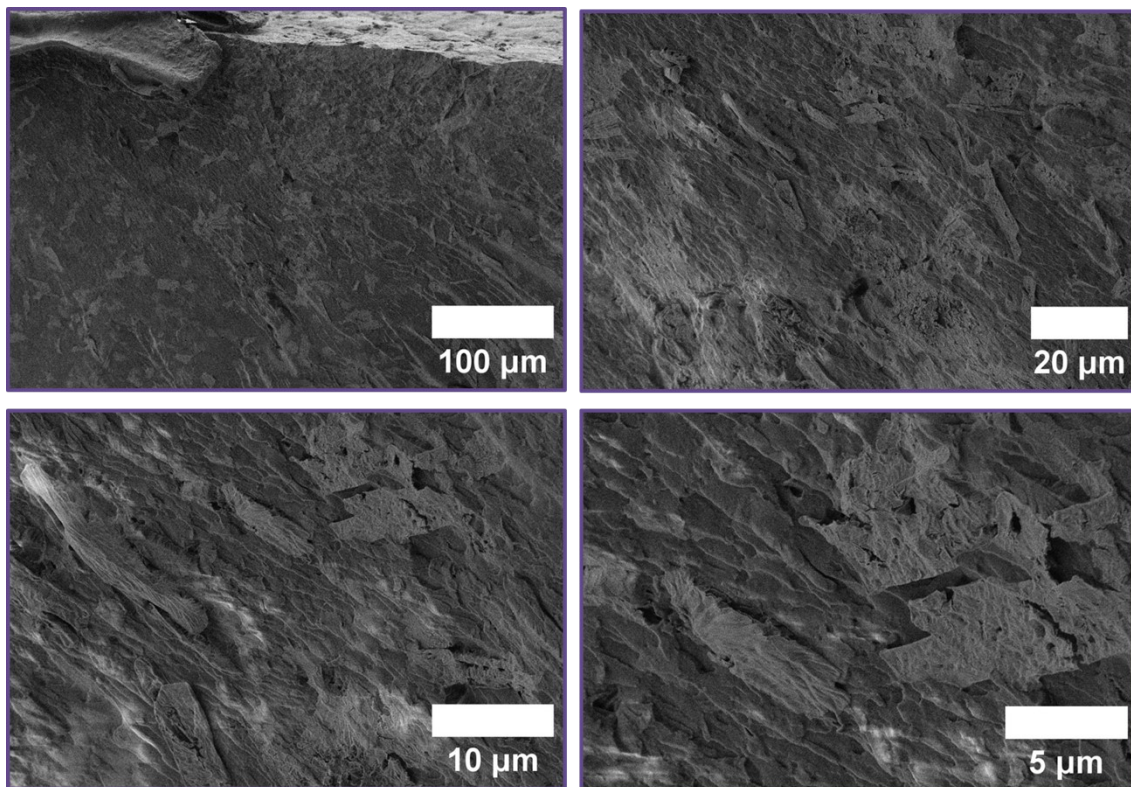


Figure S72: SEM images of recycled VU-(Als-Pri)<sub>0.5</sub> with different magnifications.

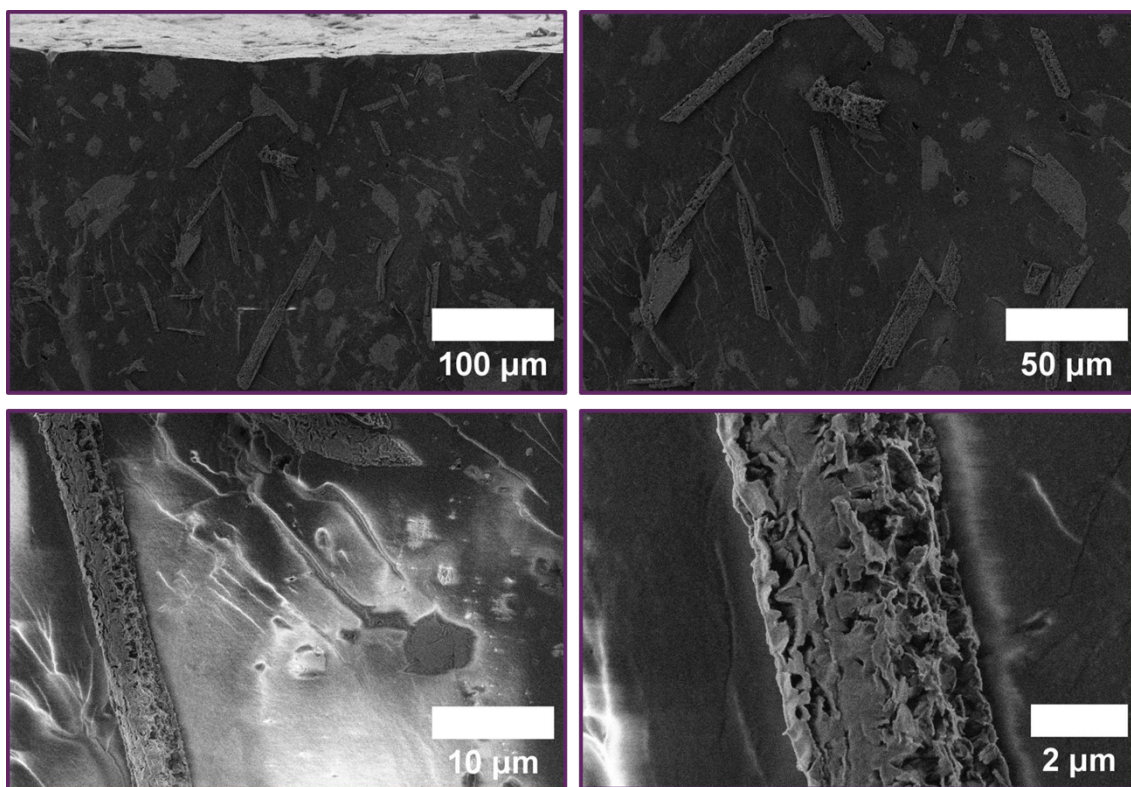


Figure S73: SEM images of recycled VU-(Als/APPD<sub>10</sub>-Pri)<sub>0.6</sub> with different magnifications.

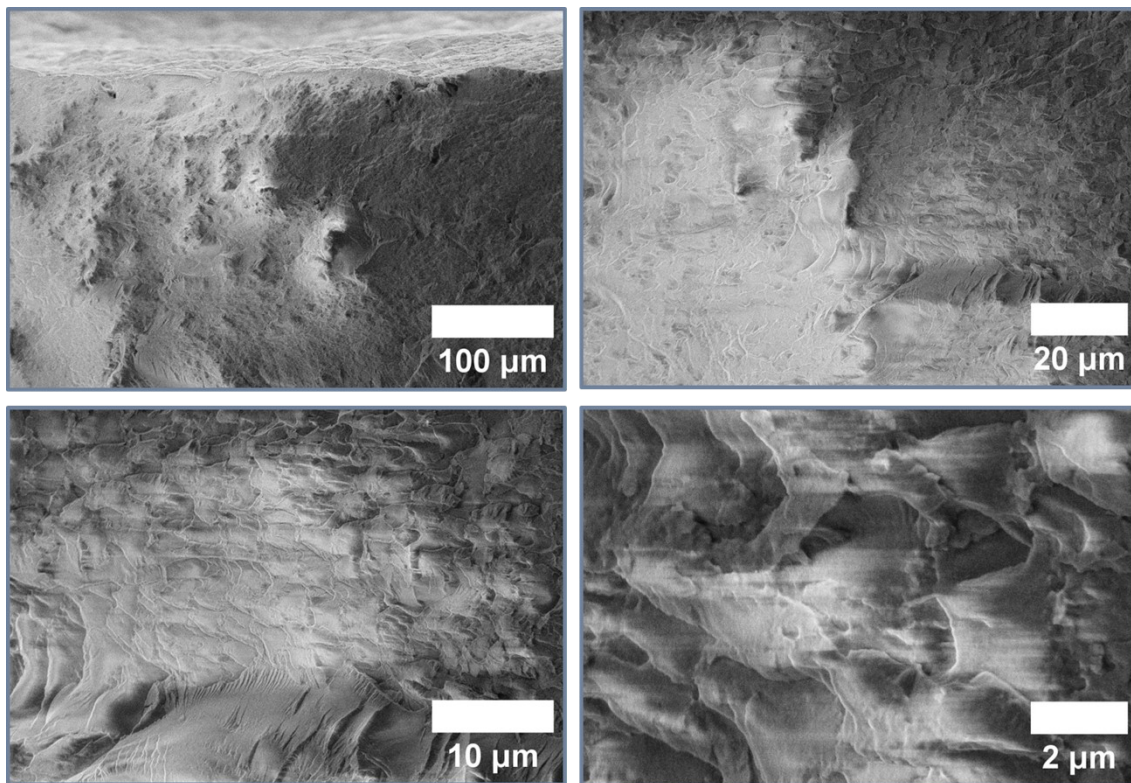


Figure S74: SEM images of recycled VU-(AlnC-Pri)<sub>0.8</sub> with different magnifications.

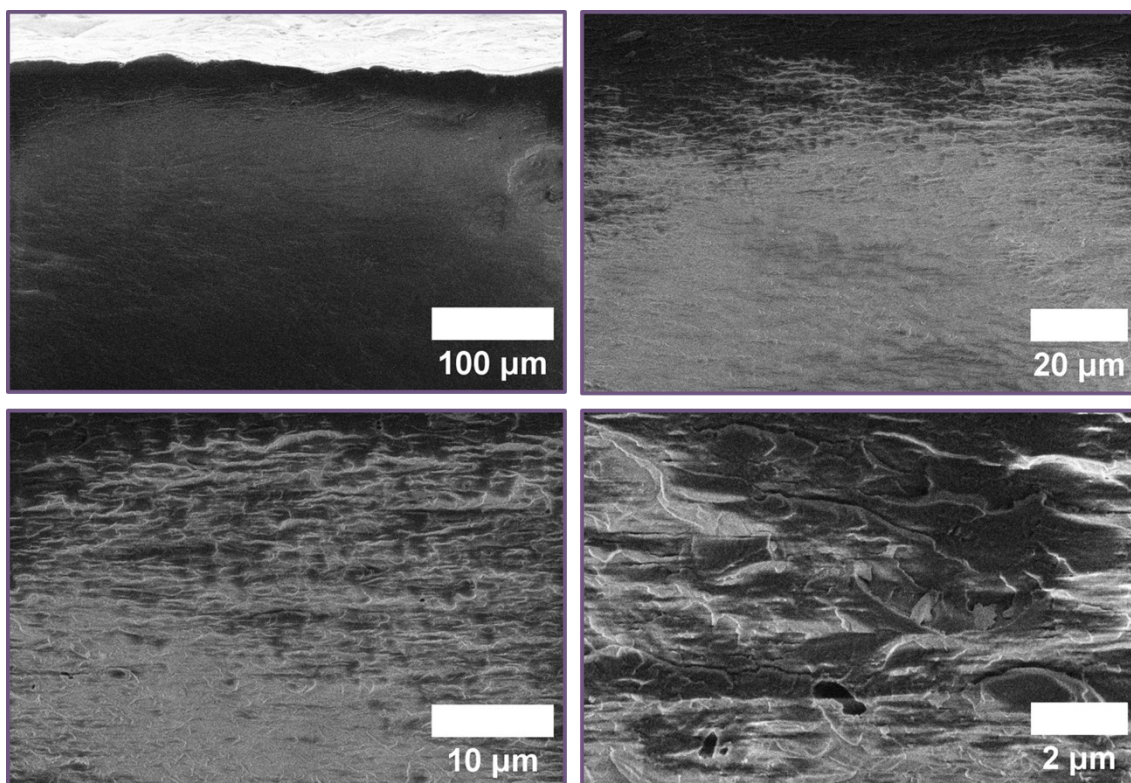
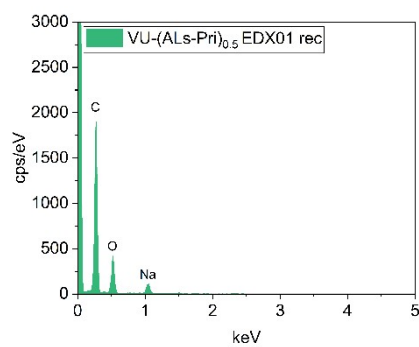
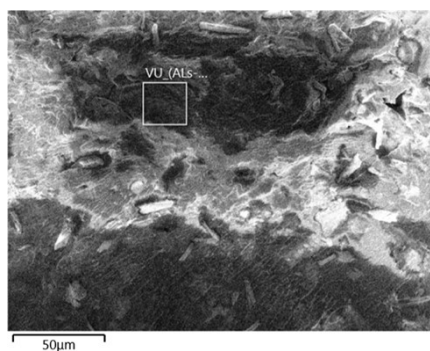


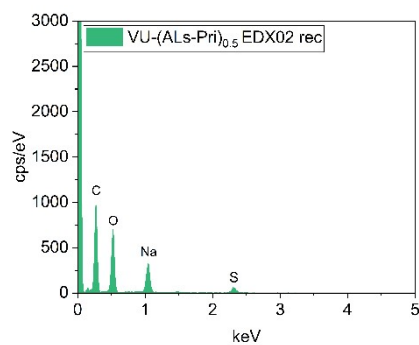
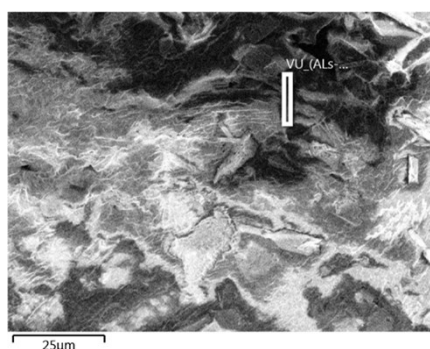
Figure S75: SEM images of recycled VU-(AlnP-Pri)<sub>0.8</sub> with different magnifications.

Table S12: EDX-measurements of VU-(ALs-Pri)<sub>0.5</sub> after recycling, showing the irradiated area (left), the EDX spectra (middle) and a table with the relative intensity of respective elements in % (right).

### VU-(ALs-Pri)<sub>0.5</sub> recycled



Element	Atom%
C	77.78
N	-
O	19.91
Na	1.89
Al	0.18
S	0.25



Element	Atom%
C	62.99
N	-
O	29.76
Na	5.88
Al	-
S	1.37

Table S13: EDX-measurements of VU-(AlS/APPD<sub>10</sub>-Pri)<sub>0.6</sub> after recycling, showing the irradiated area (left), the EDX spectra (middle) and a table with the relative intensity of respective elements in % (right).

### VU-(AlS/APPD<sub>10</sub>-Pri)<sub>0.6</sub> recycled

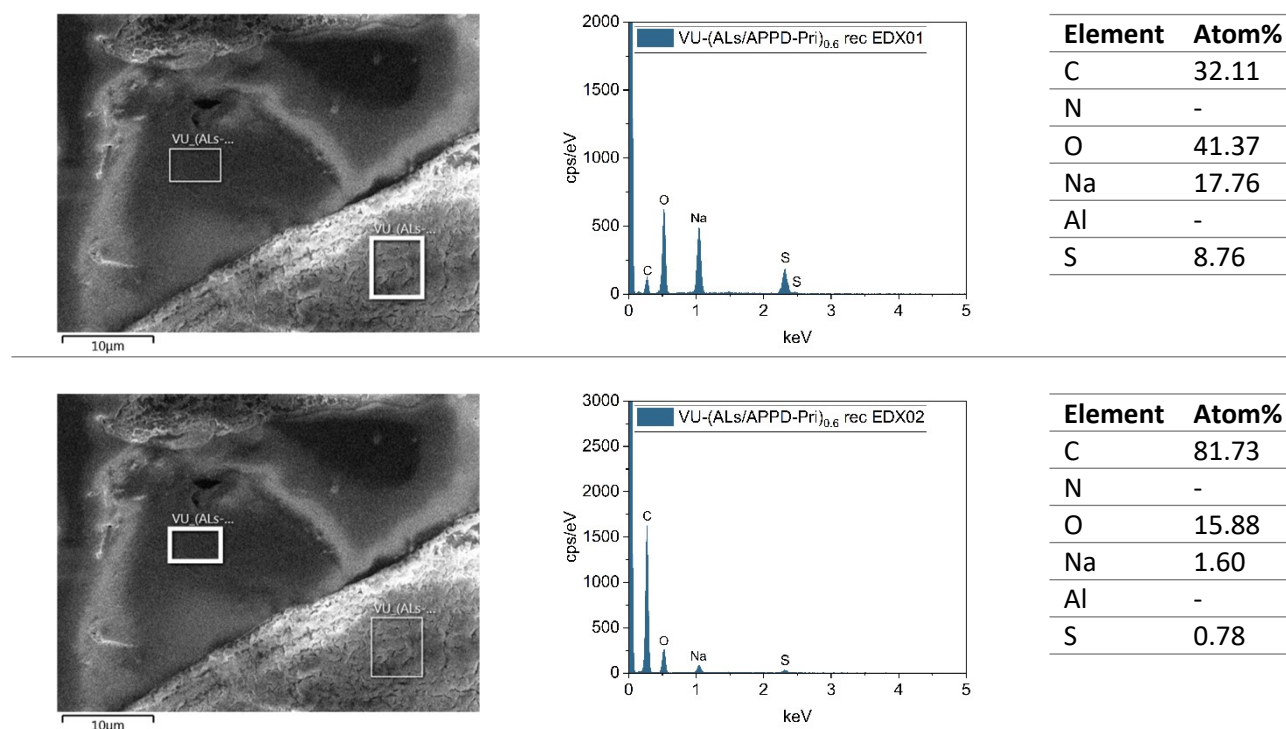


Table S14: EDX-measurements of VU-(AlnC-Pri)<sub>0.8</sub> after recycling, showing the irradiated area (left), the EDX spectra (middle) and a table with the relative intensity of respective elements in % (right).

### VU-(AlnC-Pri)<sub>0.8</sub> recycled

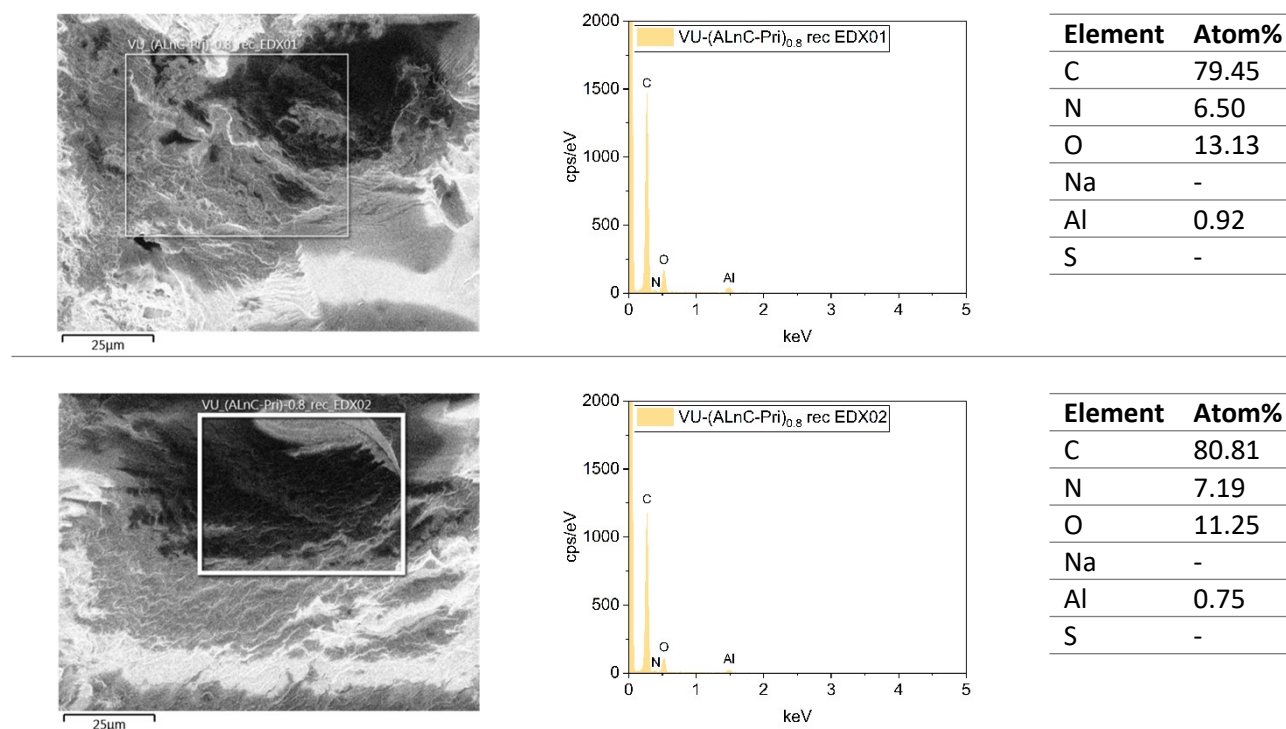


Table S15: EDX-measurements of VU-(ALnP-Pri)<sub>0.8</sub> after recycling, showing the irradiated area (left), the EDX spectra (middle) and a table with the relative intensity of respective elements in % (right).

### VU-(ALnP-Pri)<sub>0.8</sub> recycled

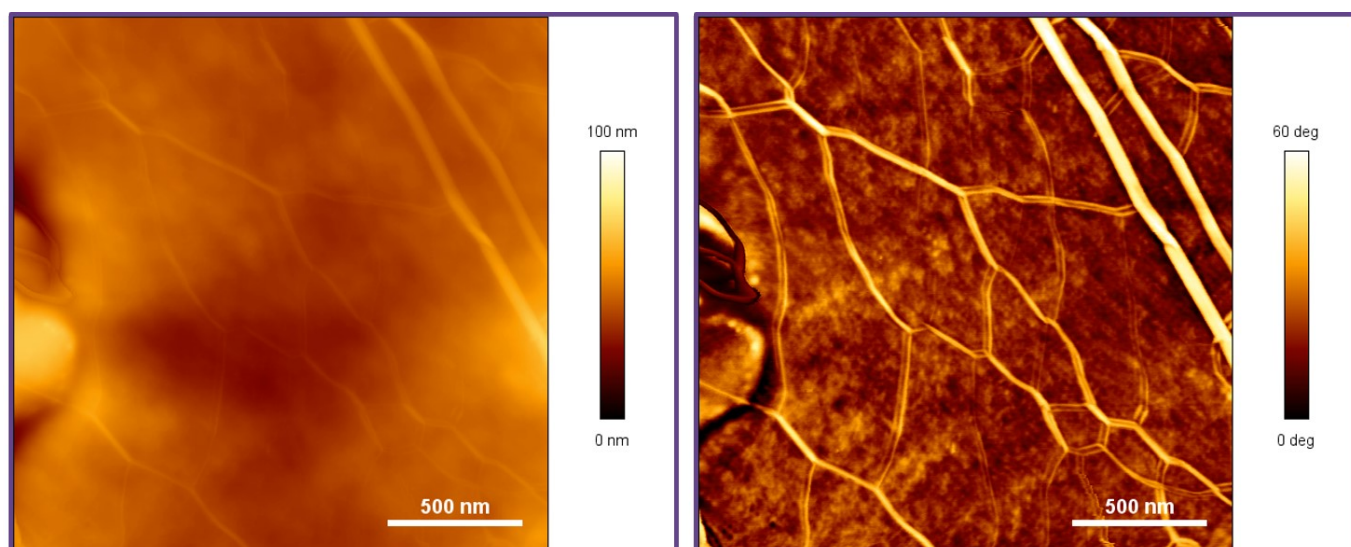
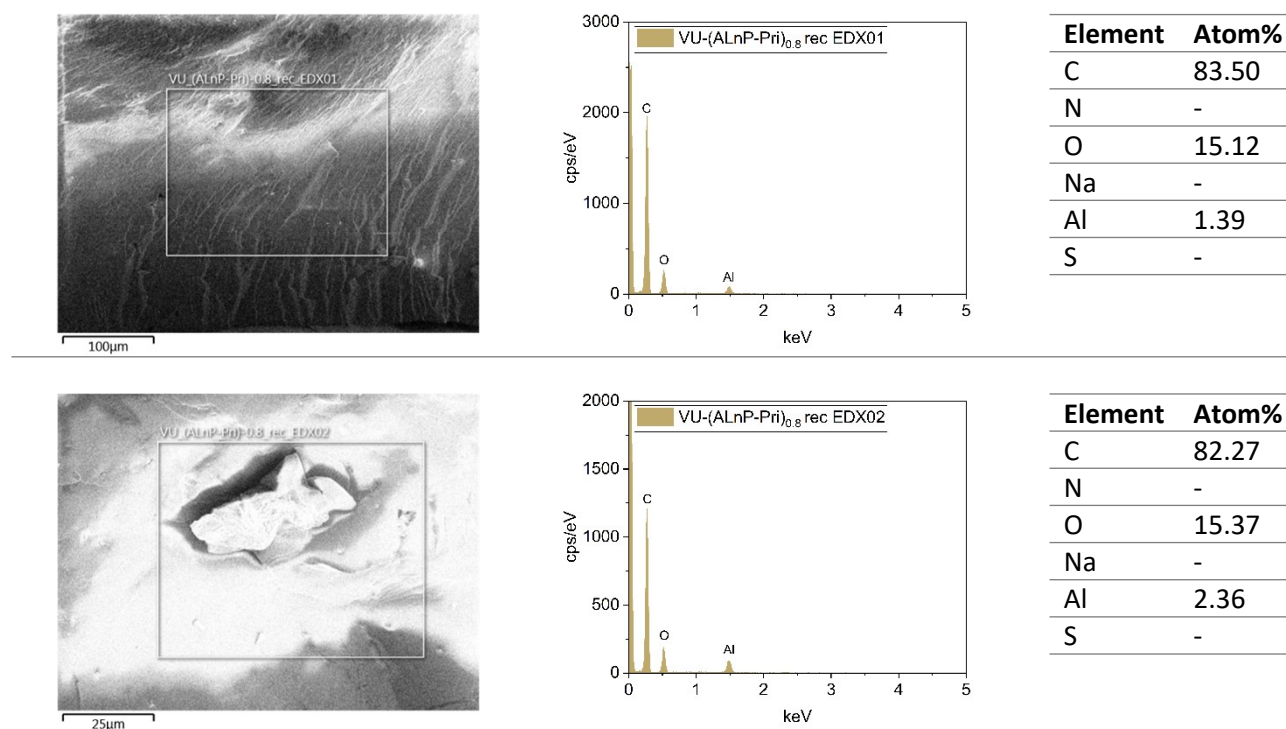


Figure S76: AFM image of recycled VU-(AlS-Pri)<sub>0.5</sub> showing the height plot (left) and the phase plot (right).

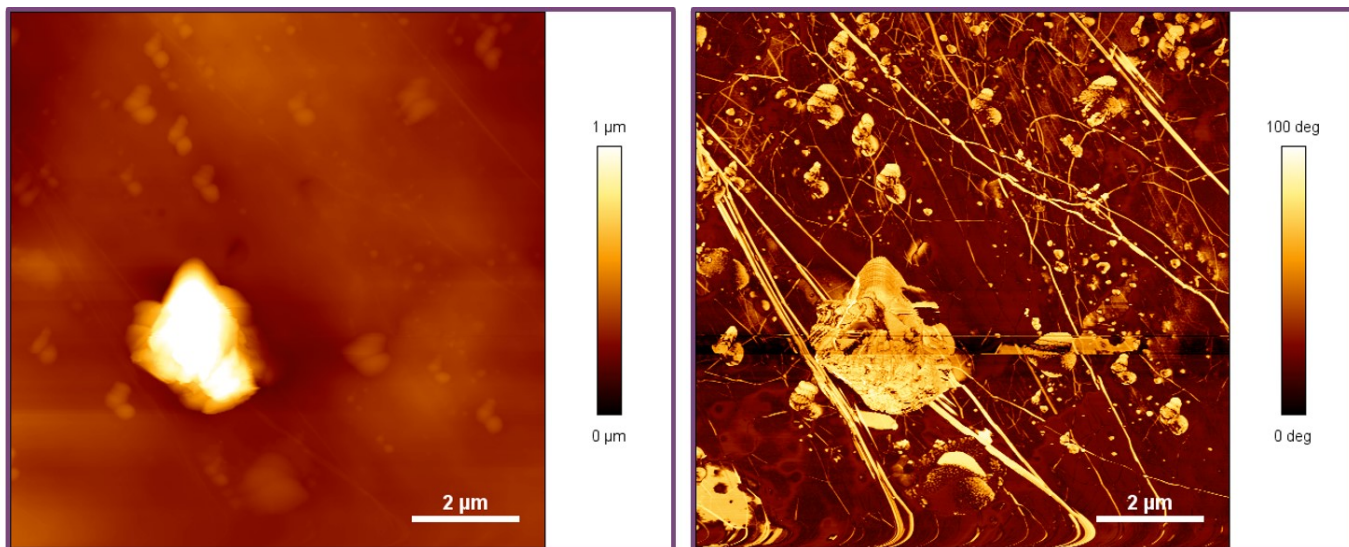


Figure S77: AFM image of recycled VU-(AlS/APPD<sub>10</sub>-Pri)<sub>0.6</sub> showing the height plot (left) and the phase plot (right).

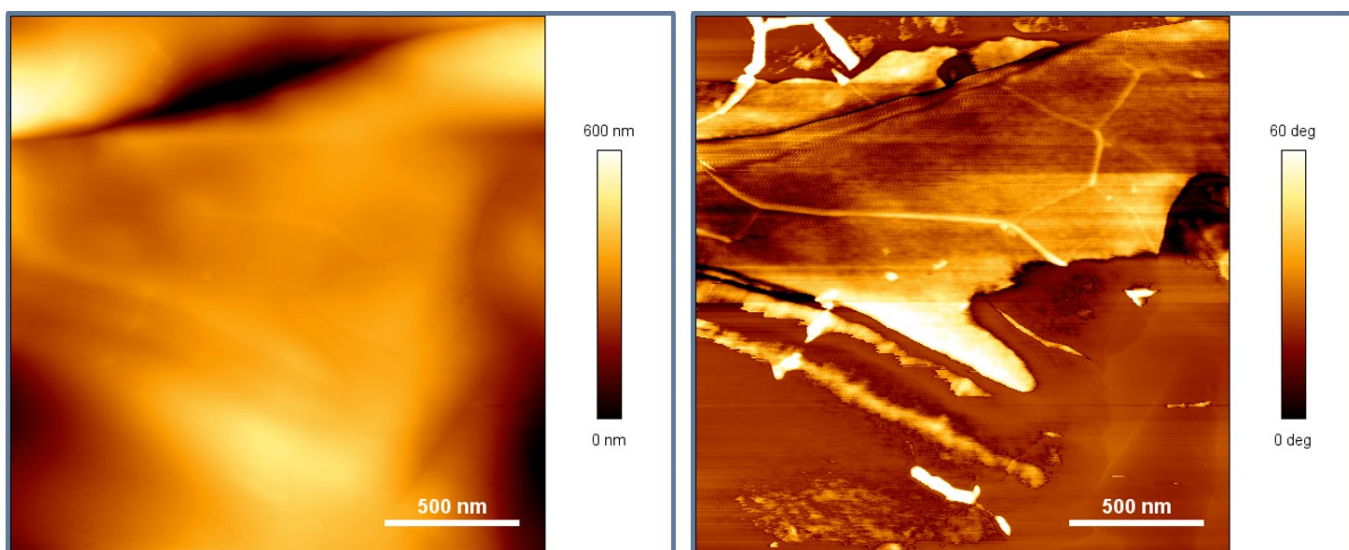


Figure S78: AFM image of recycled VU-(AlnC-Pri)<sub>0.8</sub> showing the height plot (left) and the phase plot (right).

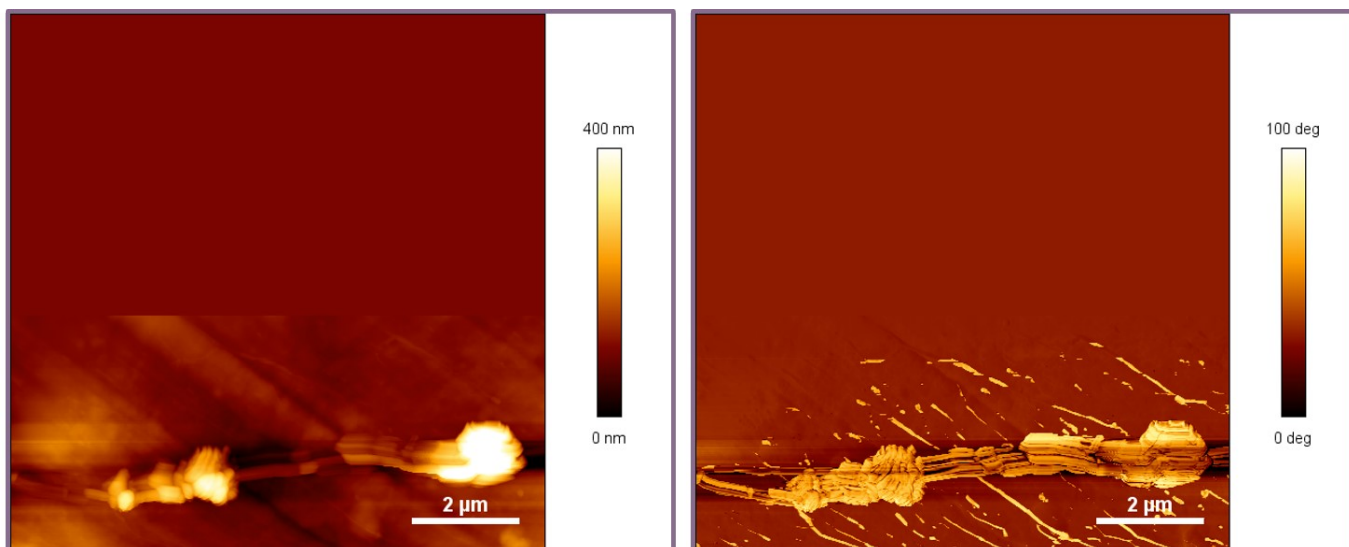


Figure S79: AFM image of recycled VU-(AlnP-Pri)<sub>0.8</sub> showing the height plot (left) and the phase plot (right).

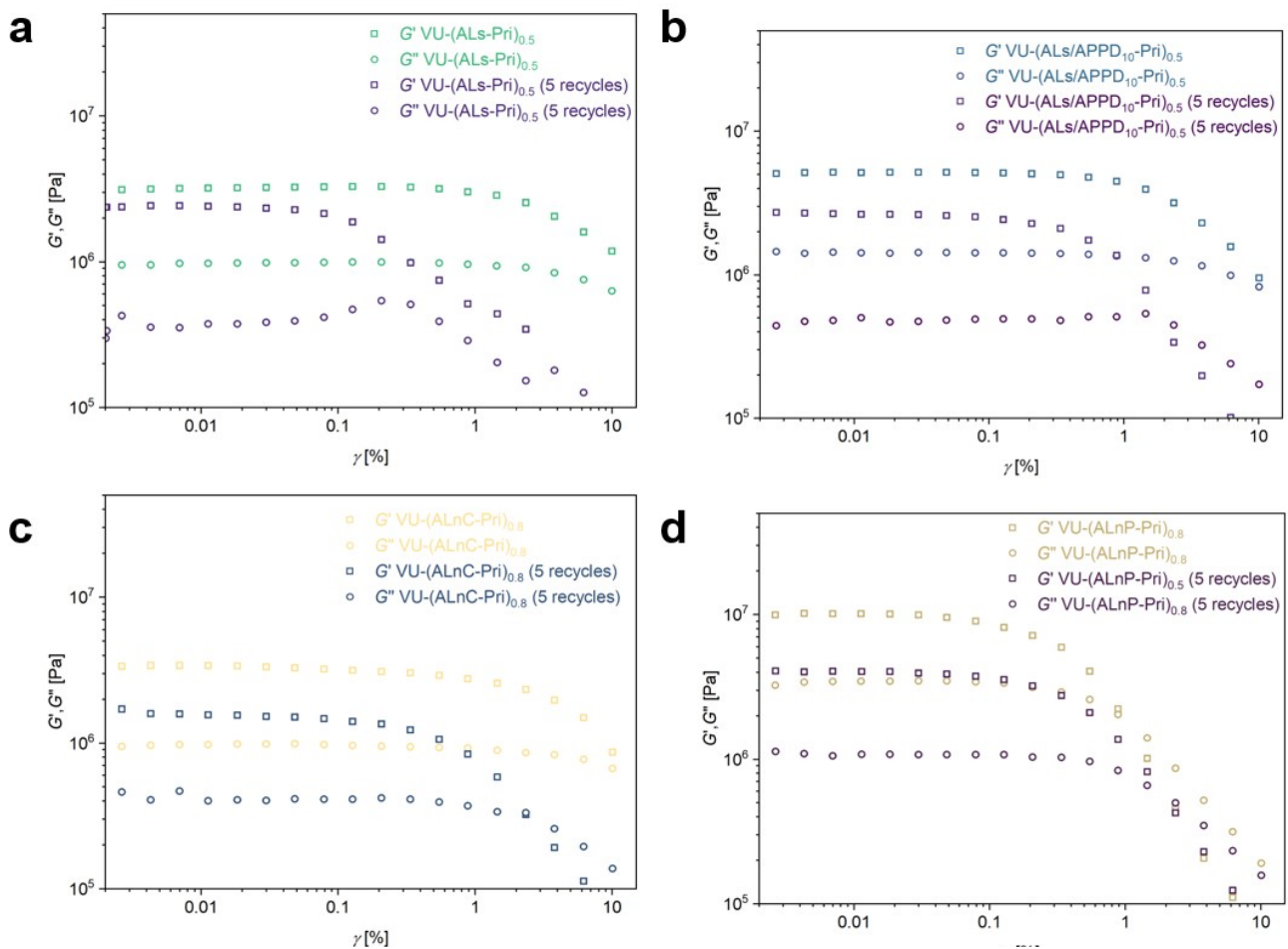


Figure S80: Amplitude sweep measurements of the recycled lignin vitrimer materials between 0.001% and 10% shear strain  $\gamma$  performed at a constant angular frequency of  $6.28 \text{ rad s}^{-1}$  of selected vitrimer materials VU-(ALs-Pri)<sub>0.5</sub> (a), VU-(ALs/APPD10-Pri)<sub>0.6</sub> (b), VU-(ALnC-Pri)<sub>0.8</sub> (c) and VU-(ALnP-Pri)<sub>0.8</sub> (d) in comparison of the pristine and five times reprocessed materials.

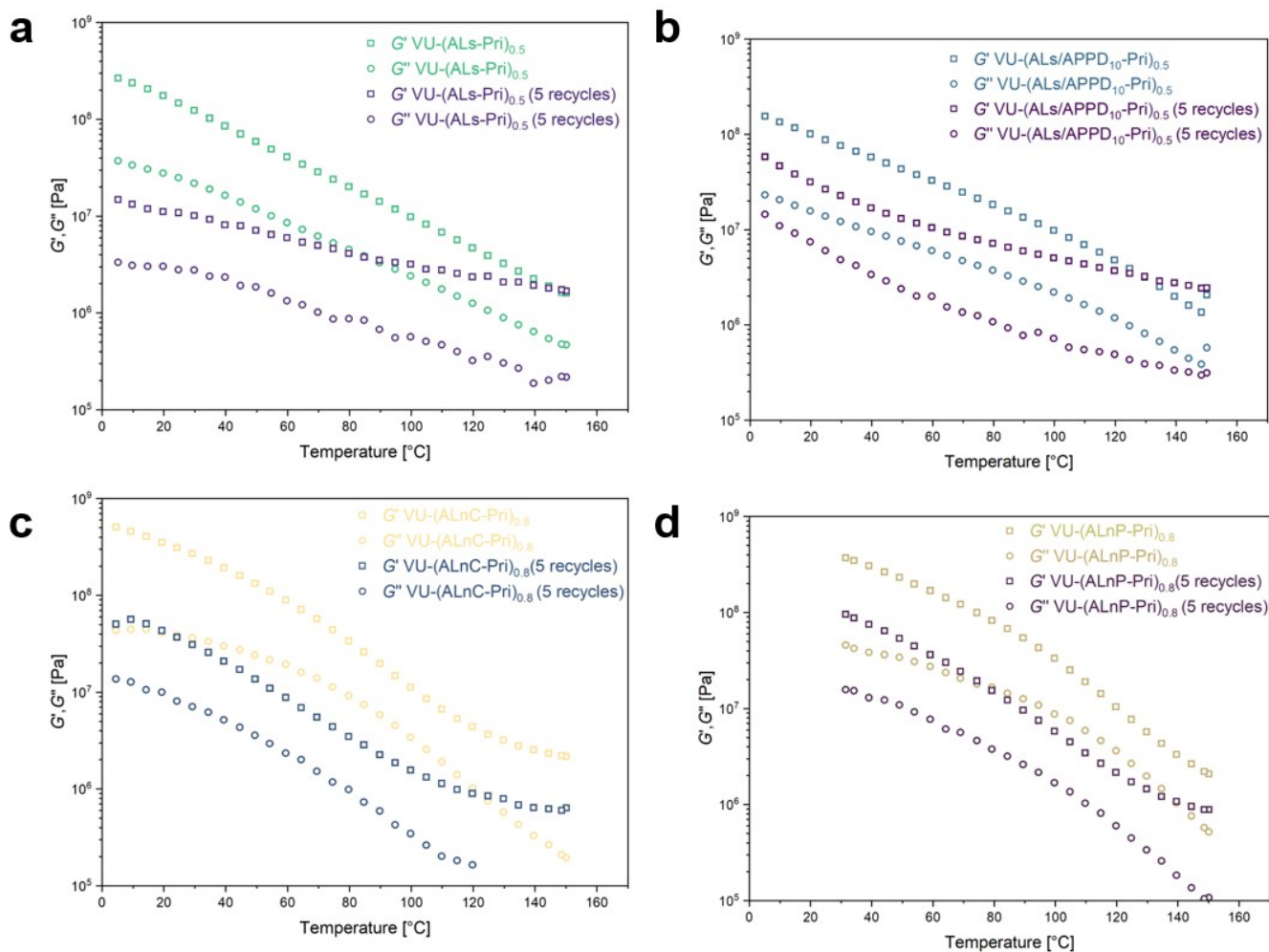


Figure S81: Temperature sweep measurements of the recycled lignin vitrimers in the temperature range of 150 °C – 0 °C performed at a constant angular frequency of 6.28 rad s<sup>-1</sup> and a constant shear strain amplitude of 0.01% of selected vitrimers VU-(ALs-Pri)<sub>0.5</sub> (a), VU-(ALs/APPD10-Pri)<sub>0.5</sub> (b), VU-(ALnC-Pri)<sub>0.8</sub> (c) and VU-(ALnP-Pri)<sub>0.8</sub> (d) in comparison of the pristine and five times reprocessed materials.

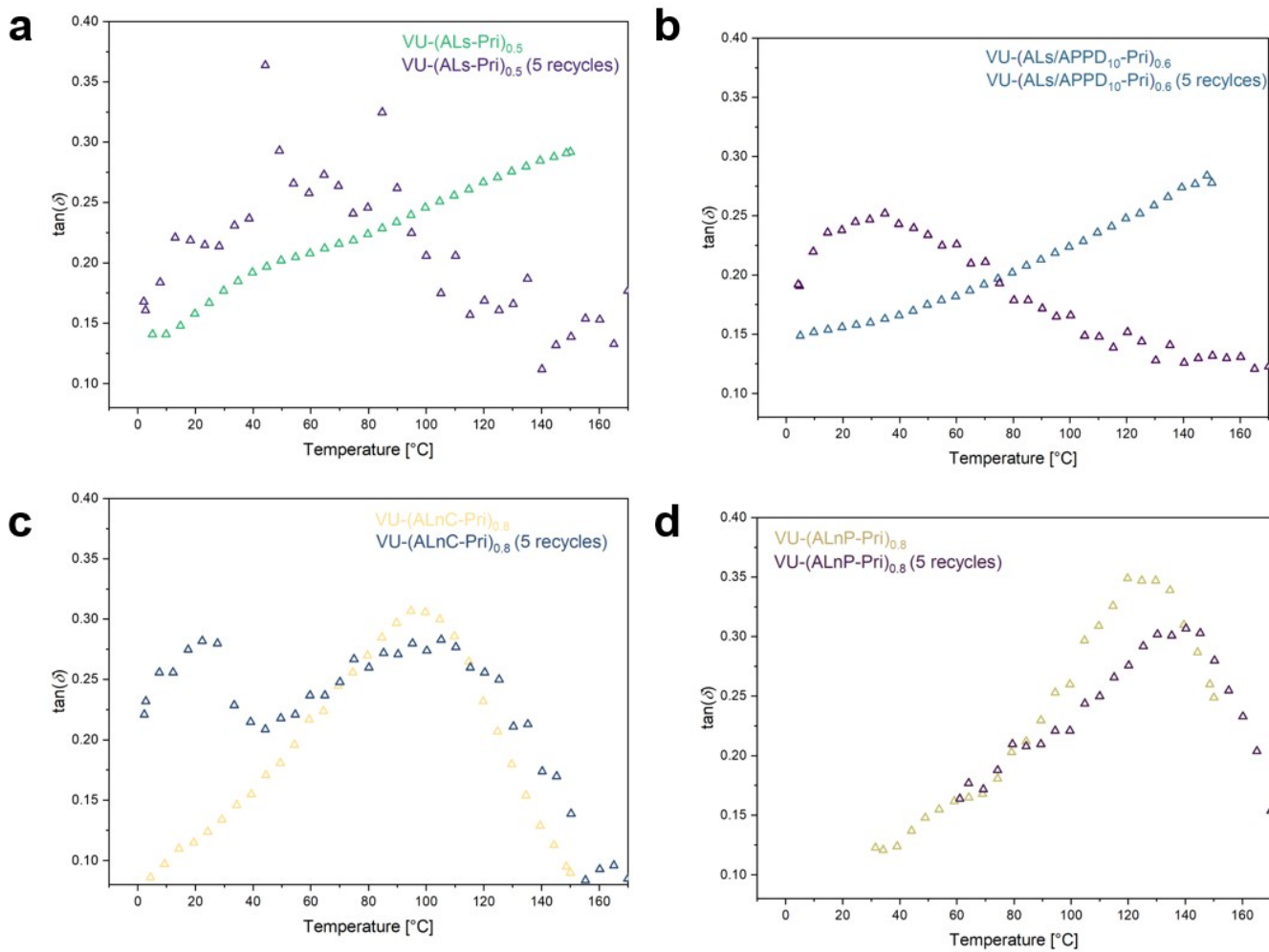


Figure S82:  $\tan(\delta)$  values calculated from the storage and loss moduli of the temperature sweep measurements of the recycled lignin vitrimers in the temperature range of 150 °C – 0 °C performed at a constant angular frequency of 6.28 rad s<sup>-1</sup> and a constant shear strain amplitude of 0.01% of selected vitrimers VU-(ALS-Pri)<sub>0.5</sub> (a), VU-(ALS/APPD10-Pri)<sub>0.6</sub> (b), VU-(ALnC-Pri)<sub>0.8</sub> (c) and VU-(ALnP-Pri)<sub>0.8</sub> (d) in comparison of the pristine and five times reprocessed materials.

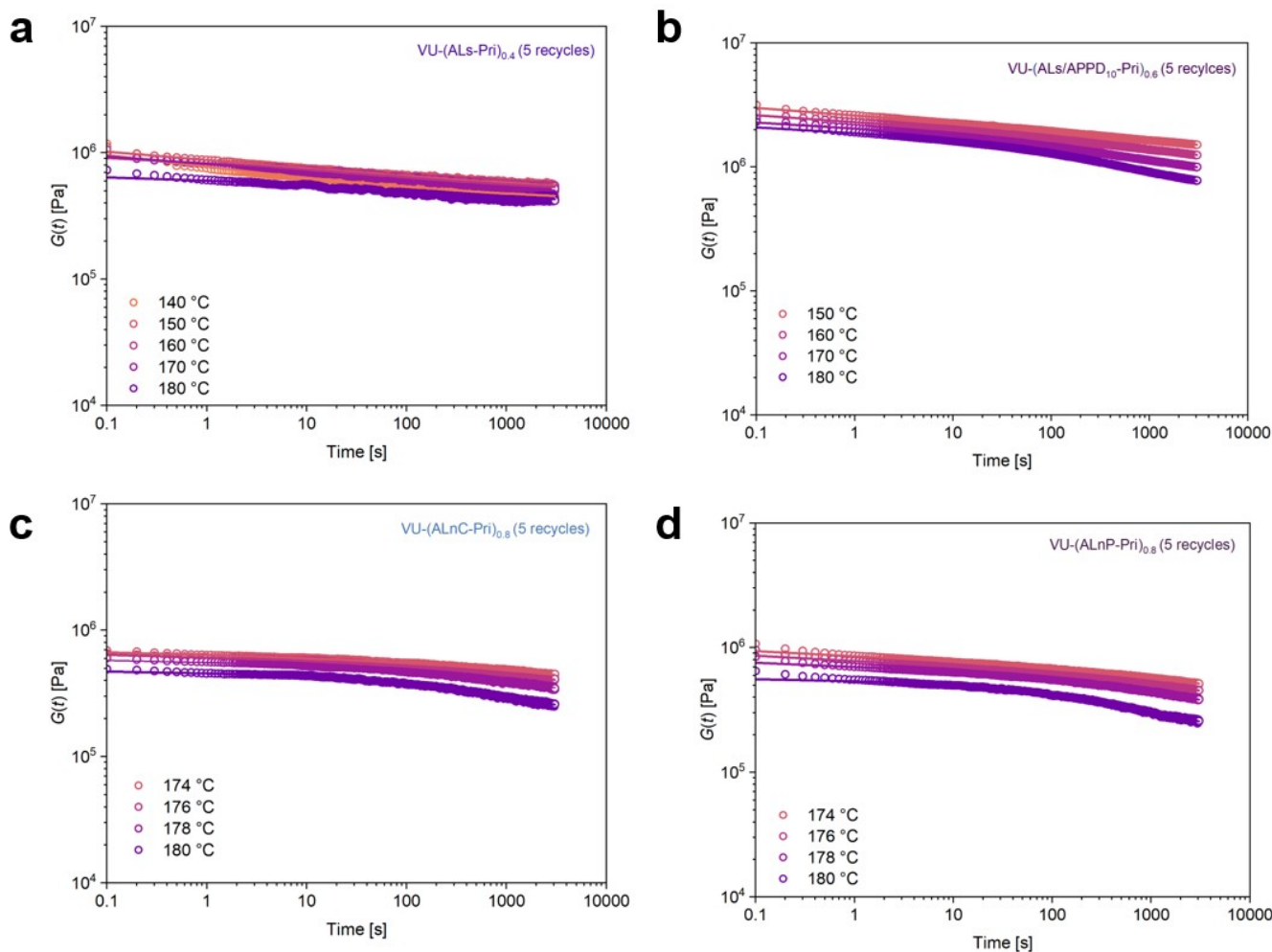


Figure S 83: Stress-relaxation measurement of selected vitrimers VU-(ALs-Pri)<sub>0.5</sub> (a), VU-(ALs/APPD10-Pri)<sub>0.6</sub> (b), VU-(ALnC-Pri)<sub>0.8</sub> (c) and VU-(ALnP-Pri)<sub>0.8</sub> (d) after five reprocessing cycles, plotting the stress-relaxation modulus  $G(t)$  versus the stress-relaxation time while applying a shear strain of 1%. The lines display the stretched exponential fit functions for the respective temperatures, calculated from the stress-relaxation data.

Table S16: Summary of the  $\beta$  and  $\langle \tau \rangle$  values for the KWW fit of the stress-relaxation measurements of the lignin vitrimers VU-(ALs-Pri)<sub>0.5</sub> and VU-(ALs/APPD-Pri)<sub>0.6</sub> after five recycling steps in the temperature range of 140 °C to 180 °C while applying a shear strain of 1%.

Sample	$\beta_{150^\circ\text{C}}$ [-]	$\beta_{160^\circ\text{C}}$ [-]	$\beta_{170^\circ\text{C}}$ [-]	$\beta_{180^\circ\text{C}}$ [-]	$\langle \tau \rangle_{150^\circ\text{C}}$ [s]	$\langle \tau \rangle_{160^\circ\text{C}}$ [s]	$\langle \tau \rangle_{170^\circ\text{C}}$ [s]	$\langle \tau \rangle_{180^\circ\text{C}}$ [s]
VU-(ALs-Pri) <sub>0.5</sub> (5x recycled)	0.052	0.188	0.097	0.380	$5.9 \cdot 10^9$	2250	$4.3 \cdot 10^5$	122
VU-(ALs/APPD <sub>10</sub> - Pri) <sub>0.6</sub> (5x recycled)	0.056	0.091	0.178	0.248	$5.5 \cdot 10^{12}$	$4.8 \cdot 10^8$	$3.40 \cdot 10^4$	3310

Table S17: Summary of the  $\beta$  and  $\langle \tau \rangle$  values for the KWW fit of the stress-relaxation measurements of the lignin vitrimers VU-(ALnC-Pri)<sub>0.8</sub> and VU-(ALnP-Pri)<sub>0.8</sub> after being 5 recycling steps in the temperature range of 170 °C to 180 °C while applying a shear strain of 1%.

Sample	$\beta_{174^\circ\text{C}}$ [-]	$\beta_{176^\circ\text{C}}$ [-]	$\beta_{178^\circ\text{C}}$ [-]	$\beta_{180^\circ\text{C}}$ [-]	$\langle \tau \rangle_{174^\circ\text{C}}$ [s]	$\langle \tau \rangle_{176^\circ\text{C}}$ [s]	$\langle \tau \rangle_{178^\circ\text{C}}$ [s]	$\langle \tau \rangle_{180^\circ\text{C}}$ [s]
VU-(ALnC- Pri) <sub>0.8</sub>	0.141	0.221	0.321	0.408	$1.81 \cdot 10^{11}$	$1.14 \cdot 10^5$	4997	1629
VU-(ALnP-Pri) <sub>0.8</sub>	0.057	0.072	0.136	0.407	$1.8 \cdot 10^{24}$	$4.1 \cdot 10^{17}$	$2.65 \cdot 10^9$	1200

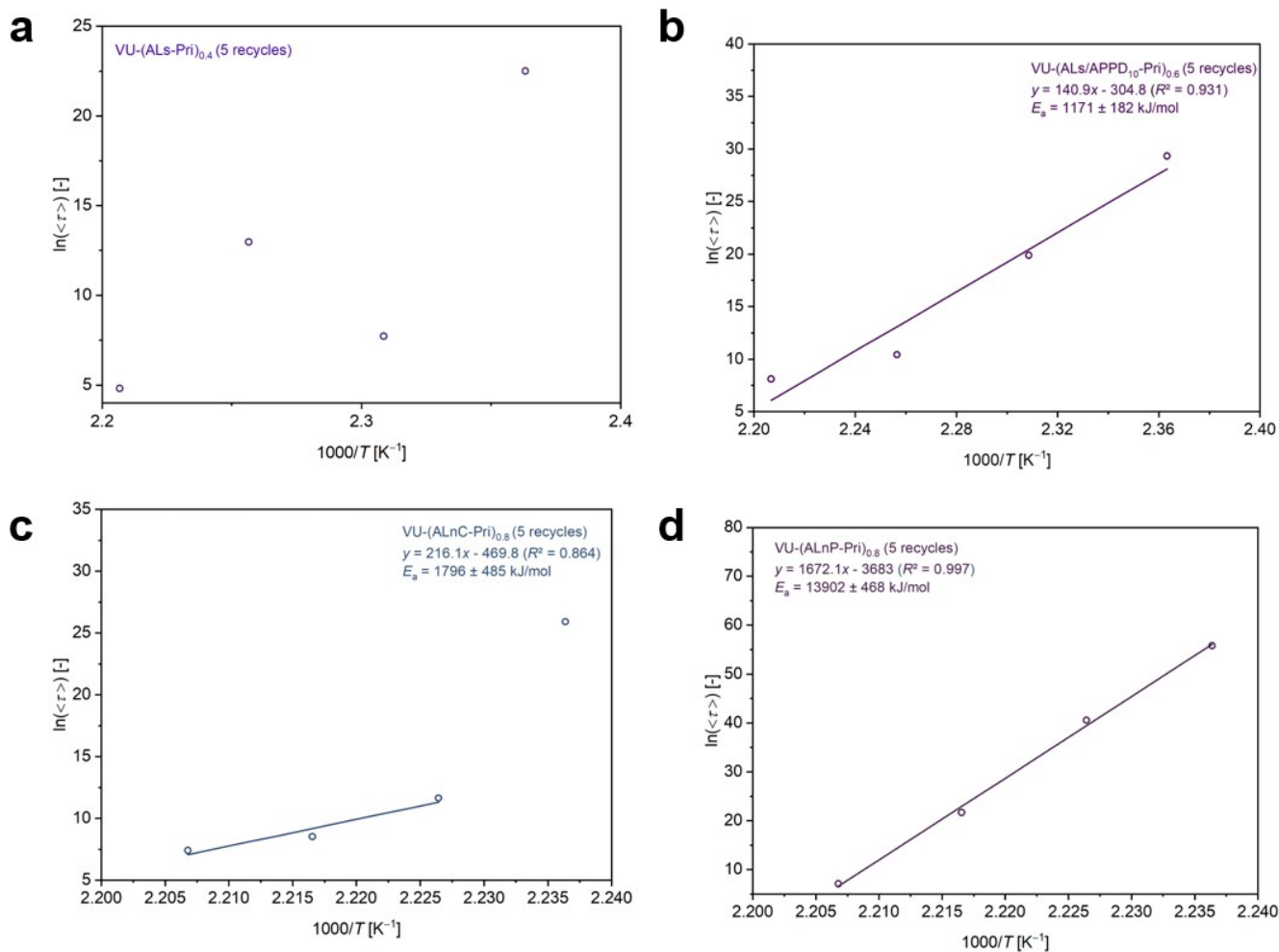


Figure S84: Plot of  $\ln \langle \tau \rangle$  versus  $1000/T$  of selected vitrimers VU-(ALs-Pri)<sub>0.5</sub> (a), VU-(ALs/APPD10-Pri)<sub>0.6</sub> (b), VU-(ALnC-Pri)<sub>0.8</sub> (c) and VU-(ALnP-Pri)<sub>0.8</sub> (d) after five reprocessing cycles while applying a shear strain of 1% to show potential stress relaxation behavior of the materials.

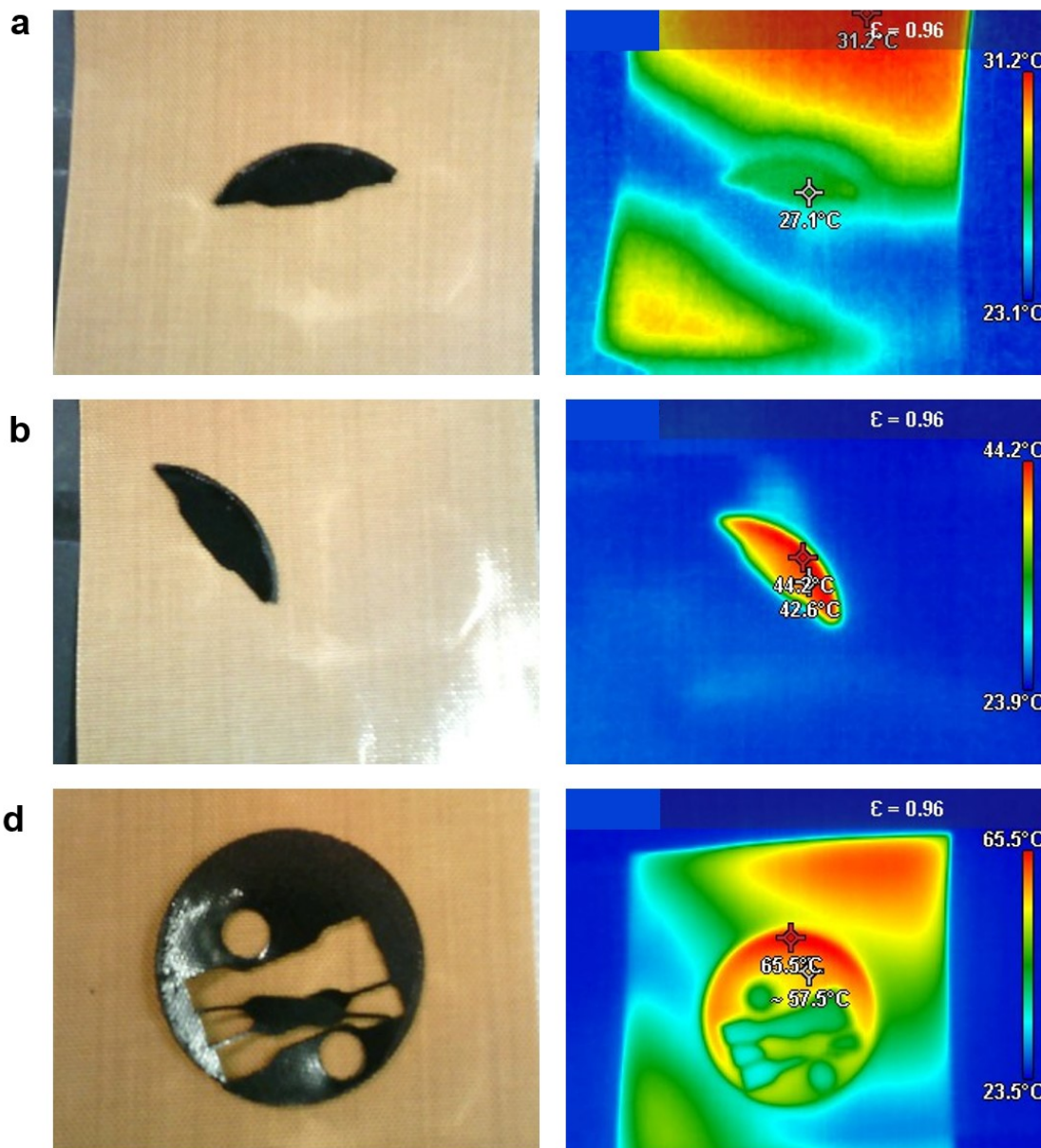


Figure S85: Pictures of the heating experiment by UV-light absorption. The setup included irradiation via an UV-light source (OmniCure 460) with a wavelength of 365 nm and an irradiation intensity of  $69 \text{ mW cm}^{-2}$ . Pictures were taken after three irradiation times. (a) Irradiation experiment with a duration of 10 s, yielding a surface temperature of  $27.1^\circ\text{C}$ . (b) Irradiation experiment with a duration of 60 s, yielding a surface temperature of  $44.2^\circ\text{C}$ . (c) Irradiation experiment with a duration of 10 s, yielding a surface temperature of  $65.5^\circ\text{C}$ . As the sheet holding the sample also heated, no significant UV-light-induced heating effect was observed.

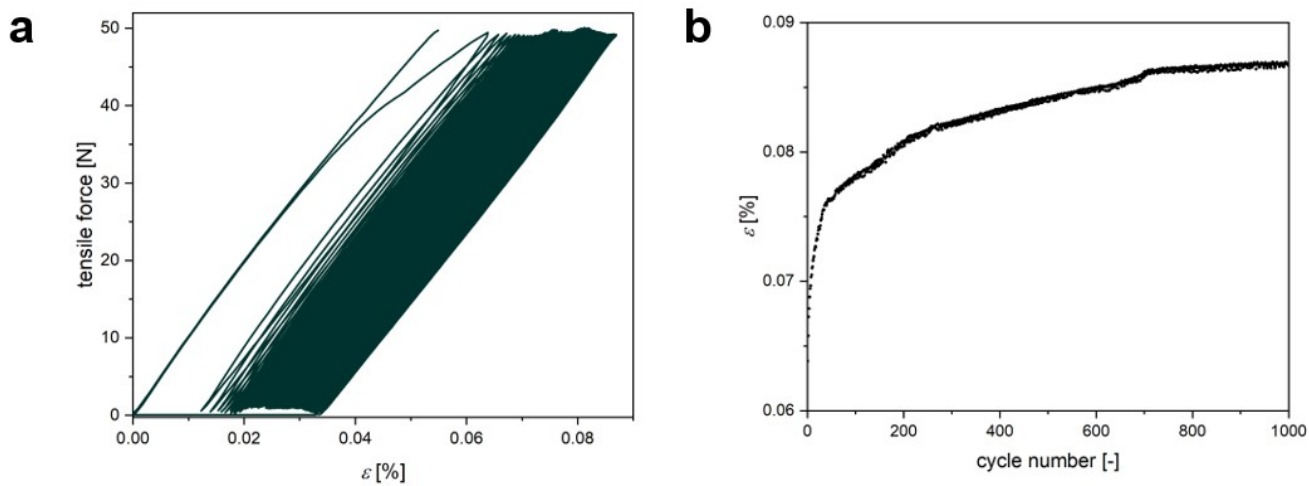


Figure S86: Durability and fatigue testing of a test sheet in a cyclic deformation test setup, displaying the tensile force plotted against the elongation (a) for 1000 cycles of repeated loading with a force of 50 N. (b) Plot of the elongation versus the cycle number, showing increasing elongation with a plateau after 700 cycles.